WIND EFFECT ON CYLINDERS OF PENTAGONAL, HEXAGONAL AND OCTAGONAL SECTIONS AT DIFFERENT POSITIONS

MST MOUSUMI RIZIA

MILITARY INSTITUTE OF SCIENCE AND TECHNOLOGY (MIST)

2018

WIND EFFECT ON CYLINDERS OF PENTAGONAL, HEXAGONAL AND OCTAGONAL SECTIONS AT DIFFERENT POSITIONS

MST MOUSUMI RIZIA
(*MSc Engg., MIST*)

A THESIS SUBMITTED
FOR THE DEGREE OF MASTER OF SCIENCE IN
MECHANICAL ENGINEERING
DEPARTMENT OF MECHANICAL ENGINEERING
MILITARY INSTITUTE OF SCIENCE AND TECHNOLOGY

2018

DEDICATION

Dedicate this thesis

To my teachers;

To my parents and family

The thesis titled **"Wind Effect on Cylinders of Pentagonal, Hexagonal and Octagonal Sections at Different Positions",** Submitted by **Mst Mousumi Rizia**, Roll No: **1016180005(P)**, Session: **April 2016**, has been accepted as satisfactory in partial fulfillment of the requirement for the degree of Master of Science in Mechanical Engineering on 9th August 2018.

BOARD OF EXAMINERS

…… Professor Dr. Md. Quamrul Islam Department of Mechanical Engineering, MIST Dhaka-1216, Bangladesh	**Chairman** **(Supervisor)**
…… Professor Dr. Mohammad Ali Department of Mechanical Engineering, BUET, Dhaka-1000, Bangladesh	**Member** **(Co-Supervisor)**
…… Brig Gen Mustafa Kamal Head, Department of Mechanical Engineering, MIST Dhaka-1216, Bangladesh	**Member** **(Ex-Officio)**
…… Professor Dr. Md. Alamgir Hossain Department of Mechanical Engineering, MIST Dhaka-1216, Bangladesh	**Member**
…… Professor Dr. Mohammad Mamun Department of Mechanical Engineering, BUET Dhaka-1000, Bangladesh	**Member** **(External)**

DECLARATION

I hereby declare that this thesis is my original work and it has been written by me in its entirety. I have duly acknowledged all the sources of information which have been used in the thesis.

This thesis has also not been submitted for any degree in any university previously.

…….

Mst Mousumi Rizia

09 August 2018

ACKNOWLEDGEMENT

First of all, my gratitude to Allah the All-Knowing and Most Merciful for the successful completion of this research work.

I wish to express my sincerest gratitude and heartfelt thanks to my supervisor Dr. Md. Quamrul Islam, Professor for his continuous guidance, inspiration, supervision and untiring support throughout the entire period of my graduate study. It is beyond doubt that without his kind support, completion of this research work would not have been possible.

I also want to express my deepest gratitude to Professor Dr. Mohammad Ali, Department of Mechanical Engineering, for his constructive suggestion and advice during several phases of this problem. His encouragement and invaluable suggestions are gratefully acknowledged.

I am also indebted to Wing Commander Dr. Vikram Deshpande, IAF, Department of Aeronautical Engineering, Lecturer Zawad Abedin, Md. Tanvir Ehsan and Lecturer Atif Yasir of Department of Mechanical Engineering, MIST for their cooperation and invaluable assistance in different aspect of the thesis.

I feel especially proud to express my appreciation to all my family members for their encouragement and support throughout this work. Their love and sacrifice made this thesis a great success in my carrier.

Special thanks to SAE Ashraf of Fluid Mechanics Laboratory of Mechanical Engineering Department of MIST and Mr. Md. Abul Kalam Azad, instructor of Fluid Mechanics Laboratory of Mechanical Engineering Department of BUET, Dhaka for their kind cooperation in constructing, fabricating and assembling different parts and components of the experimental set-up. Finally, I would like to express my sincere thanks to all members of the Department of Mechanical Engineering of MIST for their cooperation and help in the successful completion of the work.

TABLE OF CONTENTS

SUMMARY

In this research work, an experimental investigation and simulation of wind effect on pentagonal, hexagonal and octagonal cylinders were carried out. The study was performed on a group of three cylinders of the same hydraulic diameter, arranged in staggered form, one hexagonal and one pentagonal cylinder in the upstream and another octagonal cylinder in the downstream side. The cylinder's inter-spacing distances were kept fixed. The surface static pressures were measured. The test was conducted in an open circuit wind tunnel at a Reynolds number of 1.95×10^5 based on the face width of the cylinder across the flow direction in a uniform flow velocity of 14.3 m/s.

For experimental analysis, the test was carried out on the group of three cylinders at four different angles of attack i.e. 0°, 30°, 45° and 60°. The surface static pressures at the different locations of the cylinder were measured with the help of inclined multi-manometers. After that the pressure coefficients were calculated from the measured values of the surface static pressure distribution over the cylinder. Later, the drag and lift coefficients were obtained from the pressure coefficients analytically.

Simulation was carried out with similar arrangement of the cylinders keeping the same inter-spacing distances and angles of attack similar to the experimental setup. ANSYS 16 was used and corresponding coefficients of pressures, lift and drag were calculated using k-ε model. Theoretical results agree well with the experimental results.

It was also observed that at various angles of attack, the lift coefficients were insignificant compared to those for a sharp-edged cylinder. Users and specially, both engineers and architects will benefit from the outcome of this research as they will be able to design structures and buildings more efficiently. Results were expressed in the non-dimensional form for ease of usability in prototype building.

LIST OF TABLES

LIST OF FIGURES

NOMENCLATURE

A	Frontal area of the Cylinder
C_L	Coefficient of lift
C_D	Coefficient of drag
C_p	Coefficient of pressure
F_D	Drag force
F_L	Lift force
h_a	Air head
P	Static pressure on the surface of the cylinder
P_o	Ambient pressure
P	Density of air
U_∞	Free stream velocity
V	Wind speed
X	Latitude velocity of the earth
Z	Height
dp/dn	Pressure gradient
α	Angle of attack
γ_a	Specific weight of air
γ_w	Specific weight of manometer liquid (water)
Δh_w	Manometer reading
ΔP	Pressure difference
ώ	Angular velocity of the earth

CHAPTER-1

INTRODUCTION

The movement of air in any direction relative to the earth surface is called wind. It is the product of pressure gradients established between systems of high pressure to low pressure. Rather than simply flowing from low to high pressure areas, wind direction is dependent on a number of factors including terrestrial radiation, the seasonal temperature changes and the earth's rotation which is generally known as the Coriolis effect. As a result, wind in the northern hemisphere shift to the right and wind in the southern hemisphere shift to the left, so that the wind flows mostly around the high and low-pressure areas. In addition, due to the centripetal acceleration, the wind in a low-pressure system, blows in a counterclockwise and inward direction in the northern hemisphere. Whereas in northern hemisphere in high pressure systems, wind blow in a clockwise and outward direction [1]. The term 'wind' exclusively represents the horizontal wind whereas due to its relatively small vertical components, 'vertical wind' is expressed as such [1]. Meteorological observatories use anemometers to measure the wind speeds.

Wind load on structures has been considered by scientists as far back as the seventeenth century during the times of Galileo and Newton. However, it was during late 19^{th} century that the effect of wind loading on buildings and structures had been considered seriously for design purposes. Modern buildings, structures and their components are now designed to withstand the code specified wind loads. Wind loads calculation is vital in design of wind force resisting systems, e.g. structural members, components, and cladding against shear, overturning, sliding, uplift actions etc.

A good number of studies have been conducted largely on the wind effect on stand-alone buildings and structures in recent past in different corners of the world including Bangladesh due to the growing trend of high rise buildings and structures. However, till now, limited information is available concerning the flow over group of bluff bodies in staggered condition, which is definitely a significant engineering problem of considerable practical implication. With the progressing world, engineering problems concerning wind loads around a group of high rise buildings, towers, chimneys, flow induced vibration of tubes in heat exchangers, oil rigs, marine or other structures etc. need thorough aerodynamic studies. Sufficient effort has been given over past decades in research works concerning laboratory simulations, full-scale

measurements, numerical calculations and theoretical predictions and more recently simulation for flows over bodies of wide range of shapes, in pursuance to the increasing practical importance of bluff body aerodynamics. A number of structural failures prompted research work in this field that includes Smeaton, Vogt, Irminger, Eiffel and Stanton as its pioneer researchers [12]. The most likely first ever was done by Irminger in 1891 who published results of measurements on models, and later Eiffel, conducted pioneer studies on the flow velocities and tower movements in the period up to 1900, following completion of the famous tower from a laboratory at its top [12].

Although earlier, studies on wind effect were first limited to structural loading only, due to its most dramatic effects are found in their collapses; nevertheless, mid-sixties found the researchers studying environmental aspects of flow of wind around buildings/structures such as effects on pedestrians, weathering, rain penetration, ventilation, heat loss, wind noise and air pollution etc., which may be less dramatic but equally substantial. A number of works of the environmental aspects of wind was being studied at the Building Research Establishment at Garson and the University of Bristol, U. K. by a pioneer researcher Lawson [2]. It is true that researchers from all over the world have contributed greatly to the knowledge of flow over bluff bodies, but the majority of the research were conducted either on single cylinder with circular, square, octagonal, hexagonal or rectangular sections etc. or in a group with them for various flow parameters. However, till now the flow over a combination of pentagonal, hexagonal and octagonal cylinders have not been studied extensively especially in-groups, which is certainly a problem of considerable practical importance. It is believed that such study will contribute in finding the wind load of a group of buildings with pentagonal, hexagonal and octagonal shape in similar orientation which will assuredly assist engineers and architects.

1.1 Nature of the Wind

It is a well-known fact that wind speed increases with increase in height mainly due to the earth surface friction that slows down wind or air flowing near it. The general terms that differentiate winds of different average speeds are a breeze, a gale, a storm, tornado, or a hurricane. Usually very strong winds are associated with thunderstorms, cyclonic storms, dust storms or vigorous monsoons. One significant feature of the cyclonic storms over the Bangladesh region is that they rapidly weaken after crossing the coasts and move as depressions in land. The influence of a severe storm after striking the coast does not in general exceed about 60 kilometers, though sometimes, it may extend even up to 120 kilometers. Norwesters or KalBaisaki are frequent

summer occurrence that ensues for a short duration with very high wind speeds over North East of Bangladesh [12]. Here, the wind characteristics related to present study has been discussed briefly.

1.2.1 Wind Velocity

High wind velocity is associated with building and structural failure. Strong winds often have special names, including gales, hurricanes and typhoons. High velocity wind can cause unpleasant side effects as well. At any time, in addition to steady wind, there are effects of gusts, which may last for a few seconds Therefore, the wind speeds recorded at any locality are extremely variable. Short period gusts may not cause any appreciable increase in stress in main components of the building and structure due to the inertia of the buildings. The response of a building to high wind pressures depends not only upon the geographical location and characteristics of the structure itself, but also on the proximity of other impediments to air flow.

A wind from north, blowing toward the south is called a north wind, that is winds are named by the direction they come from. When a wind blows more frequently from one direction than from any other it is called a prevailing wind. Again, 'windward' refers to the direction a wind comes from while 'leeward' is the direction it blows toward. As the frictional drag declines, wind speed increases rapidly with height above the ground level. Wind is commonly not a steady current but is made up of a succession of gusts, slightly variable in direction, separated by lulls. The gustiness close to the earth is developed due to irregularities in the wind which are caused by the conventional currents. All forms of turbulence play a part in the process of transporting heat, moisture and dust into the air upward.

According to Castro, J. P. [3], a number of parameters control the flow behavior; such as (i) vortices in front of the building, (ii) opening through buildings, (iii) spacing of rows, (iv) wakes of buildings, (v) long straight streets, (vi) narrowing streets, (vii) corners and (viii) courtyards.

Mean wind speed is height dependent. Davenport, A. G. [4] has expressed this variation of wind speed as,

$$V = V_c(Z/Z_c)^a$$

Here, V = mean wind speed at a height Z,

V_c = mean wind speed (depends on the geographical locality) at Z_c,

Z_c = gradient height (a function of terrain).

Values of Z_c and the exponent 'a' suggested by Davenport, A. G. [4] are as follows:

For open terrain with very few obstacles: a = 0.16, Z_c = 300m;

For terrain uniformly covered with obstacles 10-15 m height: a = 0.28, Z_c = 430m;

For terrain with large and irregular objects: a = 0.40, Z_c = 560m.

1.2.2 Generation of Wind

Solar radiation is the source of wind energy that causes differential heating of the earth surface and the atmosphere. Lanoville A *et al* [5] mentioned that in the atmosphere there is a general convective transport of heat from lower to higher latitudes in order to make the earth's radiation imbalance. For this reason, circulation in the atmosphere of all sizes is normal, hence it is a restless medium. Wind is essentially air moving parallel with the earth's surface. Due to the gravitational equilibrium, the atmosphere is fixed to the solid-liquid earth and therefore it moves with the earth in its west to east rotational movement. Wind is collectively the air movement in addition to that associated with rotation. Horizontal motion greatly exceeds vertical motion in large-scale circulation covering several thousand miles. This is why, wind that takes several days to cross an ocean may get vertical displacement of only a few miles. In case of small-scale circulation like thunderstorms and tornadoes vertical movement quite significant. For example, air may ascend to the top of the atmosphere in about an hour during a thunderstorm [1].

Wind is no doubt, complex in origin. Its direct cause lies, generally, in the differences between atmospheric densities that in turn results in horizontal air pressure differences i.e. it is the nature's attempt to rectify pressure inequalities. Horizontal pressure differences cause pressures gradient. Ultimately, the source of average airflow generation and maintaining it against the drag is mostly due to the differences in heating and cooling between high and low latitudes despite the direct part played by pressure differences.

1.2.3 Forces Governing Winds

Total four forces function to determine the wind speed and its direction [1];

(i) pressure gradients force, (ii) Coriolis force, (iii) frictional force and (iv) centrifugal force.

i) Pressure Gradient Force

Pressure gradient forces gets air to move with increasing speed along the gradient and sets air in motion. Its magnitude is inversely proportional to the isobar spacing. Since the gradient slopes downward from high to low pressure, direction of airflow is from high to low pressure

along the pressure gradient. But earth's rotation, the movement of air particle trajectory from high to low pressure is quite indirect, except close to the equator.

ii) Coriolis Force

the rotation earth generates a deflection force that only affects the wind direction. Except at the equator, winds and all other moving objects, no matter what their direction, are deflected towards the right of the gradient in the northern hemisphere and leftward in the southern hemisphere. The force acts at right angles to the direction of motion. Coriolis force is stronger in higher latitudes. When pressure gradient is balanced by the Coriolis force, wind blows parallel with the isobars and it is called geotropic wind. The geotropic wind V_c can be estimated from the expression as suggested by Davenport, A. G. [4].

$$Vc = \frac{dp}{dn} 2\rho\omega \sin x$$

Where, (dp/dn) is the pressure gradient, 'ω' is the angular velocity of the earth, 'ρ' is the air density and 'x' is the latitude. Friction layer may be extended up to 1000 m above the earth's surface outside the atmosphere. Wind actually does blow in a direction almost parallel with the isobars with low pressure on the left and high pressure on the right in the northern hemisphere.

iii) Frictional Force

Frictional force affects both wind speed and direction. Friction between the moving air and the earth's land-sea surface tends to slow the movement of air. Surface airflow crosses isobars at an oblique angle instead of flowing parallelly to it due to the frictional effects of the land-sea surface. The wind direction angle to the isobars become wider as the friction force gets greater. For example, winds over irregular land surfaces usually form angles varying from 20^0 to 45^0 with the isobars whereas it can be as little as 10^0 over oceans [1].

iv) Centrifugal Force

This force impacts only when air moves in a curved path. Centrifugal force is a major factor only in case of strong wind and when the radius of curvature is small as they are in tropical hurricanes, tornadoes and the centers of a few usually well-developed cyclonic storms. The flow of air which is necessary to balance pressure force, Coriolis force and centrifugal force in absence of frictional force is called gradient wind. This happens at heights greater than 500 m or so [1].

1.2 Wind Loading on Structures

The effect of wind on the structure as a whole is determined by the combined action of external and internal pressures acting upon it. In all cases, the calculated wind loads act normal to the surface to which they apply. The pressures created inside a building due to access of wind through openings could be suction (negative) or pressure (positive) of the same order of intensity while that outside may also vary in magnitude with possible reversals. Thus, the design value shall be taken as the algebraic sum of the two in appropriate direction. Furthermore, the external pressures (or forces) acting on different parts of a framework do not correlate fully. Hence, there is a reduction in the overall effect.

The development of modern materials and construction techniques has resulted in the emergence of a new generation of structures. Such structures exhibit an increased susceptibility to the action of wind. Accordingly, it has become necessary to develop tools enabling the designer to estimate wind effects with a higher degree of refinement than has been previously required. It is the task of the engineer to ensure that the performance of structures subjected to the action of wind will be adequate during their anticipated life from the standpoint of both structural safety and serviceability. To achieve this end, the designer needs information regarding (i) the wind environment, (ii) the relation between that environment and the forces it induces on the structures and (iii) the behavior of the structure under the action of forces [12].

The action of wind on building considering the load effect may be classified into two major groups; the static effect and the dynamic effect. There are many other effects like generation of noise the risk of the hazard, the penetration of rain and uncomfortable wind for the pedestrians etc. but they are not usually considered for structural design. Since all wind loadings are time-dependent because of varying speeds and direction of winds, wind loading is never steady. For this reason, static load is referred to the steady (time-variant) forces and pressures tending to give the structure a steady displacement. On the other hand, dynamic effect has the tendency to set the structure oscillating. A steady wind load on a building is very difficult to achieve. In fact, always wind loads are of a fluctuating nature because of varying speeds and directions of winds. The type of wind and the stiffness and roughness of the structure determine the nature of loading on a building. When a building is very stiff the dynamic response of the structure may be neglected and only the static leads may be considered. This is because the natural frequency of an extremely stiff building is too high to be excited by wind. In the present study the effect of static loading is taken into account due to the steady wind. Since natural winds are

continually fluctuating, it is generally assumed that these fluctuations are so irregular and random that the response of a structure will not differ from that due to a steady wind of the same average speed. Because of the modern tendency to build more slender and lighter structures, the dynamic response of building and structures has been considered for study in recent years [12].

1.3 Necessity of the Study

In Bangladesh, strong wind is an annual natural hazard due to its geographical location. On the other hand, most of the existing houses and those which are going to be built in the next few decades are likely to be non-engineered, mostly with thatched roofs and are vulnerable to wind. Strong wind is causing immense losses of rural dwellers by making their houses collapse fully or partially by lifting of roof etc. Almost 70% of the population in the rural sector and 50% of the population in the urban sector are living below the poverty level with earnings too little to pay for all needs [12]. It is this group of people most impoverished that is to be provided with good housing. About 75% of the dwelling in rural areas is of kutcha construction (Mud, Bamboo, Woven Bamboo etc.) and that 23% of urban and more than 40% of rural dwellings are of a temporary nature [12]. They can rarely survive against even a moderate intensity storm. Evidence from the field in strong wind-prone areas indicates that there is a socially perceived need of more engineering knowledge and improved construction of domestic dwelling.

Bangladesh is a land hungry country. The urban population of this country is increasing at a very fast rate making the housing problem worse every day. One possible solution of the housing problem is to construct multistoried buildings. The knowledge of wind loading on a single tall building or on a group of tall buildings is essential for their economic design. The flow around a combination of pentagonal, hexagonal and octagonal model cylinder can be ideally considered analogous to that of the flow around a combination of tall pentagonal, hexagonal and octagonal shaped building. Therefore, a study of wind flow around groups of pentagonal, hexagonal and octagonal cylinders would be helpful in this respect. For designing groups of tall buildings, knowledge of the effect of wind loading on a single tall building is not sufficient because the effects of nearby buildings on the loads imposed on a structure would be quite different. In the areas with high rise buildings, other problems like unpleasant wind conditions may be developed near ground level in passages between and through buildings and many instances of such conditions, causing discomfort for the pedestrians and damage to doors

and windows in and near the passage have been reported. In order to eliminate these nuisances, architects and town planners of Bangladesh should have a better knowledge of the wind flow around the buildings, which can save precious lives and valuable properties. In the present study, it has been tried to give an understanding about the variation of wind load pattern imposed on building due to the influence of the nearby buildings. To find the complete solutions of the above-mentioned problems a more detailed study in this regard is needed.

There are many examples of failures of buildings and structures in different parts of the world, which has made the enthusiastic investigators puzzled to find the exact causes, and research works are being carried out to find the proper remedial measures for eliminating these failures. The investigators of this country may contribute a lot to the nation by conducting appropriate research work in this field.

Though the problem regarding the wind loadings on buildings and structures is common to all parts of the world and it is expected that the solution will not be significantly different from country to country, yet research work should be carried out in this field considering the climatic conditions and problem of this country so that a clear picture about the nature of wind loading can be obtained. The data from these research works should enable to the architects, engineers and town planners of Bangladesh to design buildings and structures more efficiently.

1.4 Importance of Model Study

Differences between wind tunnel and full-scale result can occur due to Reynolds number inequality, incorrect simulation of the atmospheric boundary layer and small-scale difference between wind tunnel and prototype model. In most wind tunnels tests the full-scale Reynolds number is rarely achieved. Boundary layer separation depends on Reynolds number. For sharp edged structures, separation point does not depend on Reynolds number. On the other hand, the flow field around curved surfaces is very much Reynolds number dependent, so tests on these configurations must be treated with care the crosswind scales in wind tunnels are often less than reality. This can cause underestimation of cross wind effects. The scale difference between wind tunnel model and prototype is found in the high frequency fluctuation. High peaks found on the cladding in full-scale are not found in the wind tunnel. Those effects may be caused by structural details that are not simulated in the wind tunnel model.

Both the studies with models and full-scale buildings are being performed to compare the result for varying the validity with former. Full-scale experiments are both costly and difficult to

perform. For the present study with staggered buildings full-scale experiments will not only be complex and costly but also it would be difficult to record reliable pressure distribution simultaneously on the group of buildings as there will be variation of speeds and direction of wind with time. The flow around buildings in actual environment is very complex and formulation of a mathematical model to predict the flow is very difficult. Thus, model study is a must and the results obtained under simulated condition in the laboratory are found to be quite satisfactory for practical purposes. The experimental conditions will then be simulated using software for further verification.

1.5 Objective of this Experiment

In the present experimental investigation, a pentagonal, a hexagonal and an octagonal section cylinder in combination will be taken into consideration due to the modern architectural trend of complex shaped tall tower buildings of different formations around the world. Cylinders will be located based on their hydraulic diameters. The objectives of the project are as follows:

a) To observe the pressure distribution over the cylinders distributed in a staggered manner with varying angle of attack.
b) To determine the following characteristics from static pressure distributions i.e. the wind loading of the cylinders-
    1) Coefficient of Pressure-C_p,
    2) Coefficient of Drag-$C_{D,}$
    3) Coefficient of Lift-C_L.
c) To study the comparison of theoretical values for same shapes and position using CFD.

For the application of prototype building, the results will be expressed in non-dimensional form. The findings will enable the engineers to design buildings more effectively.

1.6 Scope of the Thesis

This section contains the brief description of the different themes which has been presented in the various chapters.

Chapter 1 describes briefly about the wind characteristics and its effect on buildings and structures. Also, the aim and importance of the study has been included here.

Chapter 2 provides a brief survey of the various related literatures, specially the research works that are directly related to the present study as well as some works in line with it have been included.

The experimental set-up and the measuring equipment has been described in **Chapter 3** as a whole. This chapter also contains the detail feature of the cylinders used for the study.

The mathematical model to calculate the pressure coefficient, drag coefficient and lift coefficient along with aspects of flow modeling has been provided in **Chapter 4.**

In **Chapter 5,** the results and discussion are given which is the most important part of the thesis**.** This chapter also contains elaborate discussions on the pressure coefficient, drag coefficient and lift coefficient.

Lastly, in **Chapter 6** the conclusions and the recommendations for future researchers have been provided.

CHAPTER-2
LITERATURE REVIEW

There have been much studies made on the wind loading on buildings and structures in last few decades right after incidences of catastrophic collapses and failures on the same. With the growing population, there is increasing application of lightweight structural systems, higher strength materials, more monumental forms of construction and architectural forms of extensive range. It is clear that the possibility of any disastrous event should be avoided at any rate which needs extensive research, no matter how desirable such architectural trends become from other viewpoints. Many researchers carried out work primarily on isolated bluff bodies and later, on group of buildings and structures. Parallelly research work was also carried out on the effect of environment on the buildings. Information concerning the flow over staggered pentagonal, hexagonal and octagonal cylinder combination is not available in detail, although this is a consequential practical problem.

Background on Wind Loading

One of the pioneer researchers, Baines W. D. [6] mentions the effects of velocity distribution on wind loads and flow patterns around buildings in his paper. He measured pressure distributions on models of walls and rectangular block structures in a wind tunnel and also included tall buildings with square sections in his study. The tests were conducted both in an artificially produced velocity gradient used to simulate natural conditions and in a constant velocity field for comparison with standard procedures. He has also demonstrated that the steady pressures developed in a boundary layer are highly dependent on the mean velocity profile.

Barriga, A. R. *et al* [7] studied the effects of angle of attack, turbulence intensity and scale on the pressure distribution of a single square cylinder placed in a turbulent cross flow. They found that when the square cylinder was positioned in a cross flow with one face normal to the flow direction, only drag force was produced, but in the same flow a negative lift force was developed at small positive angle of attack, the magnitude of which was depended on the turbulence characteristics of the cross flow. It was suggested that the negative lateral forces on the square cylinder oriented at a small positive angle of attack was due to the relatively large negative pressure co-efficient in the separated zone on the windward side wall. It was also

concluded that the effect of turbulence intensity was to decrease the pressure near the front corner of the windward side wall and promote flow reattachment near the rear, giving rise to a very significant increase in aerodynamic moment.

Bearman, P. W. and Truman, D.M., [8] presented how the flow around two circular cylinders, displaced in a plane normal to the free stream, interacts as the two bodies are brought close together in their paper. Surface pressure measurements at a Reynolds number of 25000 based on the diameter of a single cylinder (d), showed the presence of a mean repulsive force between the cylinders. At gaps between 0.1d and 1d a marked asymmetry in the flow was observed with the two cylinders experiencing different drags and base pressures. The base pressure was found to change from one steady value to another or simply fluctuated between the two extremes. It was also showed how mutual interference influenced the formation of vortex streets from the two cylinders.

In an experimental investigation of wind load performed by Biswas, N. [9] on tall buildings with square cross section having five different dimensional rounded facets in a uniform flow to study its relation to drag coefficient. The study was conducted in an open circuit wind tunnel at a Reynolds number of 54000, included both on a single cylinder and a group of two cylinders with a variation in their interspacing. Remarkable effect was found on the drag coefficient in relation to the rounded facet.

Bostock, B. R. and Mair, W. A. [10] studied the forces and pressure distributions on rectangular and D-shaped cylinders placed in two-dimensional flow with a Reynolds number of 190000. A maximum drag coefficient was obtained when the height (normal to the stream) of the section was about 1.5 times the width was found for rectangular cylinders and only for a height diameter ratio less than 0.35 did the reattachments on the sides of the cylinders occur.

In their paper, Castro, J.P. and Fackwell, J.E. [3] described the flow around surface mounted cubes in uniform, irrigation and sheared turbulent flows. The shear flow simulated atmospheric boundary layer with a height ten times that of the body dimensions. They presented measurements of body surface pressure, mean and fluctuating velocities within the wake region. These measurements reflected the effects of upstream turbulence and shear on the wake flow. It was found that in the reversed flow region directly behind the body the addition of upstream turbulence and shear considerably reduced the size of cavity zone. The separating shear layers reattached to the body surface unlike the case of uniform flow. Measurements for

a variety of cube size boundary layer height ratio further revealed that reattachments occurred even for cube heights larger than the boundary layer height. They found that in the case of uniform flow approaching the cube at 45 degrees, the near wake and pressure fields were dominated by strong vortex shed from the top edge of the body.

In an experimental investigation of static pressure distributions on a group of rectangular cylinders in a uniform cross flow conducted by Islam, A. T. M. and Mandal, A. C. [11], the effects of longitudinal spacing and side dimension of the rectangular cylinders were determined. Finally, from the measured surface static pressure data, the lift and drag coefficients were calculated.

Farok, G. M. G. [12] carried out an experimental investigation of wind effect on rectangular cylinders with rounded corner where both single cylinder and group of cylinders were considered with varying inter-spacing in that study. It was observed that with the rounded corners the drag on the cylinders reduces remarkably in comparison to that on the sharp-edged cylinders.

Davis, R. W. and Moore, E. F. [13] conducted a numerical study of vortex, shedding from rectangular cylinders. They attempted to present numerical solutions for two-dimensional time dependent flow about rectangles in infinite domains and investigated the initiations and subsequent development of the vortex shedding phenomena for Reynolds number varying from 100 to 2800. The investigation yielded that the properties of these vortices were strongly dependent and lift, drag and Strouhal number were influences by the Reynolds number.

Lee, B. E. [14] conducted the study of the effect of turbulence on the surface pressure field of a square prism and measurements of the mean and fluctuating pressures on a square cylinder placed in a two-dimensional uniform and turbulent flow. It was observed that the addition of turbulence to the flow raised the base pressure and reduced the drag of the cylinder. This phenomenon was attributable to the manner in which the increased turbulence intensity thickened the shear layers, which caused them to be deflected by the downstream corners of the body and resulted in the downstream movement of the vortex formation region. The strength of the vortex shedding was shown to be reduced as the intensity of the incident turbulence was increased. Measurements of drag at various angles of attack ($0° \sim 45°$) showed that with increase in turbulence level the minimum drag occurred at smaller values of angle of attack.

Mandal, A. C. and Farok, G. M. G. [15] presented a paper on static pressure distributions on the cylinder with either square or rectangular cross-section having rounded corners. The experiment was performed for different corner radii and side dimensions of the cylinders at zero angle of attack. The wind load decreased appreciably for the cylinder with rounded corner compared to that with sharp corner. The experimental results reveal that the corner radius of the cylinder has significant effect while the side dimension has small effect on the drag coefficient.

Hussain, H. S. and Islam, O. [16] conducted experiment in a small wind tunnel and measured coefficient of pressure and coefficient of lift on circular, parabolic and elliptic shell roof in a uniform velocity. The results are estimated to be higher than that in reality as the experiment was carried out in a uniform velocity.

In an experimental investigation by Hossain, M.K.M. *et al* [17] of wind effect on staggered square and rectangular cylinders with variable longitudinal spacing, it was found that there is significant effect of inter-spacing on the wind load of cylinders.

In an experimental investigation by Islam, A. M. T. and Mandal, A. C. [18] of surface static pressure distributions on rectangular cylinders for a uniform cross-flow where the surface static pressure distribution was measured and the drag and lift coefficients were obtained. For all side ratios of the rectangular cylinders it was observed that the minimum drag occurred within 8^0 ~ 12^0 angle of attack.

In another study by Islam, A. M. T. and Mandal, A. C. [19] on surface static pressure distributions on a group of rectangular cylinders for a uniform cross flow considering the effect of side ratios and longitudinal spacing on pressure distribution. From the measured surface pressure distribution, drag and lift coefficients were obtained and it was observed that with the increase of the side ratio the drag coefficients increased in general.

In an experiment by Koeing, K. and Roshiko, A. [20], the shielding effects of various disks placed co-axially upstream of an axisymmetric flat faced cylinder were studied for different combinations of the diameter and gap ratios. For certain combinations of the diameter and gap ratios a considerable decrease in the drag was observed in such a system. Further they showed by the flow visualization technique that for such optimum shielding the upstream surface, which separated from the disk reattached smoothly onto the front edge on the downstream cylinder.

Leutheusser, J. [21] made wind tunnel tests on four typical building scale models each with different height and cross-section. For both as free standing and as a member of a group of buildings, static wind loading was found. The study yielded that the wind loading was less severe as a part of a group than when it was free standing.

Mandal, A. C. and Islam, O. [22] performed an experimental investigation of wind effect on staggered square cylinders with variable transverse and longitudinal spacing. They measured the surface static pressure distributions of each of the cylinders and then they calculated the drag and total force coefficients from the static pressure. It was observed that the net wind load on the individual cylinder of the group decreased in general; however, in some cases, high local pressure coefficient was found.

An experimental and theoretical investigation was conducted by Matsumoto, M. [23] on the aerodynamic forces acting on an oscillating square prism in a steady flow. First, a few experiments were performed to examine the aerodynamic forces in the direction of the wind stream and in a plane normal to it, acting on an oscillating square prism. Karman's theory about a thin plate was extended to the case of a square prism and the aerodynamic forces in a plane of the direction of the wind stream were obtained. A satisfactory correlation was found between the theoretical and experimental results.

Nakamura, Y. and Matskawa, T. [24] did an experimental investigation on the vortex excitation of rectangular cylinders with the long side normal to the flow in a mode of lateral translation using free and oscillation methods.

In another experiment, Nakamura, Y. and Ohya, Y. [25] studied the effects of turbulences on the mean flow past square rods. With the square face normal to the flow of square rods with different lengths, measurements were made to investigate the effects of turbulence intensity and scale on the mean flow characteristics. The length to size ratio of the rods ranged from 0.1 to 2.0 with turbulence intensity variating from 3.5% to 13%. It was found out that there were two main effects of turbulence on the mean flow past a three-dimensional sharp edged bluff body. Small-scale turbulence increased the growth rate of the shear layer, while the large-scale turbulence enhanced the roll up of the shear layer. For a square plate, both small and large-scale turbulence reduced the size of the base cavity. As the length of the square rod was increased beyond the critical (0.6 times the heights), the shear-layer-edge direct interaction

controlled the near wake eventually leading to flow reattachment. The effect of small scale turbulence was to promote the shear layer direct interaction.

Nakamura, Y. and Yujiohya [26] carried out experiments to study vortex shedding from square prisms placed in smooth and turbulent approaching flows. The velocity and pressure for the flow past prism of variable length with square section was measured and a flow visualization was made. The Square prisms were found to shed vortices in one of the two-fixed wake planes, which were parallel with the plate sides. The plane of shedding was switched irregularly from one to the other.

Roberson, J. A. *et al* [27] conducted experiments on circular cylinders, spool shaped bodies, cup-shaped bodies, square rods and rectangular rods to observe the effect of turbulence on the drag of these bodies. For square rods with their axes parallel to the flow direction it was found the C_d decreased approximately 25% when the turbulence intensity increased from 1% to 10%. A square cross-sectional rod and another rectangular rods with a length (in the free stream direction) to breadth ratio of two were used. The drag was measured with the axes of the rectangular rods oriented normal to the free stream direction. It was noted that on the sides of the square rod the pressure change with a change in turbulent intensity was about the same as for the face; while for the rectangular rod, the change in pressure on the sides was large, and it was small on the rear face. The conclusion was that the bodies, which have shapes such that reattachment of the flow is not a factor, experience an increase in C_d with the increased turbulence intensity. On the other hand, bodies for which reattachment or near reattachment of flow occur with increased turbulence may experience either a decrease or increase in C_d with increased turbulence intensity depending upon the shape of the body.

Roberson, J. A. *et al* [28] placed rectangular rods in a cross flow with the rods oriented at small angle of attack with respect to the direction to measure pressure distribution on them. The turbulence intensity of the cross flow ranged between 1% and 10% and Reynolds number was 40000 based on the minimum dimension of the rod. It was found that the free stream turbulence had a significant effect on the pressure distribution about bodies of rectangular cross-section. With small angle of attack these bodies had a significantly lower pressure on their windward side wall than did the same bodies with zero angle of attack. Tests were conducted by placing bodies of square cross-section on the floor of the wind tunnel for simulating nearly the same configuration of the buildings to study the pressure distributions. It was found that decreasing

relative height of the body had a diminishing effect on the negative pressure on the windward side wall and also critical angle of attack was increased.

Sakamoto, H. and Arie, M. [29] collected experimental data on the vortex shedding frequency behind a vertical rectangular prism and a vertical circular cylinder attached to a plane wall and immersed in a turbulent boundary layer. Their objective was to investigate the effects of the aspect ratio (height/width) of these bodies and the boundary layer characteristics on the vortex shedding frequency. The whole experiment was conducted at a turbulence level of 0.2% and free stream velocity of 20 m/s. The aspect ratio was varied from 0.5 to 0.8. The investigation revealed that arch-type vortex and the Karman-type vortex were formed behind the body, depending on the aspect ratio. At aspect ratios less than 2.0 for rectangular and 2.5 for circular cylinders, the arch-type vortex appeared. The Karman type vortex formed for the aspect ratio greater than the values above.

Vickery, B. J. [30] described in his paper the results of the measurements of fluctuating lift and drag on a long square cylinder. He attempted to establish a correlation of lift along the cylinder and the distribution of fluctuating pressure on the cross-section. The magnitude of the fluctuating lift was found to be considerably greater than that for a circular cross-section and the span wise correlation much stronger. At small angle of attack (less than 10°) turbulence caused a reduction in base suction and a decrease in fluctuating lift of about 50%. It was also reported that the presence of large-scale turbulence in the stream had a remarkable influence on both the steady and the fluctuating forces.

Besides these, many authors have performed study on flow patterns, wind loads and their effects on buildings and structures, which have been mentioned in the references. Other than the ones mentioned above, many other studies have also been done by researchers around the globe, but probably the combination of pentagonal, hexagonal and octagonal cylinders in staggered arrangement have not been deliberated. Therefore, this study would definitely add to the novel idea in regard to the wind loading on lofty structures.

CHAPTER-3
EXPERIMENTAL SETUP AND METHODOLOGY

Experiment has been carried out to find the wind load on a group of pentagonal, hexagonal and octagonal cylinders placed at the exit end of an open circuit subsonic wind tunnel. The orientation of the cylinders- one pentagonal and one hexagonal cylinder was placed at the upstream and the octagonal cylinder was at the downstream side in a uniform crossflow. An inclined multi-manometer was utilized to measure cylinder surface static pressures at different locations. This chapter systematically describes in brief about the construction of the setup including the cylinders, the wind tunnel and also the testing procedure of this research work.

3.1 Wind tunnel

The experiment was performed in an open circuit subsonic wind tunnel as shown in figure 3.1. It was a low speed wind tunnel with a maximum wind of velocity of 14.3 m/s in the test section. The successive sections of the wind tunnel comprise of a bell mouth entry, a flow straightener, a diverging section, two axial flow fans, a flow controller valve, a silencer etc. It is 5.93 meters long with a test section of 460 mm by 460 mm cross-section. A honeycomb is fixed near the end of the wind tunnel to obtain a uniform flow. The bell mouth shaped entry is convergent. Two axial flow fans are used to generate wind velocity. To power each of the fans, a motor of 2.25 kilowatt and 2900 rpm is connected. A butterfly valve is installed to control the wind speed. Immediately after the butterfly valve is a silencer as shown in the figures.

The central longitudinal axis of the wind tunnel is maintained at 990 mm a constant height from the floor. In order to ensure smooth entry of air into the tunnel and to maintain uniform flow into the duct free from outside disturbances, the converging mouth entry is incorporated in the wind tunnel. A two-stage rotating axial flow fan of 1475 rpm and 18.16 m^3/s capacity at the head of 152.4 mm of water, yields induced flow through the wind tunnel.

Just behind the axial flow fan, a butterfly valve is placed to control the airflow by means of screw thread mechanism. A silencer is fitted at the end of the flow controlling section for noise reduction of the system. This section is fitted with a honeycomb. The 1550 mm long diverging and converging section of the wind tunnel is made out of 16 SWG black sheets. To minimize expansion and contraction loss and also to reduce the possibility of flow separation, a 7° angle of divergence and convergence is made.

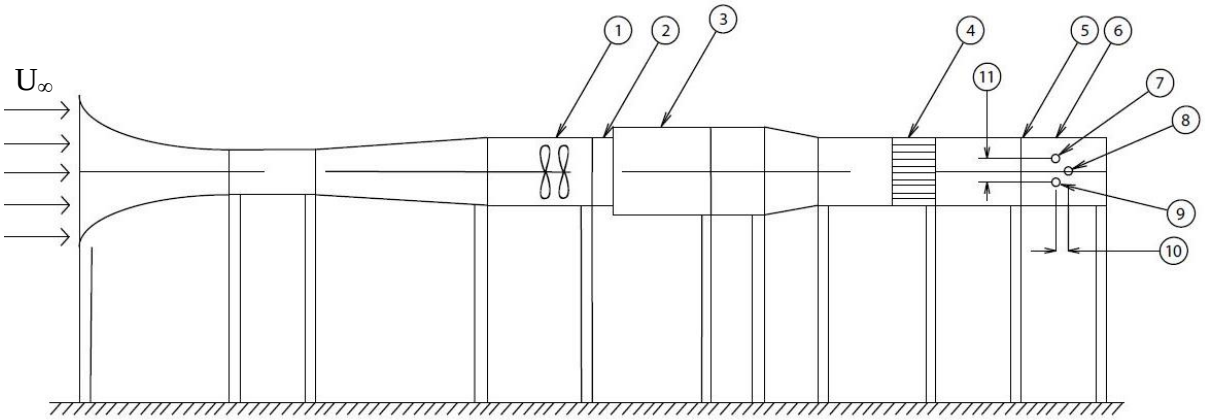

1. Fan Section
2. Valve Section
3. Silencer
4. Honey Comb
5. Exit End
6. Test Section
7. Pentagonal Cylinder
8. Octagonal Cylinder
9. Hexagonal Cylinder
10. Longitudinal Spacing, L_1
11. Transverse Spacing, L_2

Figure 3. 1: Schematic Diagram of Wind Tunnel

A digital anemometer is used for wind velocity measurement for the experimental investigation. Approximately 14.3 m/s flow velocity (U_∞) has be maintained in the test section. The measured velocity distribution was almost uniform across the tunnel test section in the upstream side of the test models. The pattern of the flow velocity in the non-dimensional form is shown in figure 3.2.

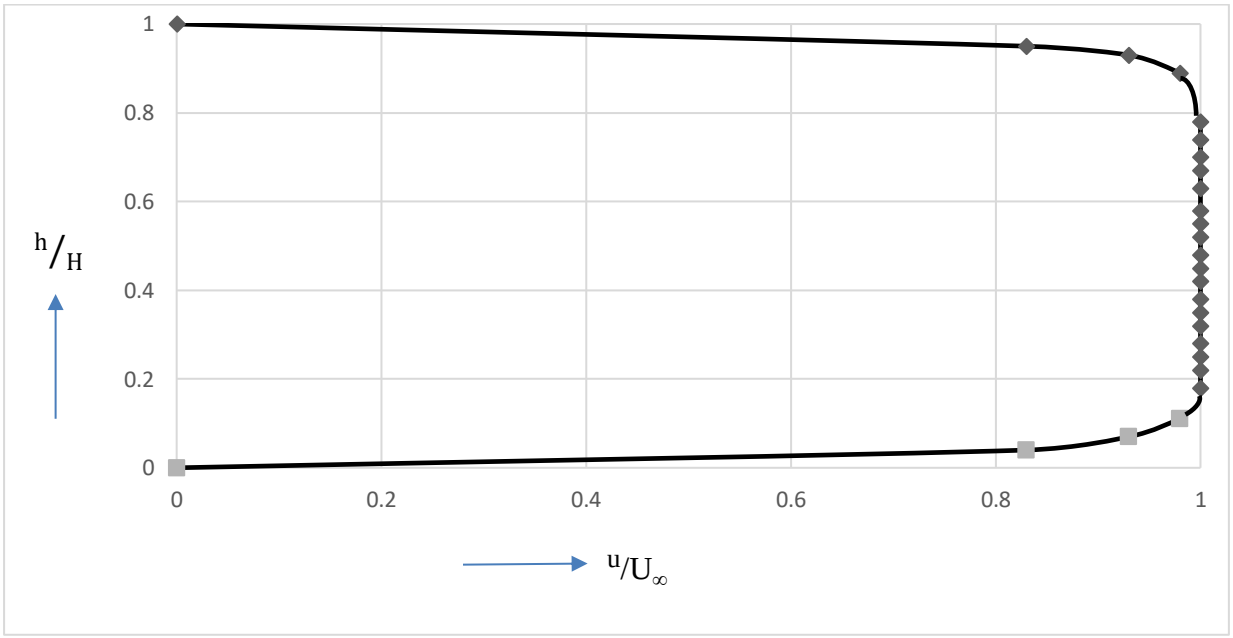

Figure 3. 2: Velocity Distribution at Upstream Side of Model

3.2 Test Section

The test was conducted in the open air at the exit end of the wind tunnel as shown in figure 3.1. A 400 mm long steel frame was fabricated for fixing the cylinder models. The top portion of the frame was at the same level of the wind tunnel at the exit end. There were no cover plates at the top or at the bottom of the extended test section. The two side walls were attached to the steel frame at the sides with the help of nut and bolt. The 460 mm distance of the side walls of the wind tunnel exit end was maintained between the extended side walls of the test section.

The sidewalls of the test section were made out of plywood. The cylinder models were fixed with the extended sidewalls. One end of the models was supported in the groove of the sidewall of the extended portion. Through this end of the cylinder, the plastic tubes were taken out for connection with the inclined multi-manometer. The manometer liquid was water. The tapping points on the sides of the pentagonal, hexagonal and octagonal model cylinders were copper made capillary tubes. These copper tubes were connected with the plastic tubes. In other side, the model cylinder was fastened with the side wall using nut and bolt. The bolt was fixed with one end of the cylinder. All three-cylinder models were correctly leveled and then carefully fixed, keeping top side of the cylinders parallel to the free stream flow direction. A standard spirit level was used for leveling of the test cylinders.

A provision for rotation at various angles of the test cylinder was kept for attaining wind load at different angles of attack. Since the top and bottom of the extended part of the wind tunnel was open; as such no correction for blockage was done in the analysis. The test cylinders were placed very close to the end of the wind tunnel so that the approach velocity on the test cylinders was approximately identical as that in the exit end of the wind tunnel.

Table 1: Experimental Conditions and Data

Room temperature = 288 K	Reynolds No, $Re = 1.95 \times 10^5$
Air speed, U_∞ = 14.3 m/s	Viscosity of air = 1.7894×10^{-5} kg/ms
Density of air = 1.225 kg/m^3	Cylinder hydraulic diameter, D = 50 mm
Spacing, L_1 = 200 mm	Spacing, L_2 = 250 mm

3.3 Construction of the Cylinders

One pentagonal, one hexagonal and one octagonal cylinder of same hydraulic diameter (Table 1) were constructed as test models. The cylinders were made of seasoned teak wood so that there would be no expansion due to the change of temperature and humidity and also to avoid bucking. Each face of the cylinder had five tapping points. Figures 3.3 and 3.4 show the tapping positions on the cross-section and on the longitudinal section of the cylinder respectively. The location of the corner tapping was at a distance of $\frac{1}{2}(\Delta d)$ whereas the distance between the consecutive tapping points was equal (Δd) in all cylinders as shown in the figure.

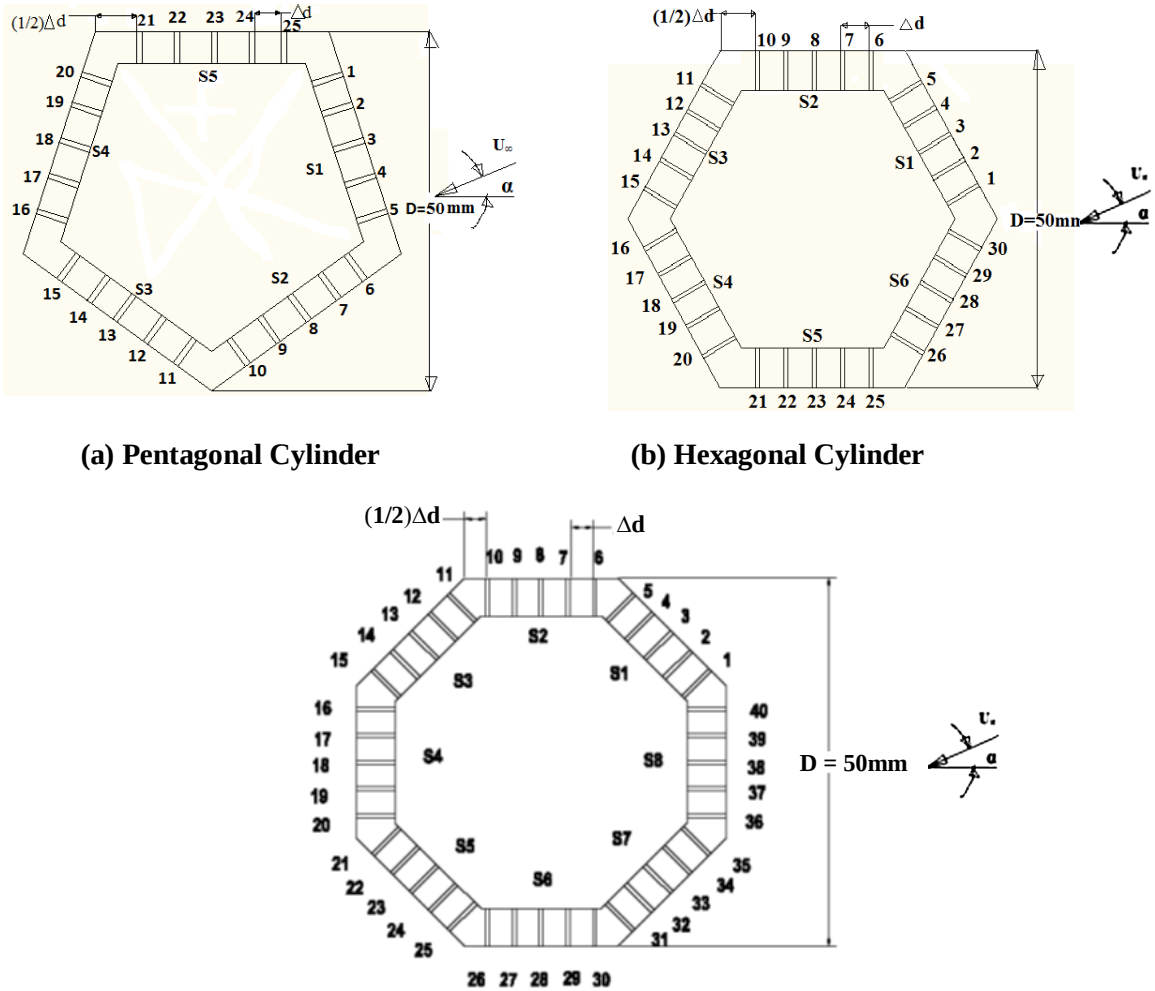

(a) Pentagonal Cylinder **(b) Hexagonal Cylinder**

(c) Octagonal Cylinder

Figure 3. 3: Tapping Positions Shown on Cross-Section of (a) Pentagonal, (b) Hexagonal and (c) Octagonal Cylinders

Each tapping was identified by a numerical number from 1 to 25 for pentagonal cylinder, from 1 to 30 for hexagonal cylinder and 1 to 40 for octagonal cylinder. From the longitudinal section view it is observed that the tapping points were not made along the cross-section of the cylinder but located within some span of the cylinder (figure 3.4) in order to avoid manufacturing problem. This would not have any effect on the experimental result due to the two-dimensional flow consideration.

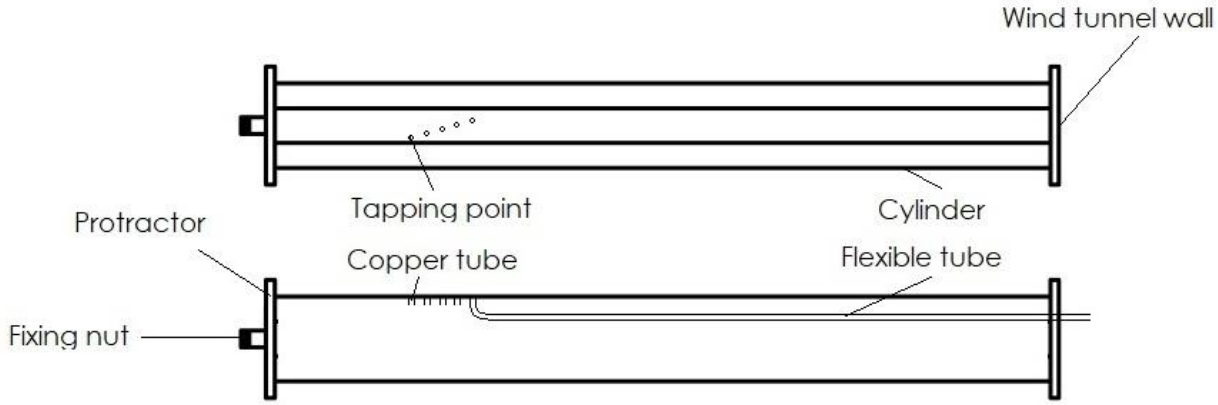

Figure 3. 4: Tapping Positions Shown on Longitudinal Section of Cylinder

The cylinder had a steel plate attached to one side to facilitate the nut and bolt fixing and other side of the cylinder was hollow through which the plastic tubes were allowed to pass via the side wall of the extended tunnel as shown in figure 3.4. The flexible plastic tubes had a 1.70mm inner diameter and were press-fitted with the copper capillary tubes at one side. At the other side the tubes were connected with the inclined multi-manometer. The tapings were made of copper tubes of 1.71mm outside diameter and approximately 10mm in length.

3.4 Cylinder Arrangement

For the experiment, a pentagonal and a hexagonal cylinder was positioned in the upstream side and another octagonal cylinder was placed centrally, in the downstream side along the uniform cross flow. The position of the group of cylinders at zero angle of attack in the wind tunnel test section is shown in figure 3.5.

The inter-spacing between upstream (pentagonal and hexagonal) and downstream (octagonal) cylinders were taken as $L_1 = 4D$ and between the two cylinders in upstream was taken as $L_2 = 5D$ (Table 1). Then static surface pressure distributions were measured on the five faces of the

pentagonal cylinder, six faces of the hexagonal cylinder and on the eight faces of the octagonal cylinder. Measurements were taken sequentially at 0˚, 30˚, 45˚ and 60˚ angles of attack at constant inter-spacing as stated above.

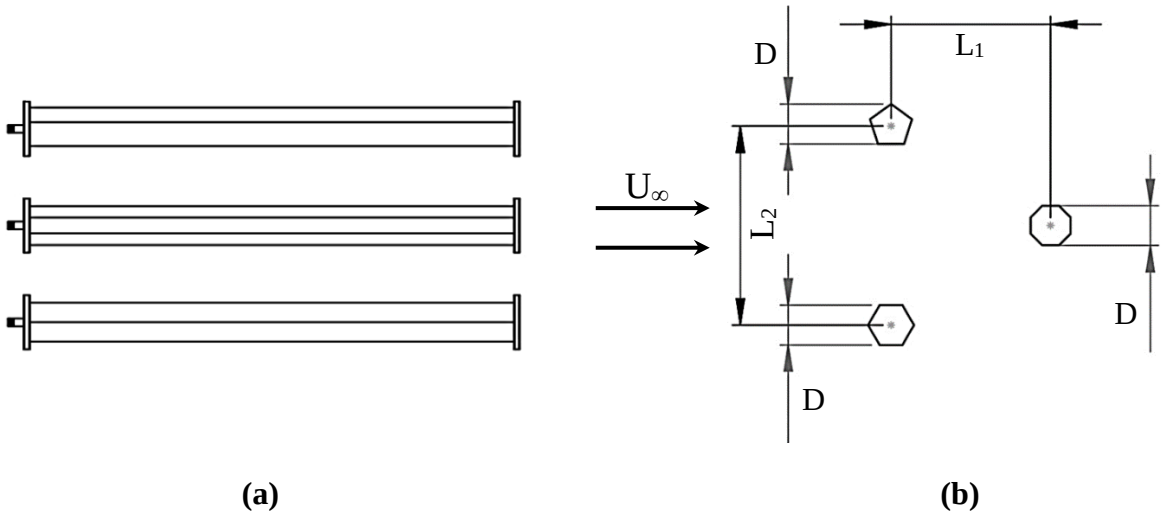

(a) **(b)**

Figure 3. 5: Schematic Representation of Experimental Setup Showing (a) Side View of Cylinders in Tunnel Test Section and (b) Position of the Group of Cylinders in Staggered Form

3.5 Measuring Equipment

A Digital anemometer was used for wind velocity measurement across the test section of the wind tunnel. Additionally, a pitot tube was used for vetting the measured velocity. The surface static pressures were measured with the help of inclined manometer. The pitot tube was connected to the inclined manometer. The inclination of the manometer was sufficient to record the pressure with reasonable accuracy. Manometer reading was done cautiously, so that no air bubble was deposited anywhere in the limb. The mean value was recorded in case of slight fluctuation in the manometer reading.

3.6 Methodology

a. At different angles of attack (α = 0˚, 30˚, 45˚ & 60˚), static pressures are measured from all the surfaces of the three-cylinder models through pressure tapings using a multi-manometer.

b. From the static pressure data:

1) Coefficient of pressure (C_p) is calculated

2) C_L and C_D at every AOA are determined for each cylinder.

c. Simulation is carried out keeping all conditions same with the experimental investigation.

d. Finally, the experimental and simulation data of C_p, C_L and C_D are analyzed and compared for the group of cylinders.

CHAPTER-4
MATHEMATICAL MODEL AND SIMULATION

The calculation procedure of finding pressure coefficients, drag and lift coefficients has been described in a nutshell in this chapter. From the measured surface static pressure on the pentagonal, hexagonal and octagonal cylinders the pressure coefficients are obtained. Then the drag and lift coefficients are found from the pressure coefficients. Drag and lift coefficients are determined numerically.

4.1 Determination of pressure coefficient

The pressure coefficient is defined as

$$C_p = \frac{\Delta P}{\frac{1}{2}\rho U_\infty^2} \tag{4.1}$$

Here, $\Delta P = P - P_0$,

Where, P = Static pressure on the surface of the cylinder,

P_0 = Ambient pressure,

ρ = Density of air,

U_∞ = Free stream velocity.

ΔP is obtained from,

$$\Delta P = \Delta h_w \times \gamma_w \tag{4.2}$$

Where, Δh_w is the manometer reading and γ_w is the specific weight of manometer liquid, which is water.

Figure 4.1 shows the section of the model pentagonal, hexagonal and octagonal cylinders with the pressure tapping points, at each of them the static pressure was recorded with the help of inclined multi-manometer. The cylinder was rotated at various angles of 0^0, 30^0, 45^0 and 60^0 for all the cylinders and at each angle surface static pressures were recorded.

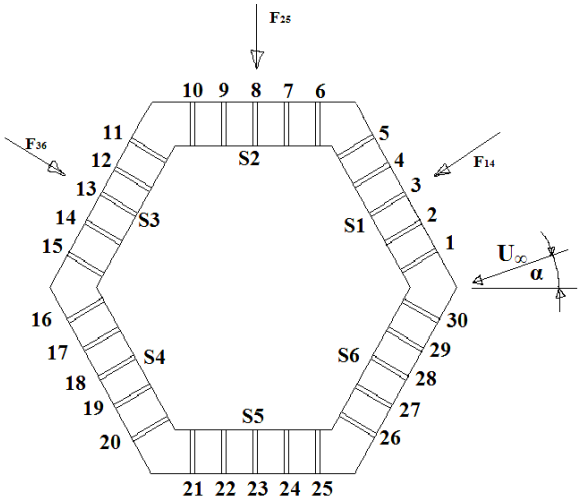

(a) Hexagonal Cylinder

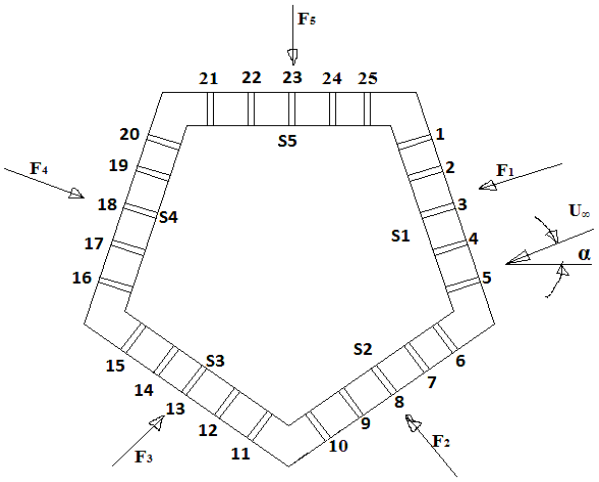

(b)Pentagonal Cylinder

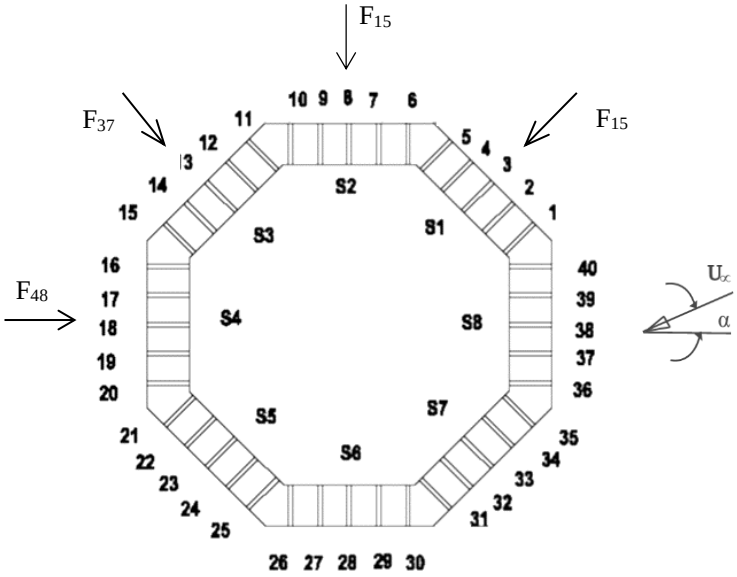

(c) Octagonal Cylinder

Figure 4. 1: Cross-section of (a) Hexagonal, (b) Pentagonal and (c) Octagonal Cylinders Showing Net forces acting on all surfaces

4.2 Determination of Drag and Lift Coefficients

Drag and lift coefficients for different types of cylinder are calculated here.

4.2.1 Pentagonal Cylinder

As shown in figure 4.1 that the cylinder has five faces S_1, S_2, S_3, S_4 and S_5. The pressure at the various tapping points along the face S_1 can be written as,

P_1 = Pressureat tapping point 1

P_2 = Pressure at tapping point 2

P_3 = Pressure at tapping point 3

P_4 = Pressure at tapping point 4

P_5 = Pressure at tapping point 5

If F_1 indicates the force along the faces S_1, then using Simpson's rule, one can find

$$F_1 = \frac{\Delta A}{3}[P_1 + 4P_2 + 2P_3 + 4P_4 + P_5]$$

If the length of the cylinder is chosen as unity, then the above expression becomes

$$F_1 = \frac{\Delta d \times 1}{3}[P_1 + 4P_2 + 2P_3 + 4P_4 + P_5]$$

$$= \frac{\Delta d}{3}[(P_1 - P_0) + 4(P_2 - P_0) + 2(P_3 - P_0) + 4(P_4 - P_0) + (P_5 - P_0) + 12P_0] \quad (4.3)$$

If the component of the force F_{d_1} occurs along the flow direction, then one can find the expression of F as F_{d_1}

$$F_{d_1} = F_1 \cos(18^0 - \alpha) \quad (4.4a)$$

Similarly the force component F_{L_1} in a direction perpendicular to the flow may be written as

$$F_{L_1} = -F_1 \sin(18^0 - \alpha) \quad (4.4b)$$

The net force F_2 along the face S_2 can be obtained in the same way as above and that is

$$F_2 = \frac{\Delta d}{3}[(P_6 - P_0) + 4(P_7 - P_0) + 2(P_8 - P_0) + 4(P_9 - P_0) + (P_{10} - P_0) + 12P_0] \quad (4.5)$$

Therefore, the components of the drag and lift forces along the face S_2 are respectively

$$F_{d_2} = -F_2 \cos(126^0 - \alpha) \tag{4.6a}$$

$$F_{L_2} = F_2 \sin(126^0 - \alpha) \tag{4.6b}$$

The net force F_3 along the face S_3 can be obtained in the same way as above and that is

$$F_3 = \frac{\Delta d}{3}[(P_{11} - P_0) + 4(P_{12} - P_0) + 2(P_{13} - P_0) + 4(P_{14} - P_0) + (P_{15} - P_0) + 12\,P_0 \tag{4.7}$$

Therefore the components of the drag and lift forces along the face S_3arerespectively

$$F_{d_3} = -F_3 \cos(54^0 - \alpha) \tag{4.8}$$

$$F_{L_3} = F_3 \sin(54^0 - \alpha) \tag{4.9}$$

The net force F_4 along the face S_4 can be obtained in the same way as above and that is

$$F_4 = \frac{\Delta d}{3}[(P_{16} - P_0) + 4(P_{17} - P_0) + 2(P_{18} - P_0) + 4(P_{19} - P_0) + (P_{20} - P_0) + 12P_0] \tag{4.10}$$

Therefore, the components of the drag and lift forces along the face S_4 are respectively

$$F_{d_4} = F_4 \cos(162^0 - \alpha) \tag{4.11}$$

$$F_{L_4} = -F_4 \sin(162^0 - \alpha) \tag{4.12}$$

The net force F_5 along the face S_5 can be obtained in the same way as above and that is

$$F_5 = \frac{\Delta d}{3}[(P_{21} - P_0) + 4(P_{22} - P_0) + 2(P_{23} - P_0) + 4(P_{24} - P_0) + (P_{25} - P_0) + 12P_0] \tag{4.13}$$

Therefore, the components of the drag and lift forces along the face S_5 are respectively

$$F_{d_5} = F_5 \cos(90^0 - \alpha) \tag{4.14}$$

$$F_{L_5} = -F_5 \sin(90^0 - \alpha) \tag{4.15}$$

Drag and lift coefficients are defined as follows

$$C_D = \frac{F_d}{\frac{1}{2}\rho A U_\infty^2} \tag{4.16}$$

$$C_L = \frac{F_L}{\frac{1}{2}\rho A U_\infty^2} \tag{4.17}$$

where, A is the frontal area of the cylinder.

The total drag force along the flow direction is

$$F_d = F_{d_1} + F_{d_2} + F_{d_3} + F_{d_4} + F_{d_5} \quad (4.18)$$

and total lift force in a direction perpendicular to flow is

$$F_L = F_{L_1} + F_{L_2} + F_{L_3} + F_{L_4} + F_{L_5} \quad (4.19)$$

Now from equations (4.16) and (4.18), the expression of drag coefficient becomes

$$C_D = \frac{F_{d_1} + F_{d_2} + F_{d_3} + F_{d_4} + F_{d_5}}{\frac{1}{2}\rho A U_\infty^2}$$

Substituting the values of F_{d_1}, F_{d_2}, F_{d_3}, F_{d_4} and F_{d_5} from equations (4.4a), (4.6a), (4.8), (4.11) and (4.14) respectively, the expression of drag coefficient becomes,

$$C_D = \frac{F_1 \cos(18^0-\alpha) - F_2 \cos(126^0-\alpha) - F_3 \cos(54^0-\alpha) + F_4 \cos(162^0-\alpha) + F_5 \cos(90^0-\alpha)}{\frac{1}{2}\rho A U_\infty^2}$$

$$\text{or, } C_D = \frac{\cos(18^0-\alpha)}{A} \cdot \frac{F_1}{\frac{1}{2}\rho U_\infty^2} - \frac{\cos(126^0-\alpha)}{A} \cdot \frac{F_2}{\frac{1}{2}\rho U_\infty^2} - \frac{\cos(54^0-\alpha)}{A} \cdot \frac{F_3}{\frac{1}{2}\rho U_\infty^2} + \frac{\cos(162^0-\alpha)}{A} \cdot \frac{F_4}{\frac{1}{2}\rho U_\infty^2} + \frac{\cos(90^0-\alpha)}{A} \cdot \frac{F_5}{\frac{1}{2}\rho U_\infty^2} \quad \ldots (4.20)$$

Now inserting the values of F_1, F_2, F_3, F_4 and F_5 from equations (4.3), (4.5), (4.7), (4.10) and (4.13) respectively,

$$C_D = \frac{\cos(18^0-\alpha)\times\Delta d}{3A} \cdot \frac{1}{\frac{1}{2}\rho U_\infty^2} \cdot [(P_1 - P_0) + 4(P_2 - P_0) + 2(P_3 - P_0) + 4(P_4 - P_0) + (P_5 - P_0) + 12P_0] - \frac{\cos(126^0-\alpha)\times\Delta d}{3A} \cdot \frac{1}{\frac{1}{2}\rho U_\infty^2} \cdot [(P_6 - P_0) + 4(P_7 - P_0) + 2(P_8 - P_0) + 4(P_9 - P_0) + (P_{10} - P_0) + 12P_0] - \frac{\cos(54^0-\alpha)\times\Delta d}{3A} \cdot \frac{1}{\frac{1}{2}\rho U_\infty^2} \cdot [(P_{11} - P_0) + 4(P_{12} - P_0) + 2(P_{13} - P_0) + 4(P_{14} - P_0) + (P_{15} - P_0) + 12P_0] + \frac{\cos(162^0-\alpha)\times\Delta d}{3A} \cdot \frac{1}{\frac{1}{2}\rho U_\infty^2} \cdot [(P_{16} - P_0) + 4(P_{17} - P_0) + 2(P_{18} - P_0) + 4(P_{19} - P_0) + (P_{20} - P_0) + 12P_0] + \frac{\cos(90^0-\alpha)\times\Delta d}{3A} \cdot \frac{1}{\frac{1}{2}\rho U_\infty^2} \cdot [(P_{21} - P_0) + 4(P_{22} - P_0) + 2(P_{23} - P_0) + 4(P_{24} - P_0) + (P_{25} - P_0) + 12P_0]$$

Now writing in terms of pressure coefficients and using 12 $P_0 = 0$ [P_0 is the ambient gauge pressure = 0] the above equation is transformed into,

$$C_D = \frac{cos(18^0-\alpha)\times\Delta d}{3A}\cdot[C_{p_1} + 4C_{p_2} + 2C_{p_3} + 4C_{p_4} + C_{p_5}] - \frac{cos(126^0-\alpha)\times\Delta d}{3A}\cdot[C_{p_6} + 4C_{p_7} + 2C_{p_8} + 4C_{P_9} + C_{p_{10}}] - \frac{cos(54^0-\alpha)\times\Delta d}{3A}\cdot[C_{p_{11}} + 4C_{p_{12}} + 2C_{p_{13}} + 4C_{p_{14}} + C_{p_{15}}] + \frac{cos(162^0-\alpha)\times\Delta d}{3A}\cdot[C_{p_{16}} + 4C_{p_{17}} + 2C_{p_{18}} + 4C_{p_{19}} + C_{p_{20}}] + \frac{cos(90^0-\alpha)\times\Delta d}{3A}\cdot[C_{p_{21}} + 4C_{p_{22}} + 2C_{p_{23}} + 4C_{p_{24}} + C_{p_{25}}] \quad (4.21)$$

Similarly, the expression of lift coefficient C_L can be obtained as,

$$C_L = -\frac{sin(18^0-\alpha)\times\Delta d}{3A}\cdot[C_{p_1} + 4C_{p_2} + 2C_{p_3} + 4C_{p_4} + C_{p_5}] + \frac{sin(126^0-\alpha)\times\Delta d}{3A}\cdot[C_{p_6} + 4C_{p_7} + 2C_{p_8} + 4C_{P_9} + C_{p_{10}}] + \frac{sin(54^0-\alpha)\times\Delta d}{3A}\cdot[C_{p_{11}} + 4C_{p_{12}} + 2C_{p_{13}} + 4C_{p_{14}} + C_{p_{15}}] - \frac{sin(162^0-\alpha)\times\Delta d}{3A}\cdot[C_{p_{16}} + 4C_{p_{17}} + 2C_{p_{18}} + 4C_{p_{19}} + C_{p_{20}}] - \frac{sin(90^0-\alpha)\times\Delta d}{3A}\cdot[C_{p_{21}} + 4C_{p_{22}} + 2C_{p_{23}} + 4C_{p_{24}} + C_{p_{25}}] \quad (4.22)$$

4.2.2 Hexagonal Cylinder

As shown in figure 4.1 that the cylinder has six faces S_1, S_2, S_3, S_4, S_5 and S_6. The pressure differences between the various tapping points on opposite faces e.g. along the face S_1 and S_4 can be obtained from-

$\Delta P_{1-20} = P_1 - P_{20}$ is the pressure difference between tapping points 1 and 20,

$\Delta P_{2-19} = P_2 - P_{19}$ is the pressure difference between tapping points 2 and 19,

$\Delta P_{3-18} = P_3 - P_{18}$ is the pressure difference between tapping points 3 and 18,

$\Delta P_{4-17} = P_4 - P_{17}$ is the pressure difference between tapping points 4 and 17 and

$\Delta P_{5-16} = P_5 - P_{16}$ is the pressure difference between tapping points 5 and 16.

If F_{14} indicates the net force along the faces S_1 and S_4, then using Simpson's rule, one can find

$$F_{14} = \frac{\Delta A}{3}[\Delta P_{1\text{-}20} + 4\Delta P_{2\text{-}19} + 2\Delta P_{3\text{-}18} + 4\Delta P_{4\text{-}17} + \Delta P_{5\text{-}16}] \quad (4.23)$$

If the length of the cylinder is chosen as unity, then the above expression becomes

$$F_{14} = \frac{\Delta d\ x\ 1}{3}[\Delta P_{1\text{-}20} + 4\Delta P_{2\text{-}19} + 2\Delta P_{3\text{-}18} + 4\Delta P_{4\text{-}17} + \Delta P_{5\text{-}16}]$$

$$= \frac{\Delta d}{3}[(P_1 - P_{20}) + 4(P_2 - P_{19}) + 2(P_3 - P_{18}) + 4(P_4 - P_{17}) + (P_5 - P_{16})]$$

$$= \frac{\Delta d}{3}[(P_1 - P_0) - (P_{20} - P_0) + 4(P_2 - P_0) - 4(P_{19} - P_0) + 2(P_3 - P_0) - 2(P_{18} - P_0)$$

$$+ 4(P_4 - P_0) - 4(P_{17} - P_0) + (P_5 - P_0) - (P_{16} - P_0)] \quad (4.24)$$

If the component of the force $F_{d_{14}}$ occurs along the flow direction, then one can find the expression of F as $F_{d_{14}}$

$$F_{d_{14}} = F_{14}\cos(30^0 - \alpha) \quad (4.25)$$

Similarly, the force component $F_{L_{14}}$ in a direction perpendicular to the flow may be written as

$$F_{L_{14}} = -F_{14}\sin(30^0 - \alpha) \quad (4.26)$$

The net force F_{25} along the faces S_2 and S_5 can be obtained in the same way as above and that is

$$F_{25} = \frac{\Delta d}{3}[(P_6 - P_0) - (P_{25} - P_0) + 4(P_7 - P_0) - 4(P_{24} - P_0) + 2(P_8 - P_0) - 2(P_{23} - P_0)$$

$$+4(P_9 - P_0) - 4(P_{22} - P_0) + (P_{10} - P_0) - (P_{21} - P_0)] \quad (4.27)$$

Therefore the components of the drag and lift forces along the faces S_2 and S_5 are respectively

$$F_{d_{25}} = F_{25}\cos(90^0 - \alpha) \quad (4.28)$$

$$F_{L_{25}} = -F_{25}\sin(90^0 - \alpha) \quad (4.29)$$

The net force F_{36} along the faces S_3 and S_6 can be obtained in the same way as above and that is,

$$F_{36} = \frac{\Delta d}{3}[(P_{11} - P_0) - (P_{30} - P_0) + 4(P_{12} - P_0) - 4(P_{29} - P_0) + 2(P_{13} - P_0) - 2(P_{28} - P_0)$$

$$+4(P_{14} - P_0) - 4(P_{27} - P_0) + (P_{15} - P_0) - (P_{26} - P_0)] \quad (4.30)$$

Therefore, the components of the drag and lift forces along the faces S_3 and $S_6$are respectively

$$F_{d_{36}} = F_{36}\cos(150^0 - \alpha) \quad (4.31)$$

$$F_{L_{36}} = -F_{36}\sin(150^0 - \alpha) \quad (4.32)$$

Drag and lift coefficients are defined as follows

$$C_D = \frac{F_d}{\frac{1}{2}\rho A U_\infty^2} \tag{4.33}$$

and $C_L = \frac{F_L}{\frac{1}{2}\rho A U_\infty^2}$ (4.34)

where, A is the frontal projected area of the cylinder.

The total drag force along the flow direction is

$$F_d = F_{d_{14}} + F_{d_{25}} + F_{d_{36}} \tag{4.35}$$

and total lift force in a direction perpendicular to flow is

$$F_L = F_{L_{14}} + F_{L_{25}} + F_{L_{36}} \tag{4.36}$$

Now from equations (4.33) and (4.35), the expression of drag coefficient becomes-

$$C_D = \frac{F_{d_{14}} + F_{d_{25}} + F_{d_{36}}}{\frac{1}{2}\rho A U_\infty^2}$$

Now substituting the values of $F_{d_{14}}$, $F_{d_{25}}$ and $F_{d_{36}}$ from equations (4.25), (4.28) and (4.31) respectively, the expression of drag coefficient becomes,

$$C_D = \frac{F_{14}\cos(30^0 - \alpha) + F_{25}\cos(90^0 - \alpha) + F_{36}\cos(150^0 - \alpha)}{\frac{1}{2}\rho A U_\infty^2}$$

$$= \frac{\cos(30^0 - \alpha)}{A} \cdot \frac{F_{14}}{\frac{1}{2}\rho U_\infty^2} + \frac{\cos(90^0 - \alpha)}{A} \cdot \frac{F_{25}}{\frac{1}{2}\rho U_\infty^2}$$

$$+ \frac{\cos(150^0 - \alpha)}{A} \frac{F_{36}}{\frac{1}{2}\rho U_\infty^2} \tag{4.37}$$

Now inserting the values of F_{14}, F_{25} and F_{36} from equations (4.24), (4.27) and (4.30) respectively, one finds

$$C_D = \frac{\cos(30^0 - \alpha) \times \Delta d}{3A} \cdot \frac{1}{\frac{1}{2}\rho U_\infty^2} \cdot [(P_1 - P_0) - (P_{20} - P_0) + 4(P_2 - P_0) - 4(P_{19} - P_0) + 2(P_3 - P_0) -$$

$$2(P_{18} - P_0) + 4(P_4 - P_0) - 4(P_{17} - P_0) + (P_5 - P_0) - (P_{16} - P_0)] + \frac{\cos(90^0 - \alpha) \times \Delta d}{3A} \cdot \frac{1}{\frac{1}{2}\rho U_\infty^2} \cdot [(P_6 -$$

$P_0) - (P_{25} - P_0) + 4(P_7 - P_0) - 4(P_{24} - P_0) + 2(P_8 - P_0) - 2(P_{23} - P_0) + 4(P_9 - P_0) - 4(P_{22} - P_0) + (P_{10} - P_0) - (P_{21} - P_0)] + \frac{cos(150^0-\alpha)\times\Delta d}{3A} \cdot \frac{1}{\frac{1}{2}\rho U_\infty^2} \cdot [(P_{11} - P_0) - (P_{30} - P_0) + 4(P_{12} - P_0) - 4(P_{29} - P_0) + 2(P_{13} - P_0) - 2(P_{28} - P_0) + 4(P_{14} - P_0) - 4(P_{27} - P_0) + (P_{15} - P_0) - (P_{26} - P_0)]$

Now writing in terms of pressure coefficients the above equation is transformed into-

$$C_D = \frac{cos(30^0-\alpha)\times\Delta d}{3A} \cdot [C_{p_1} - C_{p_{20}} + 4C_{p_2} - 4C_{p_{19}} + 2C_{p_3} - 2C_{p_{18}} + 4C_{p_4} - 4C_{p_{17}} + C_{p_5} - C_{p_{16}}] + \frac{cos(90^0-\alpha)\times\Delta d}{3A} \cdot [C_{p_6} - C_{p_{25}} + 4C_{p_7} - 4C_{p_{24}} + 2C_{p_8} - 2C_{p_{23}} + 4C_{P_9} - 4C_{p_{22}} + C_{p_{10}} - C_{p_{26}}] + \frac{cos(135^0-\alpha)\times\Delta d}{3A} \cdot [C_{p_{11}} - C_{p_{30}} + 4C_{p_{12}} - 4C_{p_{29}} + 2C_{p_{13}} - 2C_{p_{28}} + 4C_{p_{14}} - 4C_{p_{27}} + C_{p_{15}} - C_{p_{26}}]$$

Rearranging the expression of C_D becomes of the following form-

$$C_D = \frac{cos(30^0-\alpha)\times\Delta d}{3A} \cdot [(C_{p_1} + 4C_{p_2} + 2C_{p_3} + 4C_{p_4} + C_{p_5}) - (C_{p_{16}} + 4C_{p_{17}} + 2C_{p_{18}} + 4C_{p_{19}} + C_{p_{20}})] + \frac{cos(90^0-\alpha)\times\Delta d}{3A} \cdot [(C_{p_6} + 4C_{p_7} + 2C_{p_8} + 4C_{P_9} + C_{p_{10}}) - (C_{p_{21}} + 4C_{p_{22}} + 2C_{p_{23}} + 4C_{p_{24}} + C_{p_{25}}) + \frac{cos(150^0-\alpha)\times\Delta d}{3A} \cdot [(C_{p_{11}} + 4C_{p_{12}} + 2C_{p_{13}} + 4C_{p_{14}} + C_{p_{15}}) - (C_{p_{26}} + 4C_{p_{27}} + 2C_{p_{28}} + 4C_{p_{29}} + C_{p_{30}})] \quad (4.38)$$

Similarly, the expression of lift coefficient C_L can be obtained as,

$$C_L = -\frac{sin(30^0-\alpha)\times\Delta d}{3A} \cdot [(C_{p_1} + 4C_{p_2} + 2C_{p_3} + 4C_{p_4} + C_{p_5}) - (C_{p_{16}} + 4C_{p_{17}} + 2C_{p_{18}} + 4C_{p_{19}} + C_{p_{20}})] - \frac{sin(90^0-\alpha)\times\Delta d}{3A} \cdot [(C_{p_6} + 4C_{p_7} + 2C_{p_8} + 4C_{P_9} + C_{p_{10}}) - (C_{p_{21}} + 4C_{p_{22}} + 2C_{p_{23}} + 4C_{p_{24}} + C_{p_{25}})] - \frac{sin(150^0-\alpha)\times\Delta d}{3A} \cdot [(C_{p_{11}} + 4C_{p_{12}} + 2C_{p_{13}} + 4C_{p_{14}} + C_{p_{15}}) - (C_{p_{26}} + 4C_{p_{27}} + 2C_{p_{28}} + 4C_{p_{29}} + C_{p_{30}})] \quad (4.39)$$

4.2.3 Octagonal Cylinder

As shown in figure 4.1 that the cylinder has eight faces S_1, S_2, S_3, S_4, S_5 S_6, S_7 and S_8. The pressure differences between the various tapping points along the face S_1 and S_5 can be obtained from

$\Delta P_{1-25} = P_1 - P_{25}$ is the pressure difference between tapping points 1 and 25,

$\Delta P_{2-24} = P_2 - P_{24}$ is the pressure difference between tapping points 2 and 24,

$\Delta P_{3-23} = P_3 - P_{23}$ is the pressure difference between tapping points 3 and 23,

$\Delta P_{4-22} = P_4 - P_{22}$ is the pressure difference between tapping points 4 and 22,

$\Delta P_{5-21} = P_5 - P_{21}$ is the pressure difference between tapping points 5 and 21.

If F_{15} indicates the net force along the faces S_1 and S_5, then using Simpson's rule,

$$F_{15} = \frac{\Delta A}{3}[\Delta P_{1\text{-}25} + 4\Delta P_{2\text{-}24} + 2\Delta P_{3\text{-}23} + 4\Delta P_{4\text{-}22} + \Delta P_{5\text{-}21}] \quad (4.40)$$

If the length of the cylinder is chosen as unity, then the above expression becomes -

$$F_{15} = \frac{\Delta d \; x \; 1}{3}[\Delta P_{1\text{-}25} + 4\Delta P_{2\text{-}24} + 2\Delta P_{3\text{-}23} + 4\Delta P_{4\text{-}22} + \Delta P_{5\text{-}21}]$$

$$= \frac{\Delta d}{3}[(P_1 - P_{25}) + 4(P_2 - P_{24}) + 2(P_3 - P_{23}) + 4(P_4 - P_{22}) + (P_5 - P_{21})]$$

$$= \frac{\Delta d}{3}[(P_1 - P_0) - (P_{25} - P_0) + 4(P_2 - P_0) - 4(P_{24} - P_0) + 2(P_3 - P_0) - 2(P_{23} - P_0)$$

$$+4(P_4 - P_0) - 4(P_{22} - P_0) + (P_5 - P_0) - (P_{21} - P_0)] \quad (4.41)$$

If the component of the force $F_{d_{15}}$ occurs along the flow direction, then one can find the expression of F as $F_{d_{15}}$

$$F_{d_{15}} = F_{15}\cos(45^0 - \alpha) \quad (4.42)$$

Similarly the force component $F_{L_{14}}$ in a direction perpendicular to the flow may be written as

$$F_{L_{15}} = -F_{15}\sin(45^0 - \alpha) \quad (4.43)$$

The net force F_{26} along the faces S_2 and S_6 can be obtained in the same way as above and that is

$$F_{26} = \frac{\Delta d}{3}[(P_6 - P_0) - (P_{30} - P_0) + 4(P_7 - P_0) - 4(P_{29} - P_0) + 2(P_8 - P_0) - 2(P_{28} - P_0)$$

$$+4(P_9 - P_0) - 4(P_{27} - P_0) + (P_{10} - P_0) - (P_{26} - P_0)] \quad (4.44)$$

Therefore, the components of the drag and lift forces along the faces S_2 and S_5 are respectively

$$F_{d_{26}} = F_{26}\cos(90^0 - \alpha) \quad (4.45)$$

$$F_{L_{26}} = -F_{26}\sin(90^0 - \alpha) \quad (4.46)$$

The net force F_{37} along the faces S_3 and S_7 can be obtained in the same way as above-

$$F_{37} = \frac{\Delta d}{3}[(P_{11} - P_0) - (P_{35} - P_0) + 4(P_{12} - P_0) - 4(P_{34} - P_0) + 2(P_{13} - P_0) - 2(P_{33} - P_0)$$

$$+4(P_{14} - P_0) - 4(P_{32} - P_0) + (P_{15} - P_0) - (P_{31} - P_0)] \quad (4.47)$$

Therefore, the components of the drag and lift forces along the faces S_3 and S_7 are respectively-

$$F_{d_{37}} = F_{37}\, cos(\,135^0 - \alpha) \quad (4.48)$$

$$F_{L_{37}} = -F_{37}\, sin\,(\,135^0 - \alpha) \quad (4.49)$$

The net force F_{48} along the faces S_4 and S_8 can be obtained in the same way as above and that is,

$$F_{48} = \frac{\Delta d}{3}[(P_{16} - P_0) - (P_{40} - P_0) + 4(P_{17} - P_0) - 4(P_{39} - P_0) + 2(P_{18} - P_0) - 2(P_{38} - P_0)$$

$$+4(P_{19} - P_0) - 4(P_{37} - P_0) + (P_{20} - P_0) - (P_{36} - P_0)] \quad (4.50)$$

Therefore, the components of the drag and lift forces along the faces S_3 and S_7 are respectively-

$$F_{d_{48}} = F_{48}\, cos(\,180^0 - \alpha) \quad (4.51)$$

$$F_{L_{48}} = -F_{48}\, sin\,(\,180^0 - \alpha) \quad (4.52)$$

Drag and lift coefficients are defined as follows

$$C_D = \frac{F_d}{\frac{1}{2}\rho A U_\infty^2} \quad (4.53)$$

and $$C_L = \frac{F_L}{\frac{1}{2}\rho A U_\infty^2} \quad (4.54)$$

where, A is the frontal projected area of the cylinder.

The total drag force along the flow direction is

$$F_d = F_{d_{15}} + F_{d_{26}} + F_{d_{37}} + F_{d_{48}} \quad (4.55)$$

and total lift force in a direction perpendicular to flow is

$$F_L = F_{L_{15}} + F_{L_{26}} + F_{L_{37}} + F_{L_{48}} \quad (4.56)$$

Now from equations (4.53) and (4.55), the expression of drag coefficient becomes-

$$C_D = \frac{F_{d_{15}} + F_{d_{26}} + F_{d_{37}} + F_{d_{48}}}{\frac{1}{2}\rho A U_\infty^2}$$

Now substituting the values of $F_{d_{15}}, F_{d_{26}}, F_{d_{37}}$ and $F_{d_{48}}$ from equations (4.42), (4.45), (4.48) and (4.51) respectively, the expression of drag coefficient becomes,

$$C_D = \frac{F_{15}\cos(45^0-\alpha) + F_{26}\cos(90^0-\alpha) + F_{37}\cos(135^0-\alpha) + F_{48}\cos(180^0-\alpha)}{\frac{1}{2}\rho A U_\infty^2}$$

$$= \frac{\cos(45^0-\alpha)}{A}\cdot\frac{F_{15}}{\frac{1}{2}\rho U_\infty^2} + \frac{\cos(90^0-\alpha)}{A}\cdot\frac{F_{26}}{\frac{1}{2}\rho U_\infty^2} + \frac{\cos(135^0-\alpha)}{A}\frac{F_{37}}{\frac{1}{2}\rho U_\infty^2}$$

$$+ \frac{\cos(180^0-\alpha)}{A}\frac{F_{48}}{\frac{1}{2}\rho U_\infty^2} \qquad (4.57)$$

Now inserting the values of $F_{d_{15}}$, $F_{d_{26}}$, $F_{d_{37}}$ and $F_{d_{48}}$ from equations (4.41), (4.44), (4.47) and (4.50) respectively, one finds

$$C_D = \frac{\cos(45^0-\alpha)}{3A}\cdot\frac{\Delta d}{\frac{1}{2}\rho U_\infty^2}\cdot[(P_1-P_0)-(P_{25}-P_0)+4(P_2-P_0)-4(P_{24}-P_0)+2(P_3-P_0)-2(P_{23}-P_0)+4(P_4-P_0)-4(P_{22}-P_0)+(P_5-P_0)-(P_{21}-P_0)] + \frac{\cos(90^0-\alpha)}{3A}\cdot\frac{\Delta d}{\frac{1}{2}\rho U_\infty^2}\cdot[(P_6-P_0)-(P_{30}-P_0)+4(P_7-P_0)-4(P_{29}-P_0)+2(P_8-P_0)-2(P_{28}-P_0)+4(P_9-P_0)-4(P_{27}-P_0)+(P_{10}-P_0)-(P_{26}-P_0)] + \frac{\cos(135^0-\alpha)}{3A}\frac{\Delta d}{\frac{1}{2}\rho U_\infty^2}\cdot[(P_{11}-P_0)-(P_{35}-P_0)+4(P_{12}-P_0)-4(P_{34}-P_0)+2(P_{13}-P_0)-2(P_{33}-P_0)+4(P_{14}-P_0)-4(P_{32}-P_0)+(P_{15}-P_0)-(P_{31}-P_0)] + \frac{\cos(180^0-\alpha)}{3A}\frac{\Delta d}{\frac{1}{2}\rho U_\infty^2}\cdot[(P_{16}-P_0)-(P_{40}-P_0)+4(P_{17}-P_0)-4(P_{39}-P_0)+2(P_{18}-P_0)-2(P_{38}-P_0)+4(P_{19}-P_0)-4(P_{37}-P_0)+(P_{20}-P_0)-(P_{36}-P_0)]$$

Now writing in terms of pressure coefficients the above equation is transformed into-

$$C_D = \frac{\cos(45^0-\alpha)\times\Delta d}{3A}\cdot[C_{p_1}-C_{p_{25}}+4C_{p_2}-4C_{p_{24}}+2C_{p_3}-2C_{p_{23}}+4C_{p_4}-4C_{p_{22}}+C_{p_5}-C_{p_{21}}] + \frac{\cos(90^0-\alpha)\times\Delta d}{3A}\cdot[C_{p_6}-C_{p_{30}}+4C_{p_7}-4C_{p_{29}}+2C_{p_8}-2C_{p_{28}}+4C_{P_9}-4C_{p_{27}}+C_{p_{10}}-C_{p_{26}}] + \frac{\cos(135^0-\alpha)\times\Delta d}{3A}\cdot[C_{p_{11}}-C_{p_{35}}+4C_{p_{12}}-4C_{p_{34}}+2C_{p_{13}}-2C_{p_{33}}+4C_{p_{14}}-4C_{p_{32}}+C_{p_{15}}-C_{p_{31}}] + \frac{\cos(180^0-\alpha)\times\Delta d}{3A}\cdot[C_{p_{16}}-C_{p_{40}}+4C_{p_{17}}-4C_{p_{39}}+2C_{p_{18}}-2C_{p_{38}}+4C_{p_{19}}-4C_{p_{37}}+C_{p_{20}}-C_{p_{36}}]$$

Rearranging the expression of C_D becomes of the following form-

$$C_D = \frac{\cos(45^0-\alpha)\times\Delta d}{3A}\cdot[(C_{p_1}+4C_{p_2}+2C_{p_3}+4C_{p_4}+C_{p_5})-(C_{p_{25}}+4C_{p_{24}}+2C_{p_{23}}+4C_{p_{22}}+C_{p_{21}})] + \frac{\cos(90^0-\alpha)\times\Delta d}{3A}\cdot[(C_{p_6}+4C_{p_7}+2C_{p_8}+4C_{P_9}+C_{p_{10}})-(C_{p_{30}}+4C_{p_{29}}+2C_{p_{28}}+4C_{p_{27}}+C_{p_{26}})] + \frac{\cos(135^0-\alpha)\times\Delta d}{3A}\cdot[(C_{p_{11}}+4C_{p_{12}}+2C_{p_{13}}+4C_{p_{14}}+C_{p_{15}})-(C_{p_{35}}+4C_{p_{34}}+2C_{p_{33}}+4C_{p_{32}}+C_{p_{31}})] + \frac{\cos(180^0-\alpha)\times\Delta d}{3A}\cdot[(C_{p_{16}}+4C_{p_{17}}+2C_{p_{18}}+4C_{p_{19}}+4C_{p_{20}})-(C_{p_{40}}+4C_{p_{39}}+2C_{p_{38}}+C_{p_{37}}+C_{p_{36}})]] \qquad (4.58)$$

Similarly, the expression of lift coefficient C_L can be obtained as,

$$C_L = -\frac{sin(45^0-\alpha)\times\Delta d}{3A}\left[\left(C_{p_1} + 4C_{p_2} + 2C_{p_3} + 4C_{p_4} + C_{p_5}\right) - \left(C_{p_{25}} + 4C_{p_{24}} + 2C_{p_{23}} + 4C_{p_{22}} + C_{p_{21}}\right)\right] - \frac{sin(90^0-\alpha)\times\Delta d}{3A}\cdot[(C_{p_6} + 4C_{p_7} + 2C_{p_8} + 4C_{P_9} + C_{p_{10}}) - (C_{p_{30}} + 4C_{p_{29}} + 2C_{p_{28}} + 4C_{p_{27}} + C_{p_{26}})] - \frac{sin(135^0-\alpha)\times\Delta d}{3A}\cdot[(C_{p_{11}} + 4C_{p_{12}} + 2C_{p_{13}} + 4C_{p_{14}} + C_{p_{15}}) - (C_{p_{35}} + 4C_{p_{34}} + 2C_{p_{33}} + 4C_{p_{32}} + C_{p_{31}})] - \frac{cos(180^0-\alpha)\times\Delta d}{3A}\cdot[(C_{p_{16}} + 4C_{p_{17}} + 2C_{p_{18}} + 4C_{p_{19}} + 4C_{p_{20}}) - (C_{p_{40}} + 4C_{p_{39}} + 2C_{p_{38}} + C_{p_{37}} + C_{p_{36}})] \quad (4.59)$$

4.3 Aspect of the Flow Modeling

The Navier-Stokes equations are a combination of continuity, momentum and energy equations. CFD (Computational Fluid Dynamics) solver is used to solve these equations for different flow types. For turbulent flows, additional transport equations are also needed to be solved. Therefore, the governing equations for the incompressible turbulent wind flow around the different shape of cylinders, is the RANS (Reynolds-averaged Navier Stokes) equations given as follows:

$$\frac{\partial u_i}{\partial x_i} = 0 \quad (4.60)$$

$$\frac{\partial}{\partial x_j}(\rho u_j u_i) = -\frac{\partial p}{\partial x_j} + \frac{\partial}{\partial x_j}[\mu(\frac{\partial u_i}{\partial x_j} + \frac{\partial u_j}{\partial x_i}) - \rho\overline{u_i' u_j'}] \quad (4.61)$$

The turbulent wind flow around the group of cylinders is simulated by k-ε turbulence model, which is one of the most popular models used in CFD to simulate mean flow characteristics for turbulent flow conditions. The standard k-ε model of turbulence is a computational procedure to the system, based on a model transport equation for the turbulent kinetic energy (k) and its dissipation rate (ε). It is a two-equation model in which the solution of two separate transport equations allows the turbulence velocity and length scales to be independently determined. The model transport equation for k is derived from the exact equation and that of ε is obtained using physical reasoning and bears little resemblance to its mathematically exact counterpart. In the derivation of the k-ε model, flow is assumed as fully turbulent and the effect of molecular viscosity is considered as negligible. The following two equations represent the transport of turbulent kinetic energy, k and its rate of dissipation rate, ε respectively:

$$\frac{\partial}{\partial t}(\rho k) + \frac{\partial}{\partial x_i}(\rho k u_i) = \frac{\partial}{\partial x_j}\left[\left(\mu + \frac{\mu_t}{\sigma_k}\right)\frac{\partial k}{\partial x_j}\right] + P_k + P_b - \rho\epsilon - Y_M + S_k \quad (4.62)$$

$$\frac{\partial}{\partial t}(\rho\epsilon) + \frac{\partial}{\partial x_i}(\rho\epsilon u_i) = \frac{\partial}{\partial x_j}\left[\left(\mu + \frac{\mu_t}{\sigma_\epsilon}\right)\frac{\partial \epsilon}{\partial x_j}\right] + C_{1\epsilon}\frac{\epsilon}{k}(P_k + C_{3\epsilon}P_b) - C_{2\epsilon}\rho\frac{\epsilon^2}{k} + S_\epsilon \qquad (4.63)$$

Where, u_i represents velocity component in corresponding direction. These two equations are used avoiding time dependent term in order to make the steady condition. In these equations, $P_k = -\rho\overline{u_i' u_j'}\frac{\partial u_i}{\partial x_j}$ represents the generation of turbulent kinetic energy due to the mean velocity gradients. To evaluate P_k in a manner consistent with the Boussinesq hypothesis, $P_k = \mu_t S^2$, where S is the modulus of the mean rate of strain tensor ($S = \sqrt{2S_{ij}S_{ij}}$). With the mean strain rate is given by, $S_{ij} = \frac{1}{2}\left(\frac{\partial u_i}{\partial u_j} + \frac{\partial u_j}{\partial x_i}\right)$; where P_b is the generation of turbulent kinetic energy due to buoyancy. It is calculated $P_b = \beta g_i \frac{\mu_t}{Pr_t}\frac{\partial T}{\partial x_j}$; where, β is coefficient of thermal expansion, g_i is the component of the gravitational vector in i-th direction and Pr_t is the turbulent Prandtl number for energy and Y_M represents the contribution of fluctuating dilation in compressible turbulence to the overall dissipation rate. In the present model, $Y_M = 0$ as compressibility effect is neglected for incompressible flow. $C_{1\epsilon}$, $C_{2\epsilon}$ and $C_\mu$are constants; σ_k and σ_ε are the turbulent Prandtl numbers for k and ε, and $S_t$and S_ε are user defined source items respectively. $S_t$and S_ε are user defined source items respectively. The turbulent viscosity μ_t is computed by combining k and ε as $\mu_t = C_\mu(k^2/\varepsilon)$. In order to make good agreement with the experimental results, the values of the various constants were chosen as: $C_{1\epsilon} = 1.44$, $C_{2\epsilon} = 1.92$, $C_\mu = 0.09$, $\sigma_k = 1.0$ and $\sigma_\varepsilon = 1.3$. Non-dimensional pressure, drag and lift coefficients were defined as, $C_p = 2(P - P_0)/\rho U_0^2$, $C_D = 2F_D/\rho U_0^2$ *and* $C_L = 2F_L/\rho U_0^2$ respectively, where, P_0 is the free stream pressure, F_D is the drag force and F_L is the lift force.

4.4.1 Geometrical Setup

The three different shape of cylinders are used in staggered form for this analysis. Their arrangement is similar to that of the experimental setup with the pentagonal and hexagonal shapes placed in upstream and octagonal shape placed in downstream position (Fig 4.2). ANSYS 16 software is used for geometrical design as well as solver purpose.

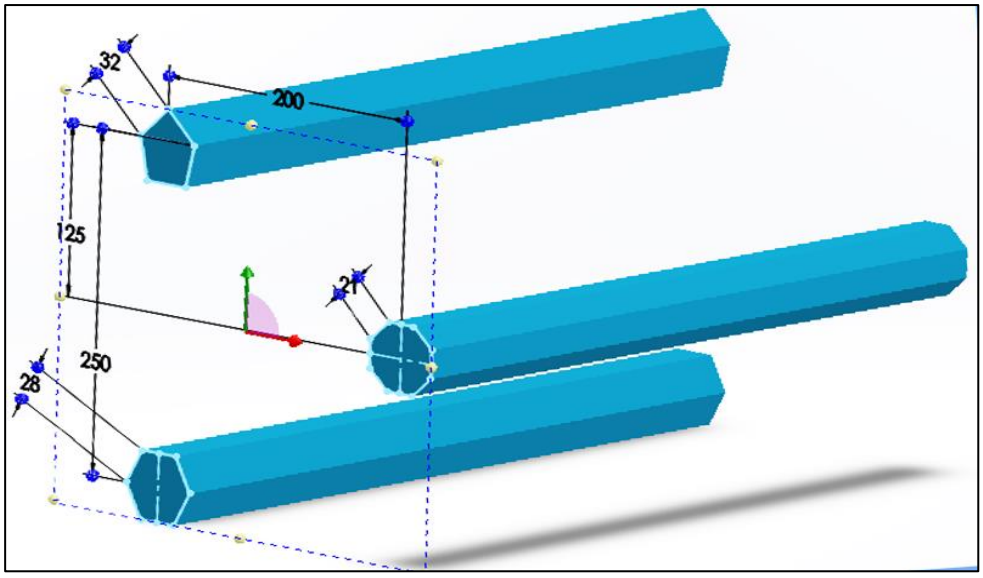

Figure 4. 2: Arrangement and dimension (in mm) of the cylinders

Numerical results are highly influenced by the dimensions of the geometrical domain. As shown in Fig 4.3, the boundaries with respect to the cylinders in upstream for front, top and bottom are chosen as 12D and for rear boundary, it is 36D with respect to the octagonal cylinder at downstream from the origin, where hydraulic diameter, D = 50 mm for all three cylinders. The dimensions of the computational flow domain for the simulation purpose are given below.

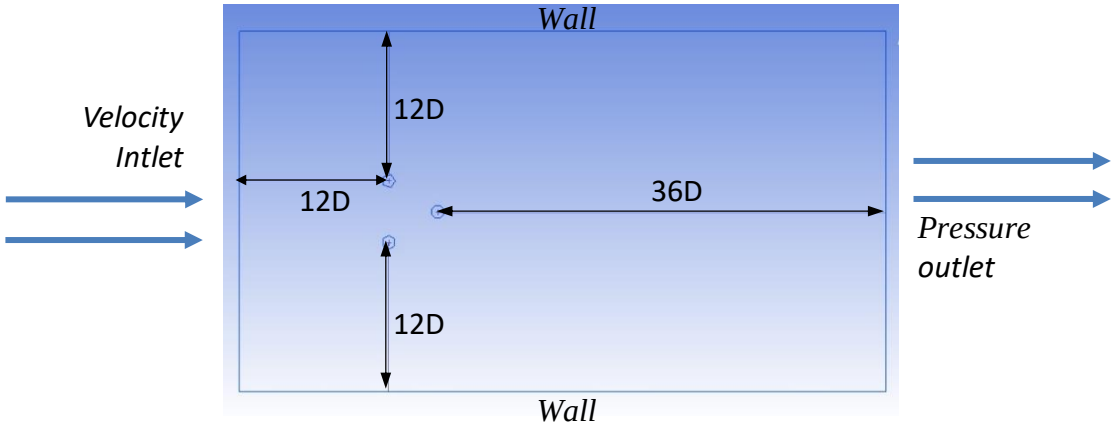

Figure 4. 3: Computational Flow Domain

4.4.2 Initial Condition and Boundary Condition

To set initial and boundary data for the k-ε turbulence model, turbulence intensity (*I)* is specified, which is the ratio of characteristic turbulent eddy velocity to free stream velocity or the average velocity; $I=\sqrt{\frac{1}{3}(\overline{u'^2}+\overline{v'^2}+\overline{w'^2})}/U_{ref}$ *or* $I = \sqrt{(2/3k)}/U_{ref}$, where 'I' is a dimensionless quantity. For the flow simulation, low turbulence intensity is considered. The value of 'I' is

calculated from $I = 0.16Re^{-(1/8)}$. As boundary condition on $\epsilon = (0.164k^{1.5}/0.07L)$. Based on this boundary condition, the k-ε turbulence model is applied to evaluate the two-dimensional flow simulation around the group of cylinders.

4.4.3 Meshing and Computational Method

Flow domains are split into smaller sub domains in order to analyze fluid flow. The governing equations are then discretized and solved inside each of these sub domains. An unstructured two-dimensional meshing was done consisting of quadrilateral shaped elements, to get better control of the mesh and also to reduce numerical error. The meshing resolution was greater in regions where greater computational accuracy was needed i.e. at the faces of the cylinders. Turbulent flow is assumed and the free stream temperature, air density, viscosity are assumed similar to experimental conditions (Table 1). Calculations are done for combination of the three cylinders at 0˚, 30˚, 45˚ and 60˚ angles of attack. Medium mesh smoothing was chosen to enhance element shapes and overall mesh quality.

Table 2: **Mesh Data, Sizing and Quality**

Type of cell	Quadrilateral
Nodes: 184215	Elements: 183189
Minimum cell size	1.5052×10^{-003}m
Maximum cell	0.301040m
Minimum Orthogonal Quality	5.11734×10^{-01}
Maximum Ortho Skew	4.88266×10^{-01}
Maximum Aspect Ratio	6.51241

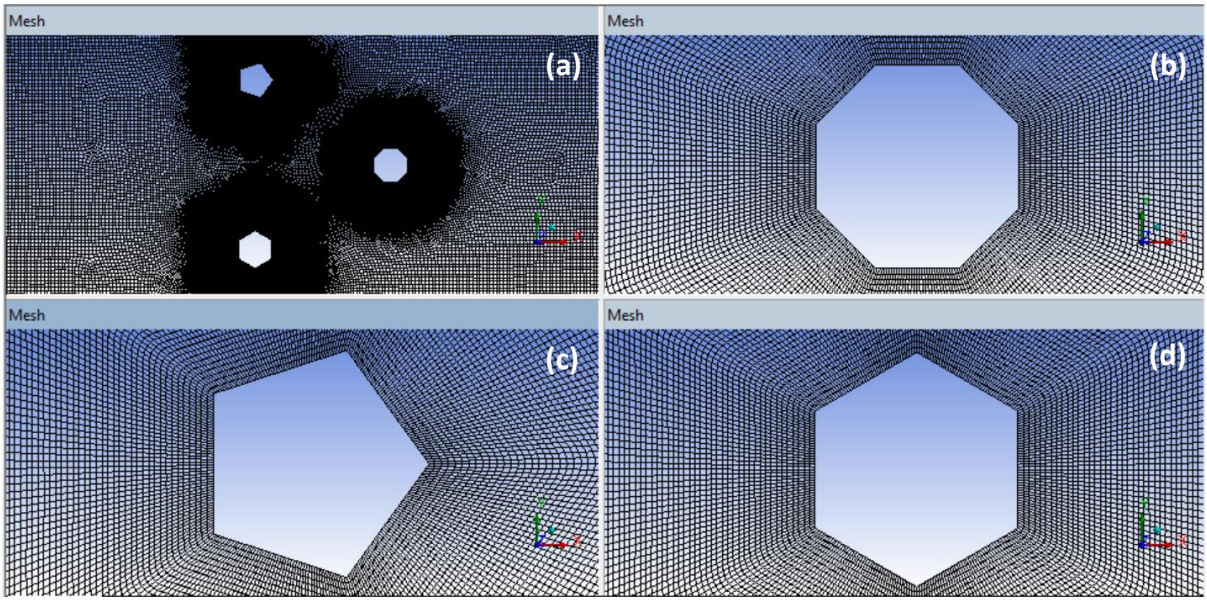

Figure 4. 4: Mesh at 0˚ Angle of Attack around (a) the combination of three cylinders, (b) Octagon at downstream, (c) Pentagon and (d) Hexagon at upstream position

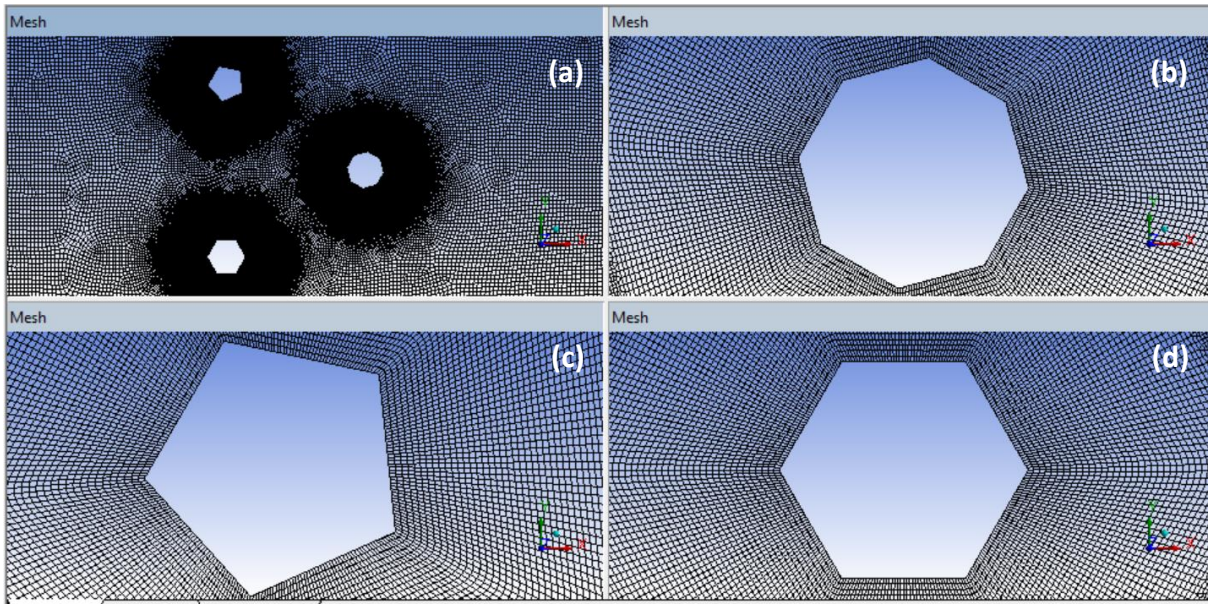

Figure 4. 5: Mesh at 30˚ Angle of Attack around (a) the combination of three cylinders, (b) Octagon at downstream, (c) Pentagon and (d) Hexagon at upstream position

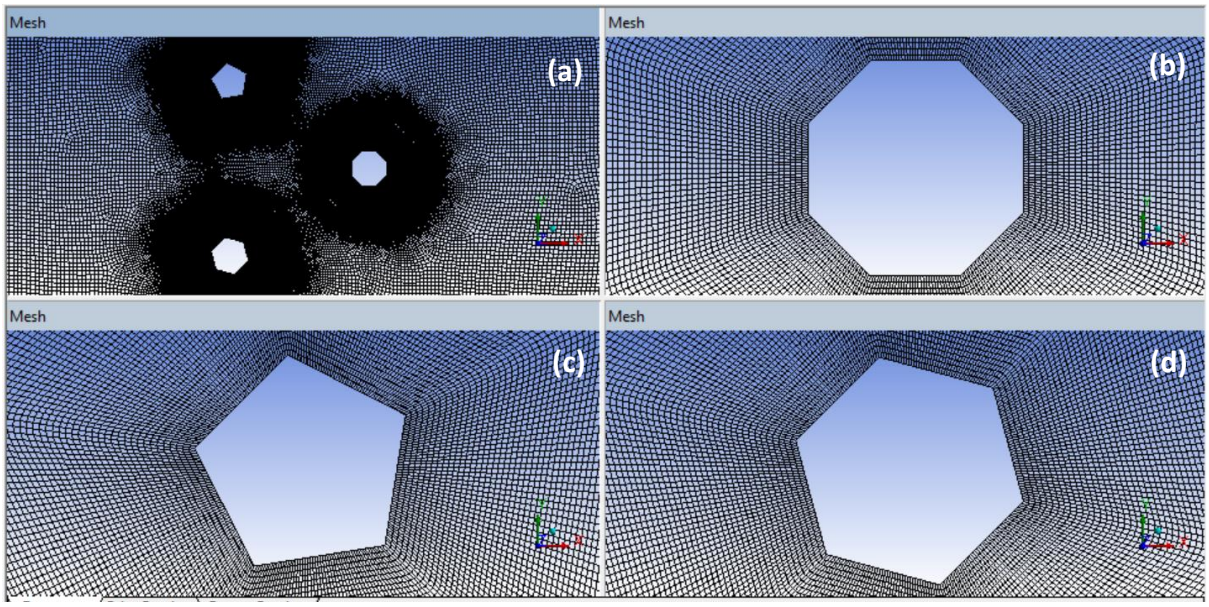

Figure 4. 6: **Mesh at 45˚ Angle of Attack around (a) the combination of three cylinders, (b) Octagon at downstream, (c) Pentagon and (d) Hexagon at upstream position**

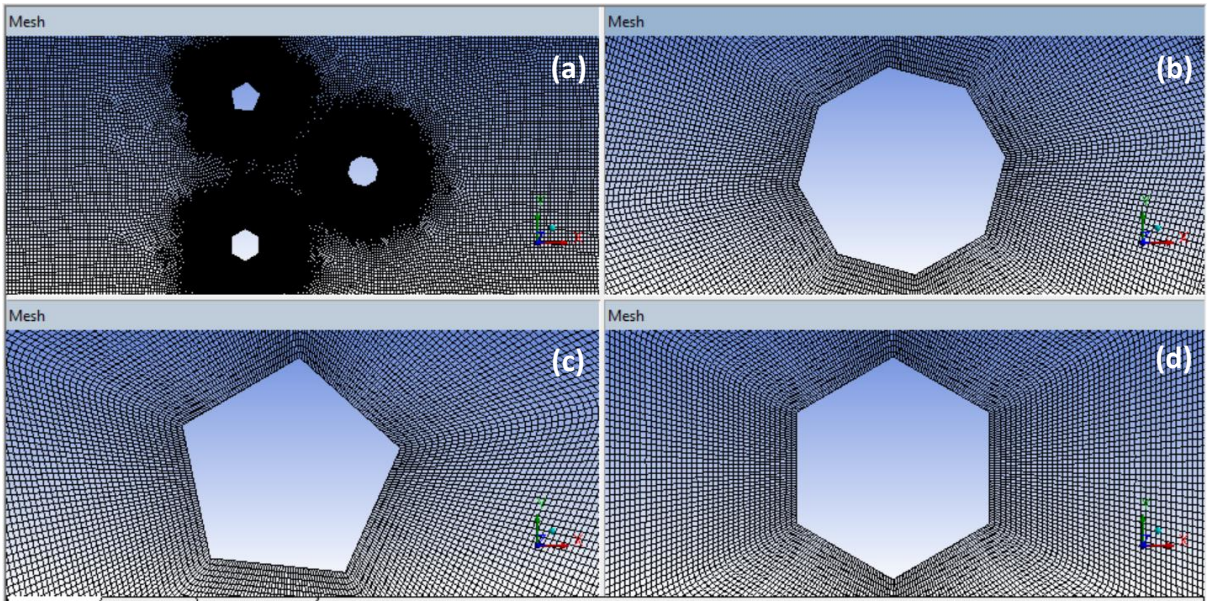

Figure 4. 7: **Mesh at 60˚ Angle of Attack around (a) the combination of three cylinders, (b) Octagon at downstream, (c) Pentagon and (d) Hexagon at upstream position**

To test the grid independency a finer mesh, made of 223017 elements, 224140 number of nodes is compared with a mesh of 129845 elements and 131060 number of nodes with the same input. The drag co-efficient found for the finer mesh is 0.861, 0.906 and 0.537 for pentagonal, hexagonal and octagonal cylinders respectively. These values vary with that of the other mesh by 0.0546%, 0.0022% and 0.0037% respectively, which is concurrent to the independency test.

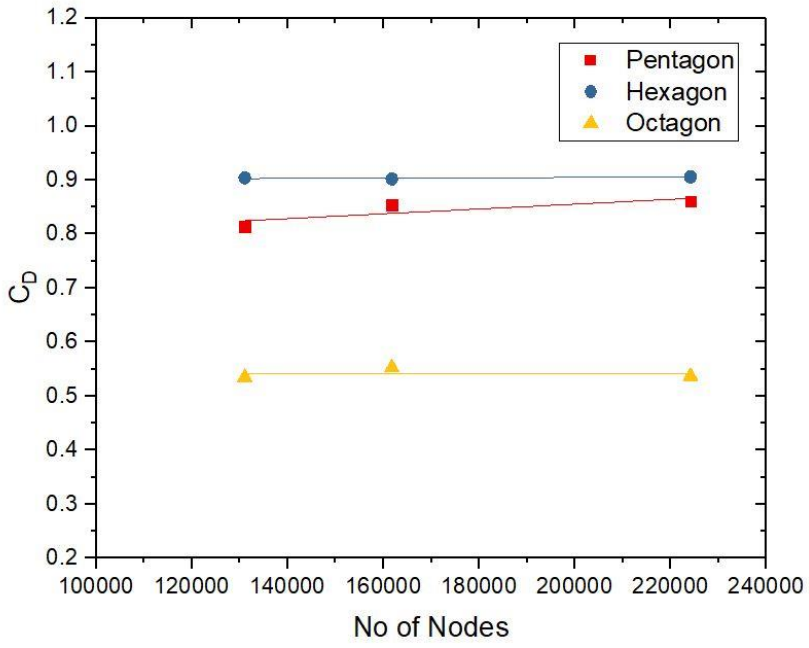

Figure 4. 8: Grid Independency Analysis

As per the analysis done on drag co-efficient vs number of nodes, it is seen that after a certain number of grid cells, there are no variation on computational results. Around 184215 number of nodes is chosen for further analysis. Overall, the Y Plus (y+) value does not cross 60% which gives a fairly good meshing accuracy for this turbulence modelling.

CHAPTER-5
RESULTS AND DISCUSSIONS

The results of the experimental and numerical investigation regarding the surface static pressure coefficients, drag and lift coefficients have been discussed in this chapter. At first, the static pressure coefficients on the surface of the pentagonal, hexagonal and octagonal cylinders at 0°, 30°, 45° and 60° angles of attack are taken into consideration. Next, the distributions of the static pressure coefficients on the surface of the staggered cylinders obtained from numerical study is compared at the same angles of attack. Finally, the calculated drag and lift coefficients for the group of cylinders are presented.

5.1 Distribution of Pressure, Drag and Lift Coefficients

In this section the distributions of the pressure coefficients for pentagonal, hexagonal and octagonal cylinders at different angles of attack have been presented. Pressure coefficients have been calculated from the measured values of the surface static pressures. Next by the numerical integration method of the pressure coefficients, drag and lift coefficients have been found.

In order to relate pressure distribution around any shape, at first a typical flow over the single square cylinder has been discussed prior to detailed discussion on the results of the experimental investigation. As shown in figure 5.1, its angles of attack are studied from zero degrees to 45° angles of attack [39]. Although the pentagonal, hexagonal and octagonal cylinders will give a bit different flow pattern, formation of the vortex pair will be similar. The path of the shear layers is altered from their point of origin at the front corners of the square cylinder to the vortex formation region as the angle of attack increases. The shear layers which typically originate at the front corners of the square, curve outward and form the familiar vortex street in the wake close behind the body in the absence of turbulence in the incident flow. The back-surface pressure varies depending on the distance of these vortices. The longer the distance of the vortices is from the body, higher is the back pressure and vice versa. As a result, pressure decreases at the rear surface of the model cylinder at higher angle of attack in contrast to an increase in pressure at smaller angle of attack. [40]

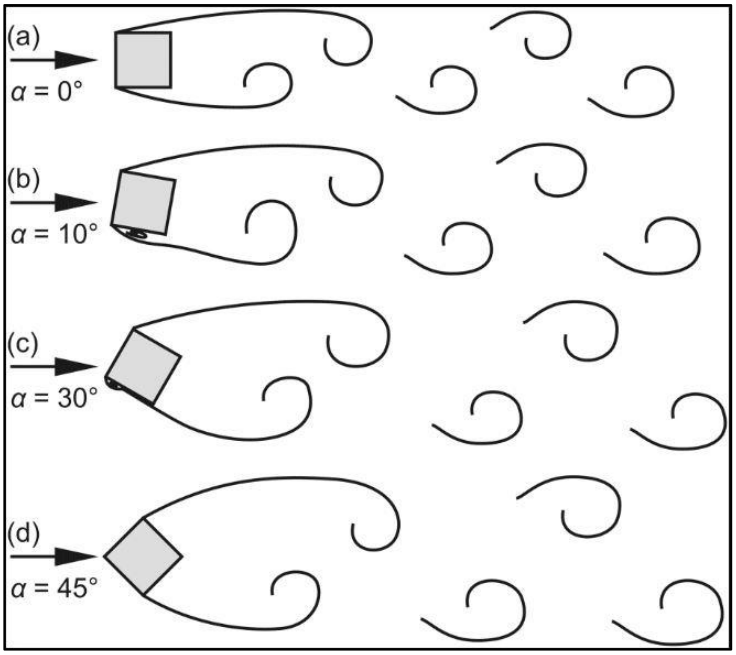

Figure 5. 1: **Typical Vortex Pattern in the Downstream of Square Cylinder [39]**

All three cylinders have five tapping points on each surface which have been numbered for ease of identification. At different angles of attack (Angle of Attack), the distributions of pressure coefficients at different tapping points for pentagonal, hexagonal and octagonal cylinders have been shown for relative study in figures 5.2 to 5.4.

Comparative data of pressure coefficient at different faces of pentagonal shape from experimental analysis (Annex B) and simulation at different angles of attack has been shown in figures 5.5 to 5.8. Similarly, the distributions of static pressure coefficients at different angles of attack for hexagonal and octagonal shapes have been presented in figures 5.9 to 5.12 and figures 5.13 to 5.16.

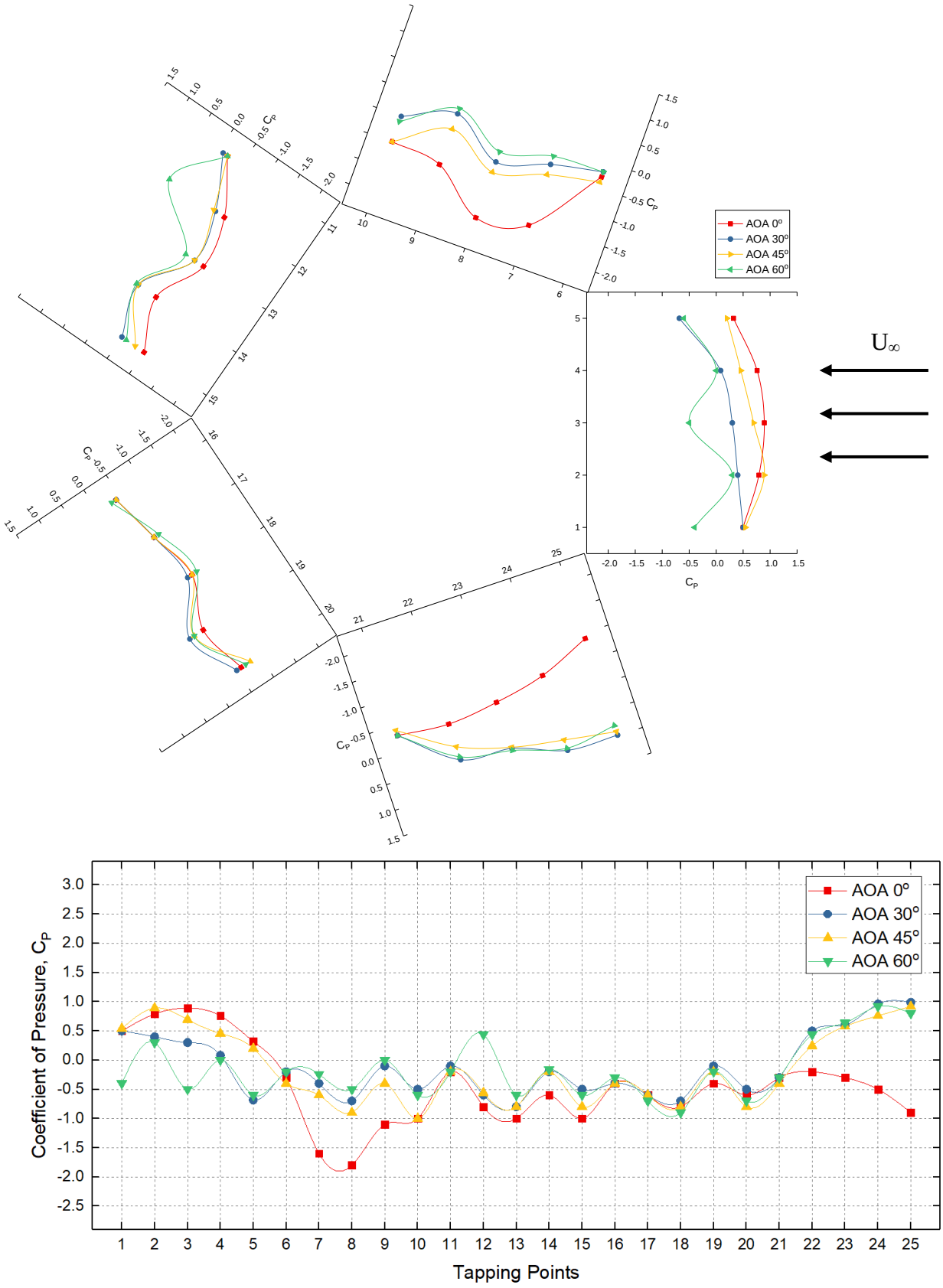

Figure 5. 2: Distribution of Pressure Coefficient on Five Faces of Pentagonal Cylinder at Different Angles of Attack

Pentagonal cylinder is placed in the upstream side above the hexagonal cylinder. As shown in figures 5.5 to 5.8, the variation and comparison of experimental and simulation values of the coefficient of pressure at different angles of attack can be visualized. The surface with tapping points 1 to 5 is placed perpendicular to the wind. At an angle of attack of 0˚, the wind facing side has developed maximum static pressure, which is in lined with the stagnation characteristics. With the increase in Angle of Attack, the position of higher static pressure changes. Other than that, slight fluctuation of magnitudes in experimental and numerical investigations are noticeable. This deviation could be attributed to the smooth surface considered in simulation which helps airflow to easily glide over its surface rather than the surface roughness in practical case for the experimental cylinder. Overall the similar trend of the graph of coefficient of pressure in both cases confirms the cogency.

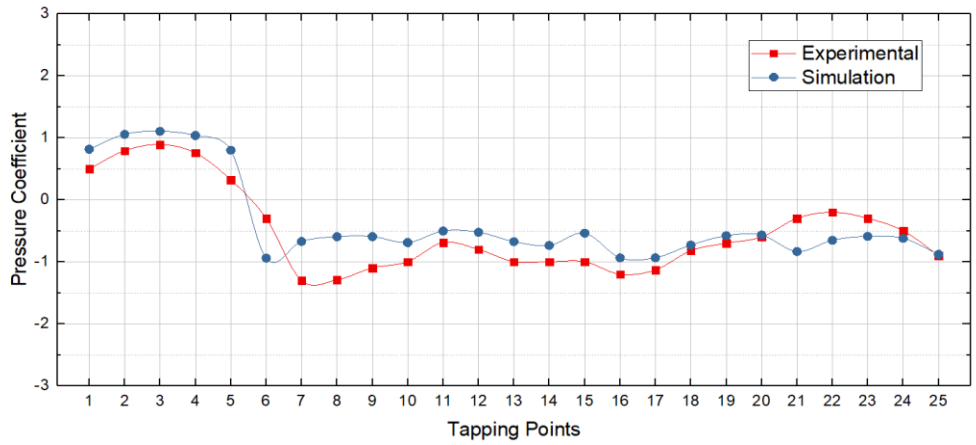

Figure 5. 3: Distribution of Pressure Coefficient on Pentagonal Cylinder at 0^0 Angle of Attack

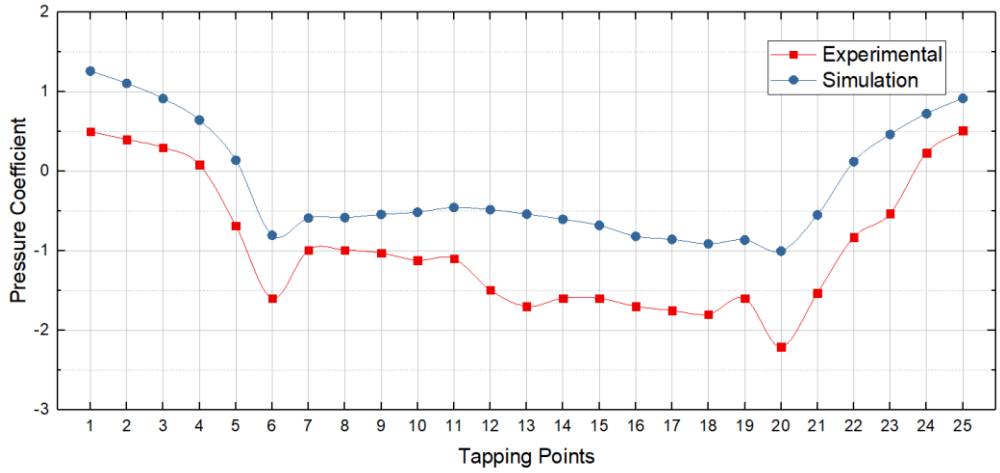

Figure 5. 4: Distribution of Pressure Coefficient on Pentagonal Cylinder at 30^0Angle of Attack

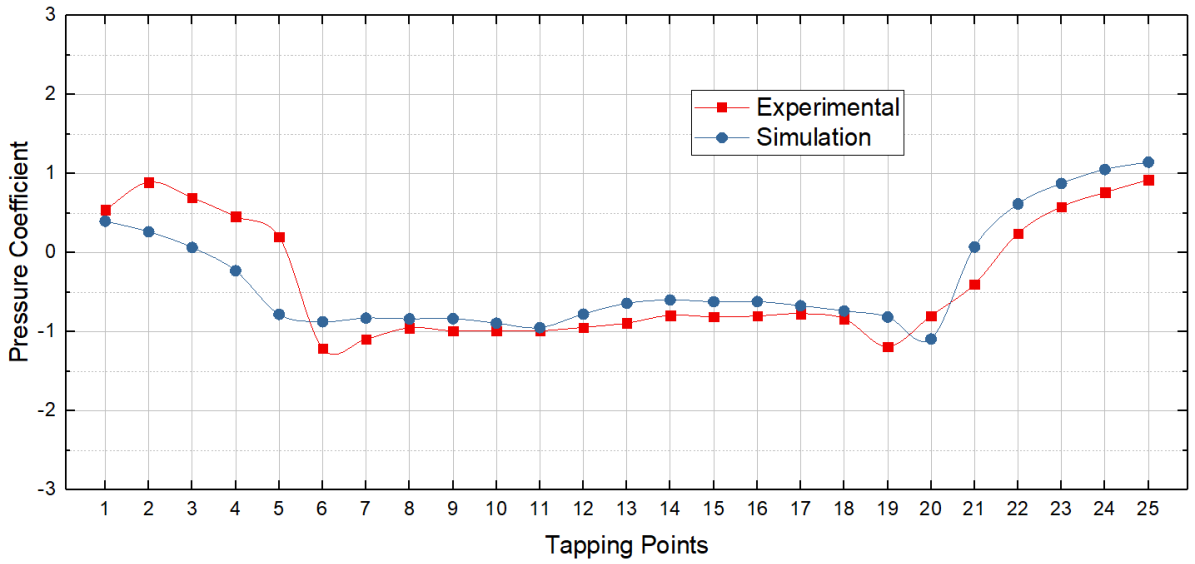

Figure 5. 5: Distribution of Pressure Coefficient on Pentagonal Cylinder at 45^0 Angle of Attack

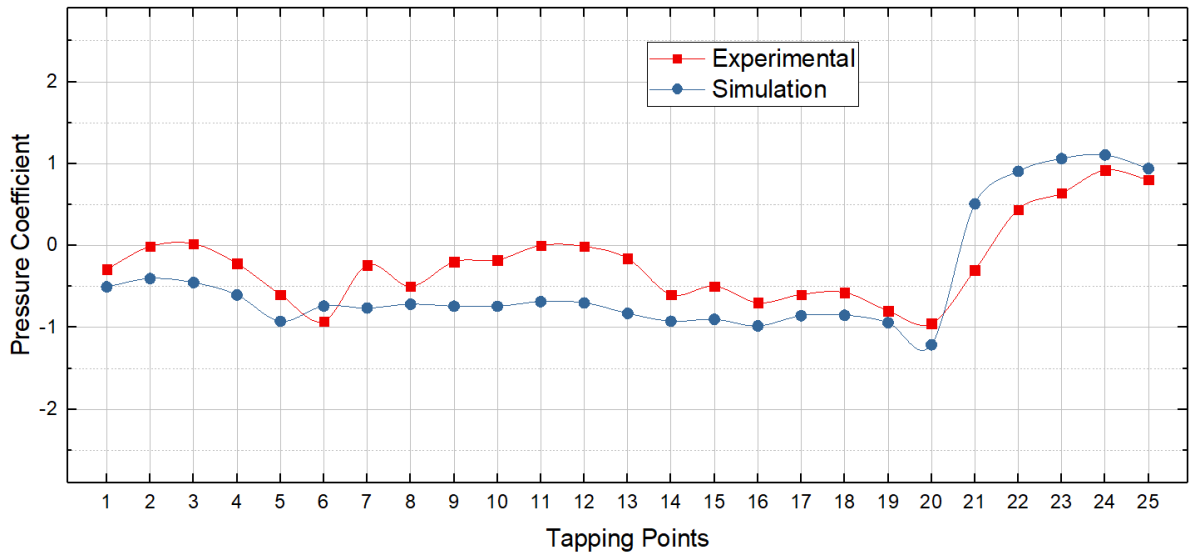

Figure 5. 6: Distribution of Pressure Coefficient on Pentagonal Cylinder at 60^0 Angle of Attack

Hexagonal cylinder is placed in the upstream side right below the pentagonal cylinder in a parallel position. The variation of coefficient of pressure at different angles of attack is shown in figures 5.9 to 5.12. Tapping points 1 to 5 in the wind facing side is shown in the sketch earlier. A well-matched pattern of distribution of pressure of coefficient for both experimental and simulation results is observed. At an angle of attack of 0˚, the wind facing side has developed high static pressure, but the maximum is observed at 30˚ Angle of Attack due to the leading corner of the cylinder, which indicates the stagnation.

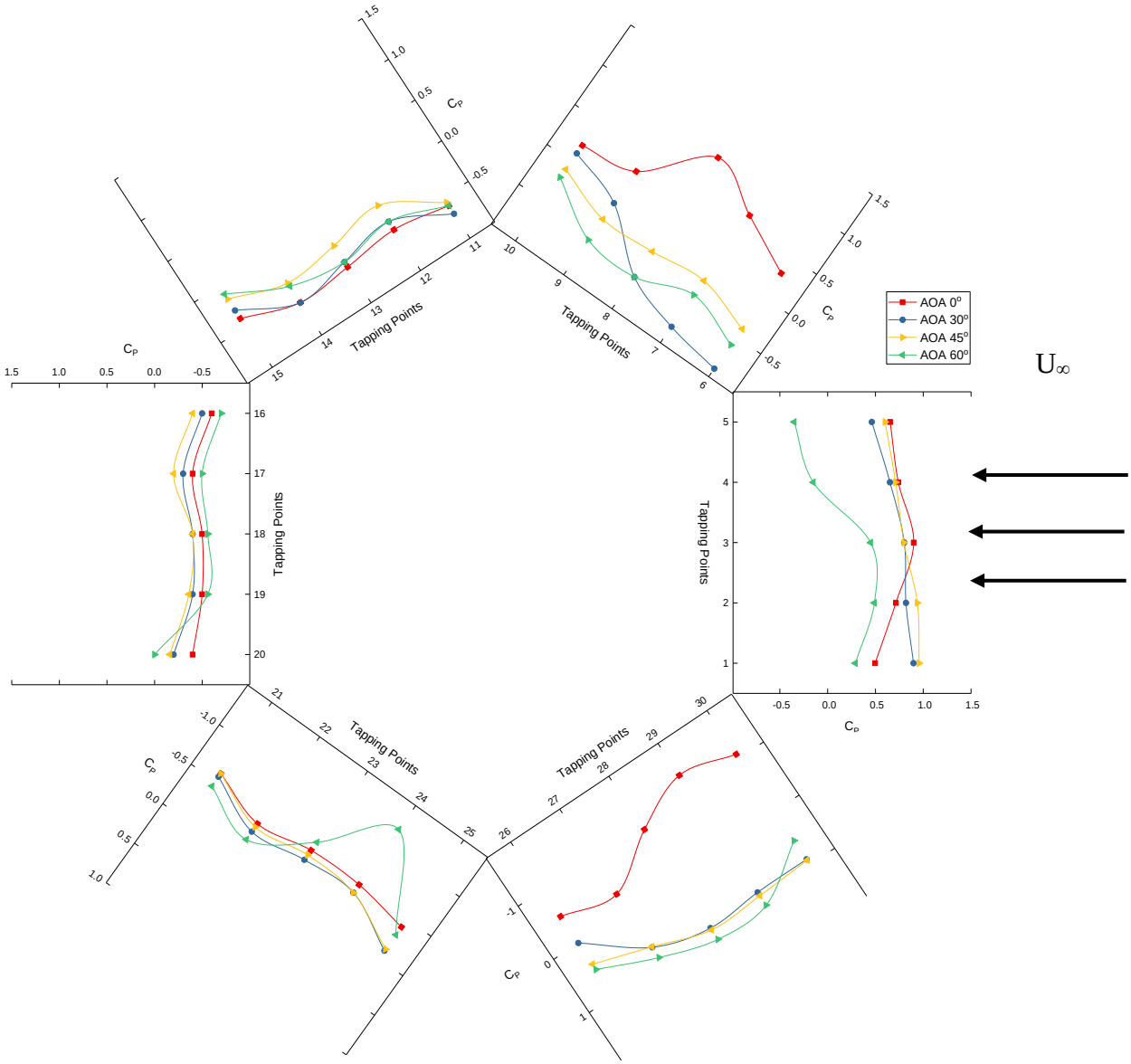
AOA 0°
AOA 30°
AOA 45°
AOA 60°
U∞
Cp
Tapping Points

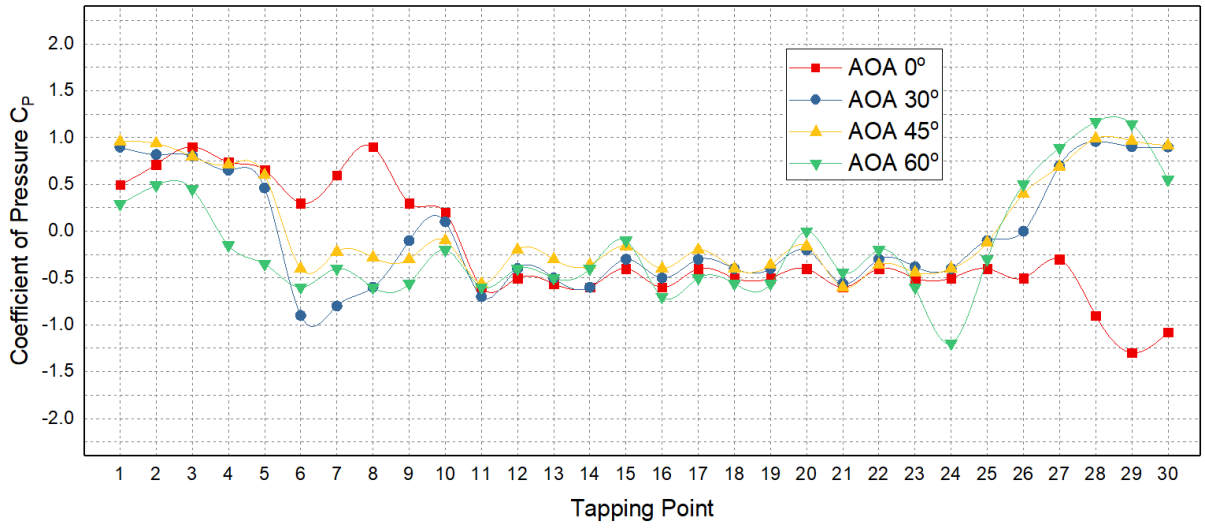
AOA 0°
AOA 30°
AOA 45°
AOA 60°
Coefficient of Pressure Cp
Tapping Point

Figure 5. 7: Distribution of Pressure Coefficient on Six Faces of Hexagonal Cylinder at Different Angles of Attack

Similar higher coefficient of pressure is observed at 60˚ Angle of Attack at a surface with tapping point 26 to 30 as it then faces the wind flow at the front. It is decreased in other four faces of the cylinder. Because of the back flow, in the opposite side of the wind loading, the coefficient of pressure is increased in a fragment. As the Angle of Attack increases, the distribution of coefficient of pressure is symmetric in front and back faces. When experimental and numerical investigations are compared, similar to pentagonal cylinder, due to the smoothness of the surface in case of simulation a magnitude variation is observed. However, the similar graphical trend of coefficient of pressure shows that numerical results and experimental results agree.

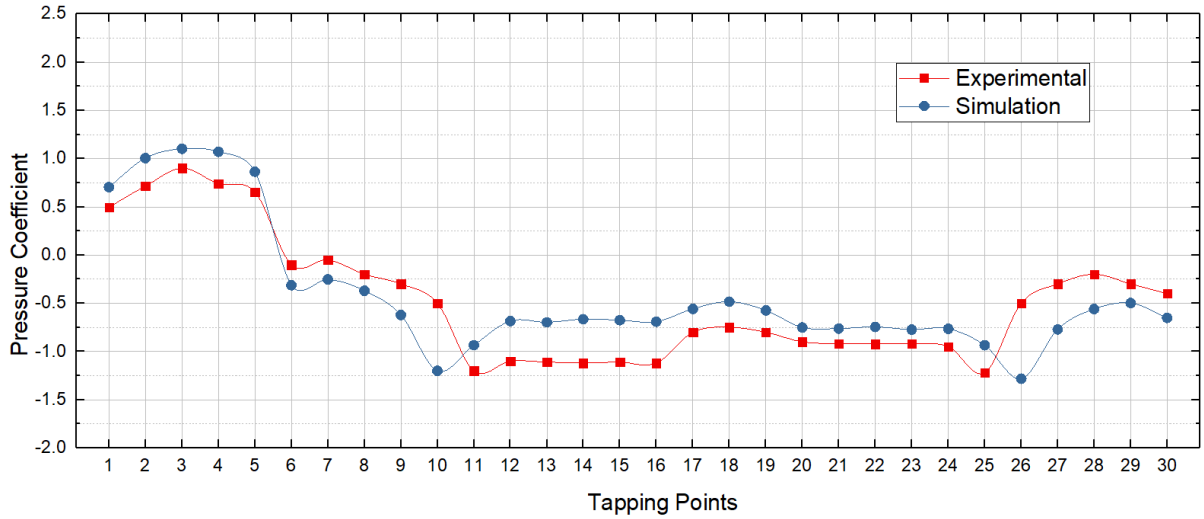

Figure 5. 8: Distribution of Pressure Coefficient on Hexagonal Cylinder at 0^0 Angle of Attack

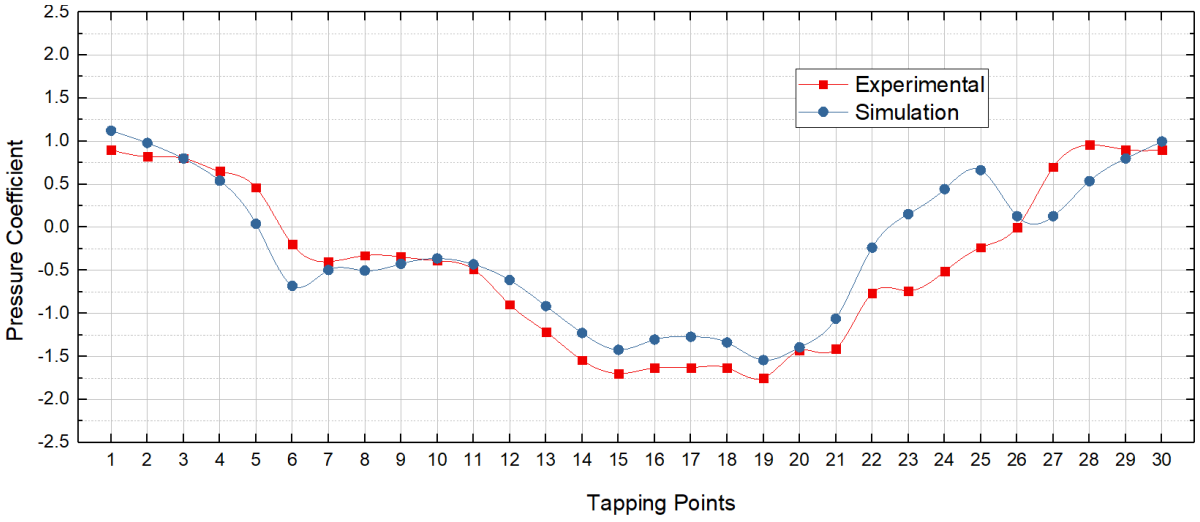

Figure 5. 9: Distribution of Pressure Coefficient on Hexagonal Cylinder at 30^0 Angle of Attack

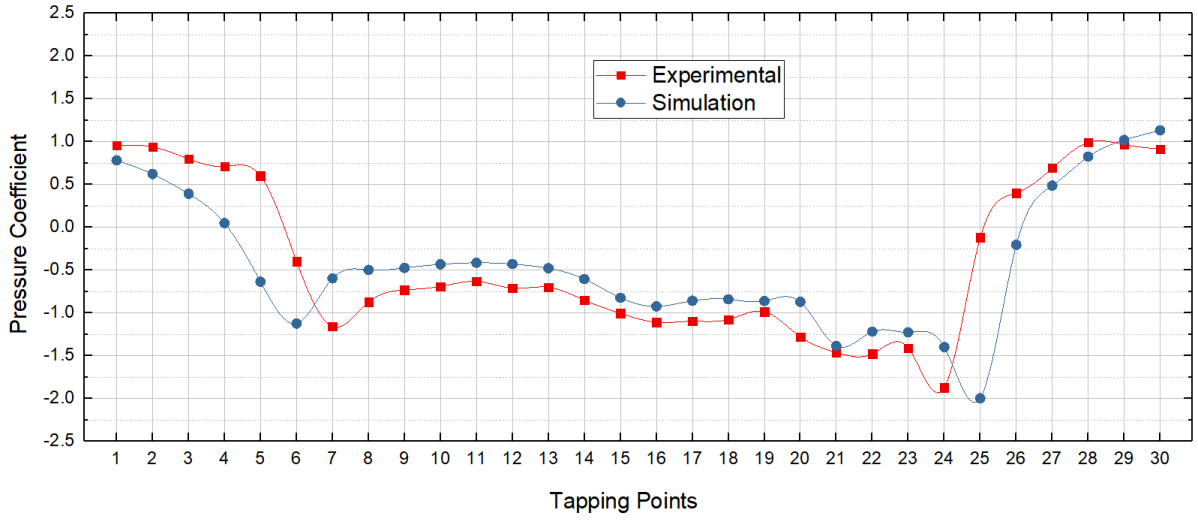

Figure 5. 10: Distribution of Pressure Coefficient on Hexagonal Cylinder at 45^0 Angle of Attack

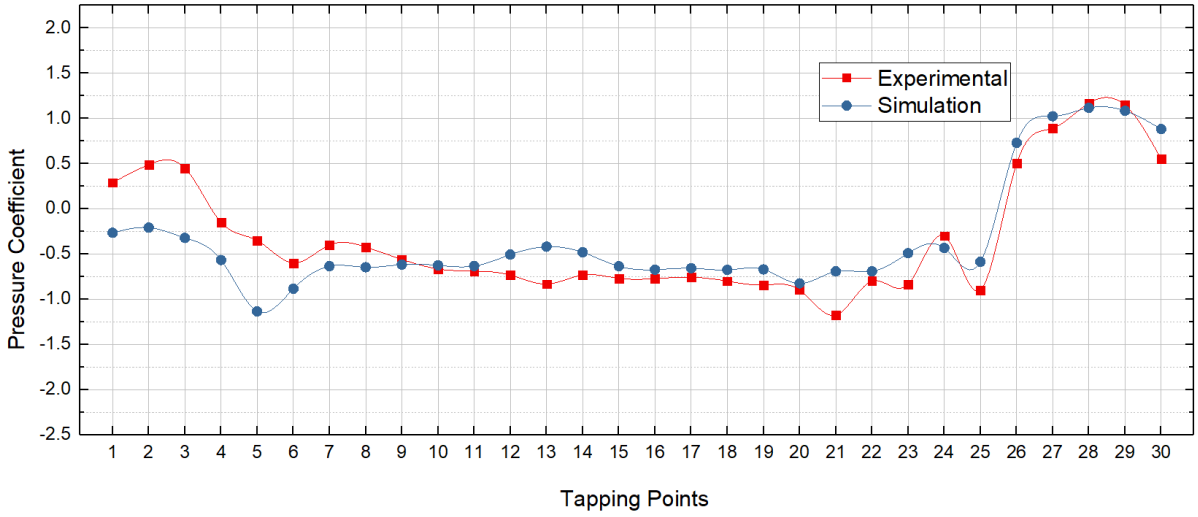

Figure 5. 11: Distribution of Pressure Coefficient on Hexagonal Cylinder at 60^0 Angle of Attack

Now, octagonal cylinder is placed in the downstream side. At different angles of attack, the variation of coefficient of pressure is shown in figures 5.13 to 5.16. Tapping points 1 to 5 is the wind facing side, as shown in the sketch earlier. From the comparison of experimental and simulation result, usual pattern can be observed. At an angle of attack of 0˚, the wind facing side has developed high static pressure, which indicates the stagnation. It is decreased in subsequent two faces of the cylinder. In the opposite side of the wind loading, the coefficient of pressure is increased in smaller amount. This is because of the back flow.

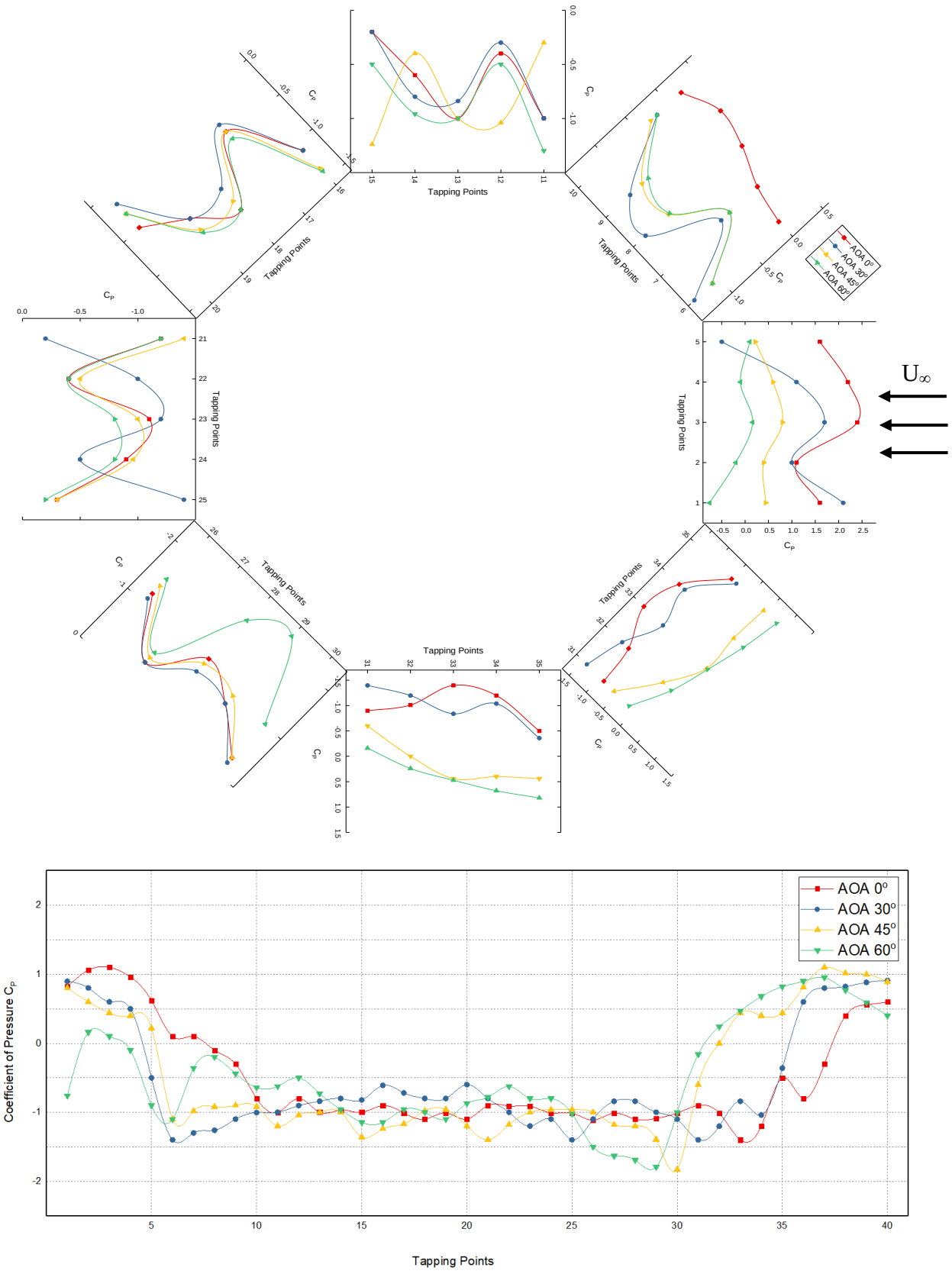

Figure 5. 12: Distribution of Pressure Coefficients at Different Angles of Attack on Octagonal Cylinder

However, maximum static pressure occurs at Angle of Attack 30˚ when the octagonal corner faces the front with a decrease observed in all other faces. As the Angle of Attack increases to 45˚, the distribution of coefficient of pressure is symmetric in front and back faces. In the Angle of Attack of 60˚, the cylinder assumes a similar orientation of 0˚ Angle of Attack. The location of the stagnation is changed to the front facing surface but the graph trend is found to be similar to that of 0˚ Angle of Attack. Apart from that, if experimental and numerical investigations are compared, similar to the other cylinders, due to the smoothness of the surface in case of simulation a difference is magnitude is observed. Similar graph pattern of the coefficient of pressure in both cases confirms the validity of the experiment.

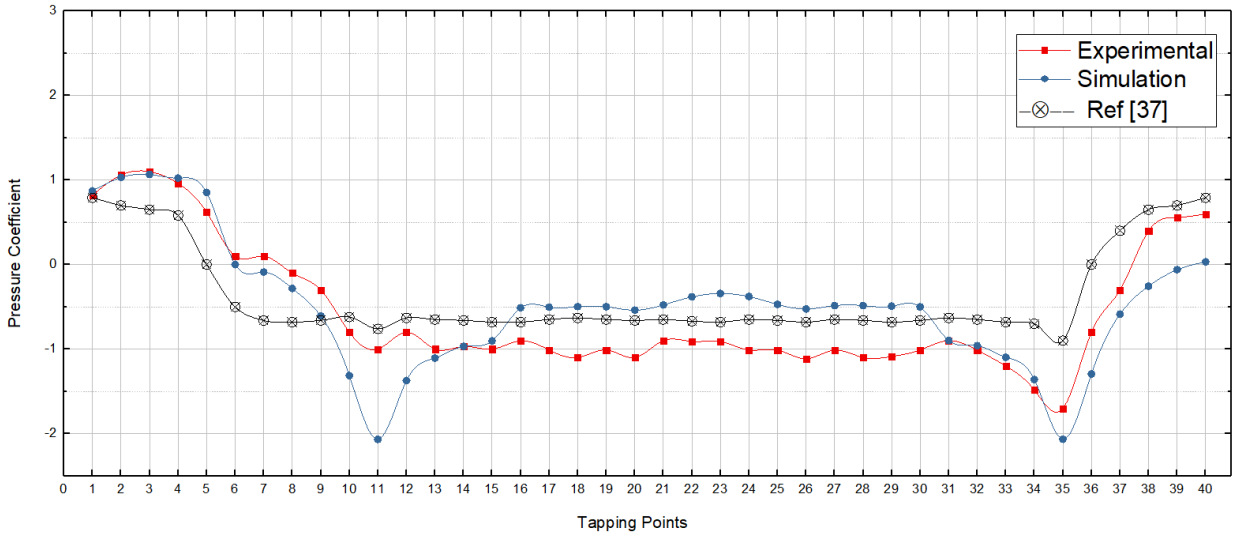

Figure 5. 13: Distribution of Pressure Coefficient on Octagonal Cylinder in a group and for a single octagonal cylinder [37] at 0^0Angle of Attack

The coefficient of pressure of octagonal section in the downstream of the group of cylinders is compared with the one obtained for a single octagonal section placed in airstream [37]. On careful observation, a similar trend is observed. The deviations found for the experimental and simulation data for the octagonal section as part of a group are due to the influence on the airflow in its upstream side caused by the presence of pentagonal and hexagonal sections.

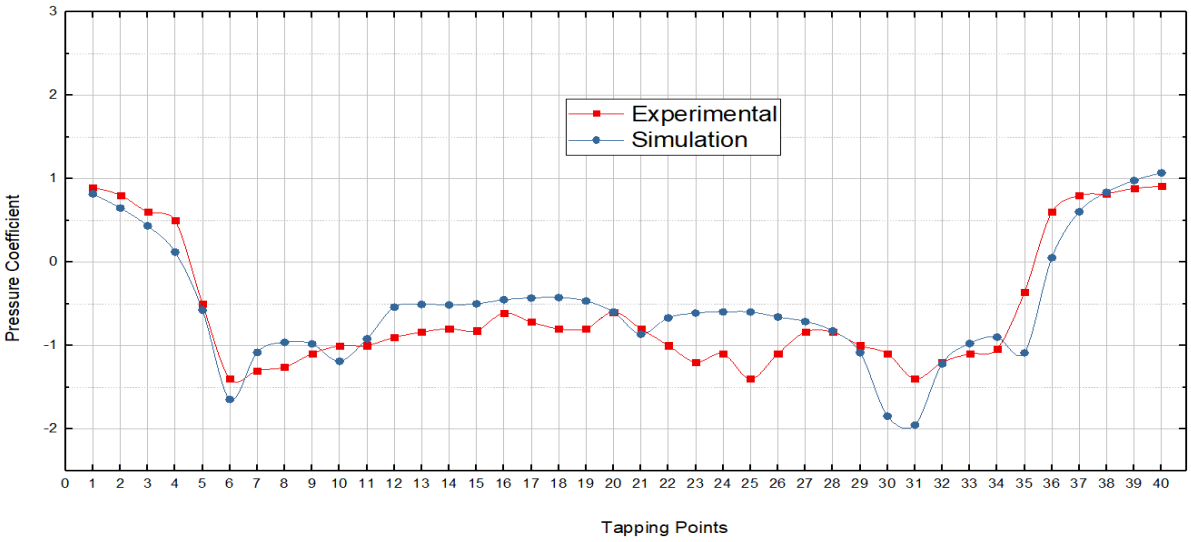

Figure 5. 14: Distribution of Pressure Coefficient on Octagonal Cylinder at 30^0Angle of Attack

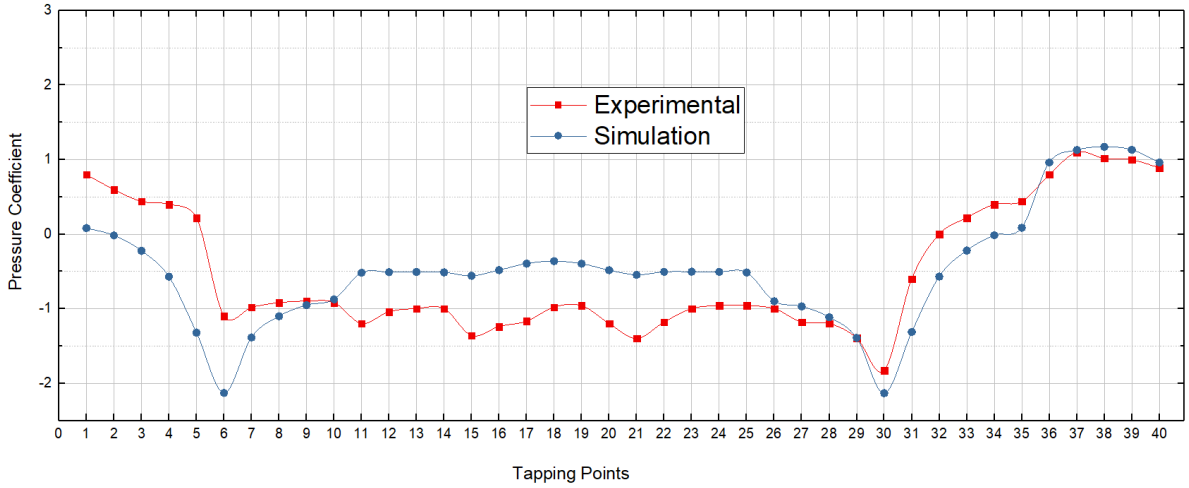

Figure 5. 15: Distribution of Pressure Coefficient on Octagonal Cylinder at 45^0Angle of Attack

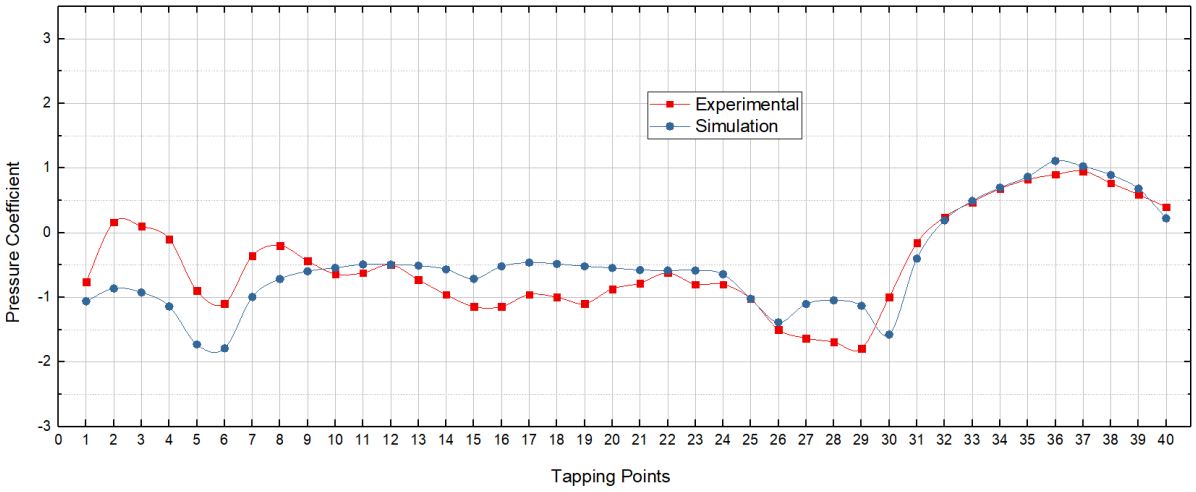

Figure 5. 16: Distribution of Pressure Coefficient on Octagonal Cylinder at 60^0Angle of Attack

5.2 Pressure Contour, Velocity Streamline and Velocity Contour

The pressure contours, are represented in figures 5.17 to 5.20, figures 5.21 to 5.24 and figures 5.25 to 5.28 respectively. The pressure contour provides a visual understanding of the coefficient of pressure distribution for the three cylinders in staggered form as discussed previously. As per the scale on left, red and orange colours indicate higher pressure, whereas green and yellow colours indicate comparatively lower pressure zones. At 30° Angle of Attack, due to the front facing corners in all three cylinders, highest pressure, larger pressure zone with highest back pressure is found. At 45° Angle of Attack, least back pressure is observed than any other Angle of Attack.

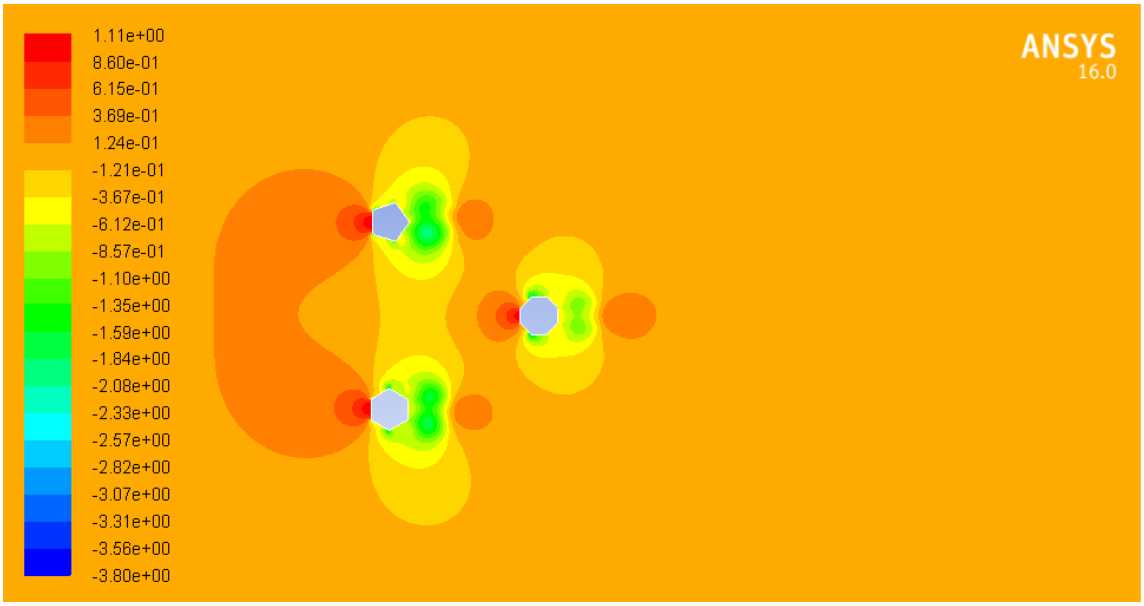

Figure 5. 17: Contours of Pressure Coefficient at 0^0 Angle of Attack

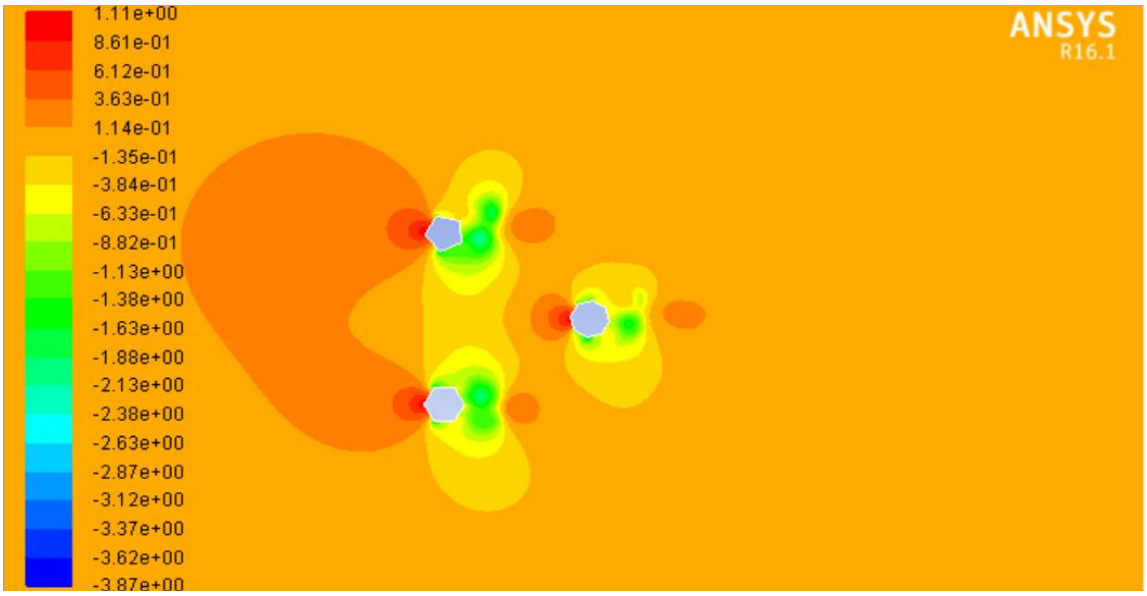

Figure 5. 18: Contours of Pressure Coefficient at 30^0 Angle of Attack

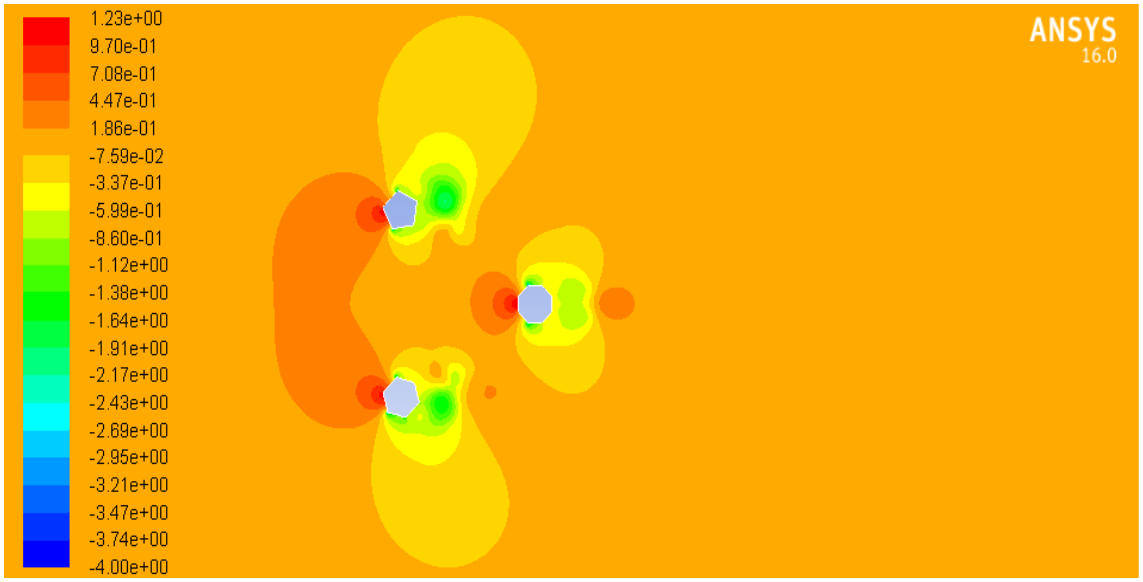

Figure 5. 19: Contours of Pressure Coefficient at 45^0 Angle of Attack

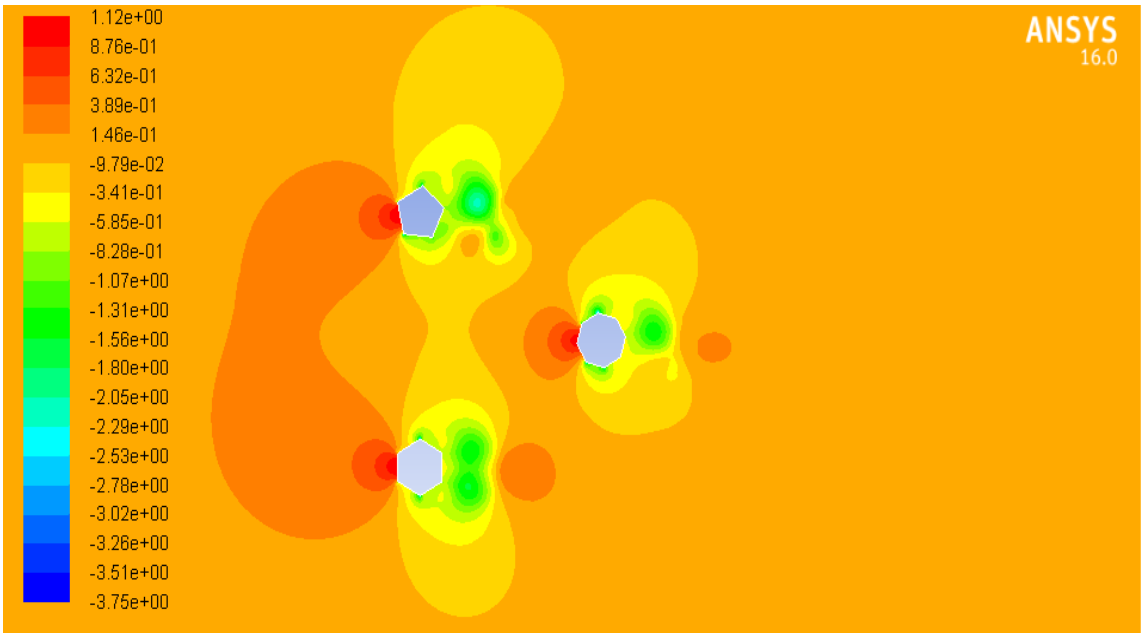

Figure 5. 20: Contours of Pressure Coefficient at 60^0 Angle of Attack

Velocity streamline and velocity contour provide an excellent impression of the flow in 2D to help easily understand the change in velocity and flow of air around the group of cylinders. From the figure 5.21 to 5.24, it can be noticed that flow separation is created in the wake region at angles of attack of 30˚ and 45˚. In case of 30˚ and 60˚ Angle of Attack, backflow is present. Due to the extended corners towards the front of all three cylinders, maximum flow disturbance can be observed at Angle of Attack 30˚. Also, the velocity is higher at adjacent surface of the wind facing side as the wind flows through the contact surface.

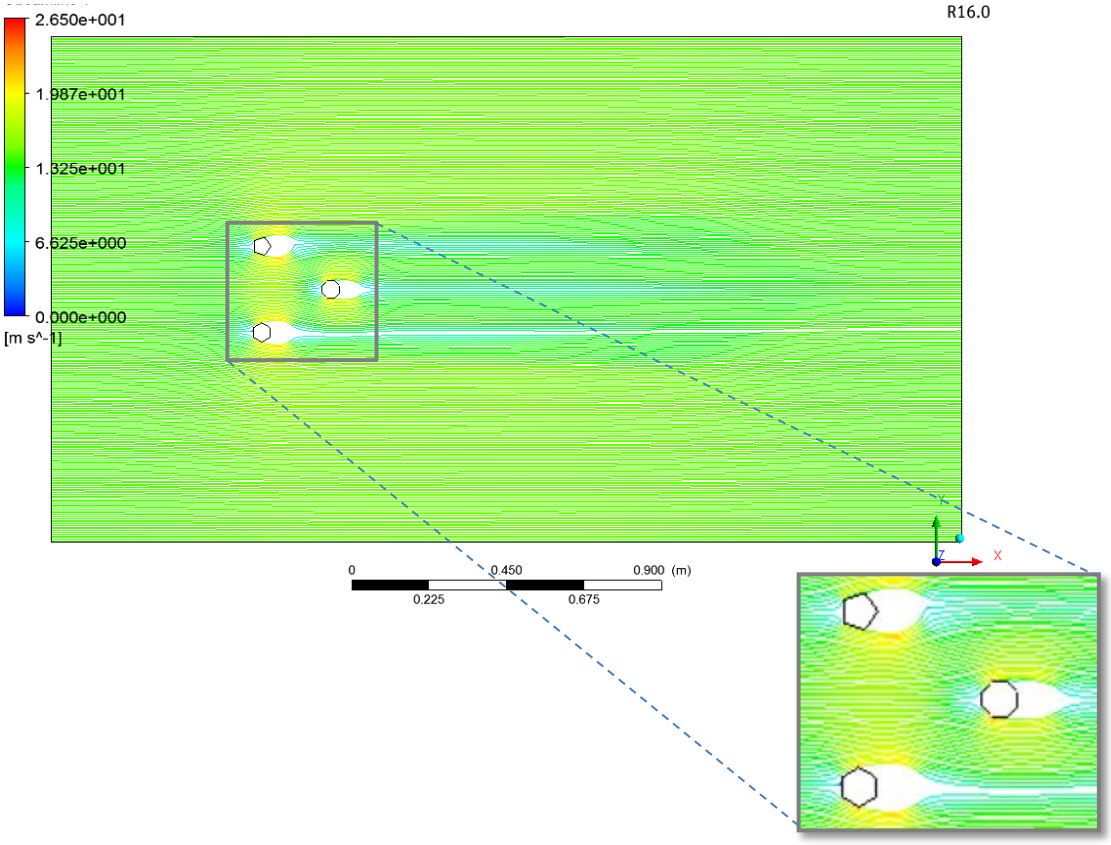

Figure 5.21: Velocity Streamline at 0^0 Angle of Attack

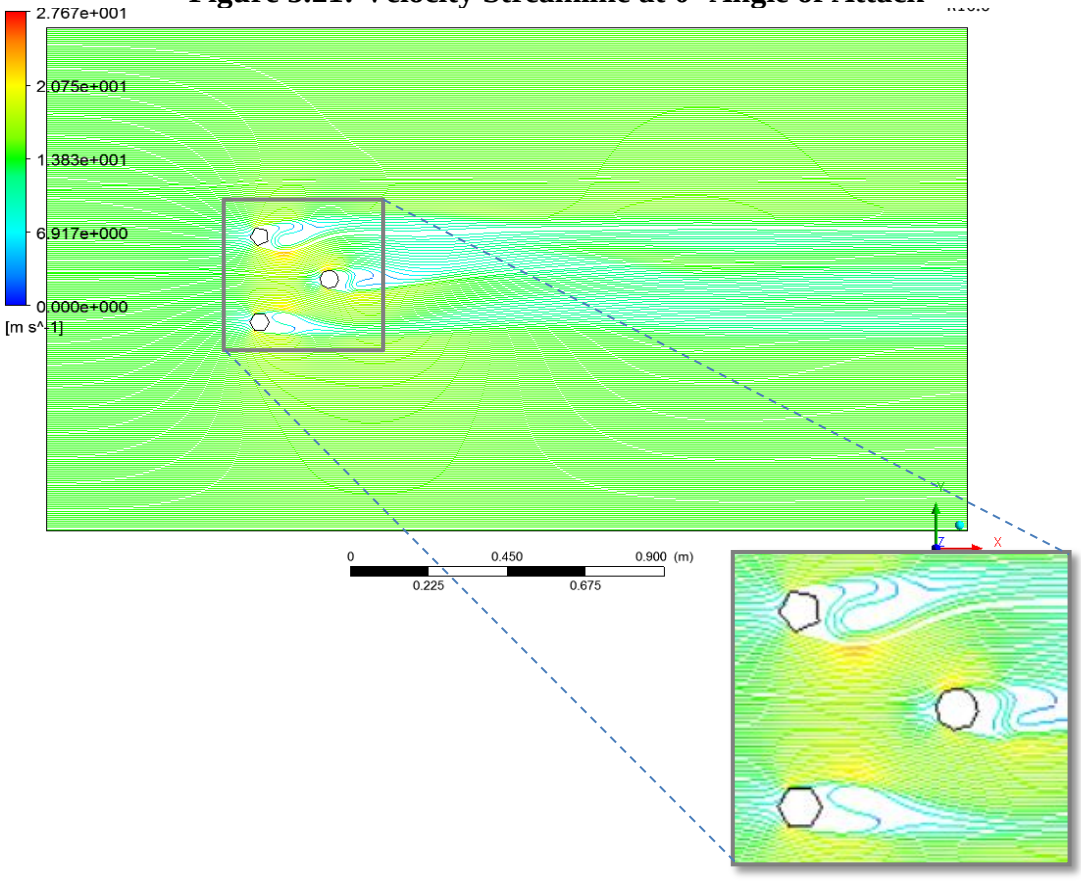

Figure 5.22: Velocity Streamline at 30^0 Angle of Attack

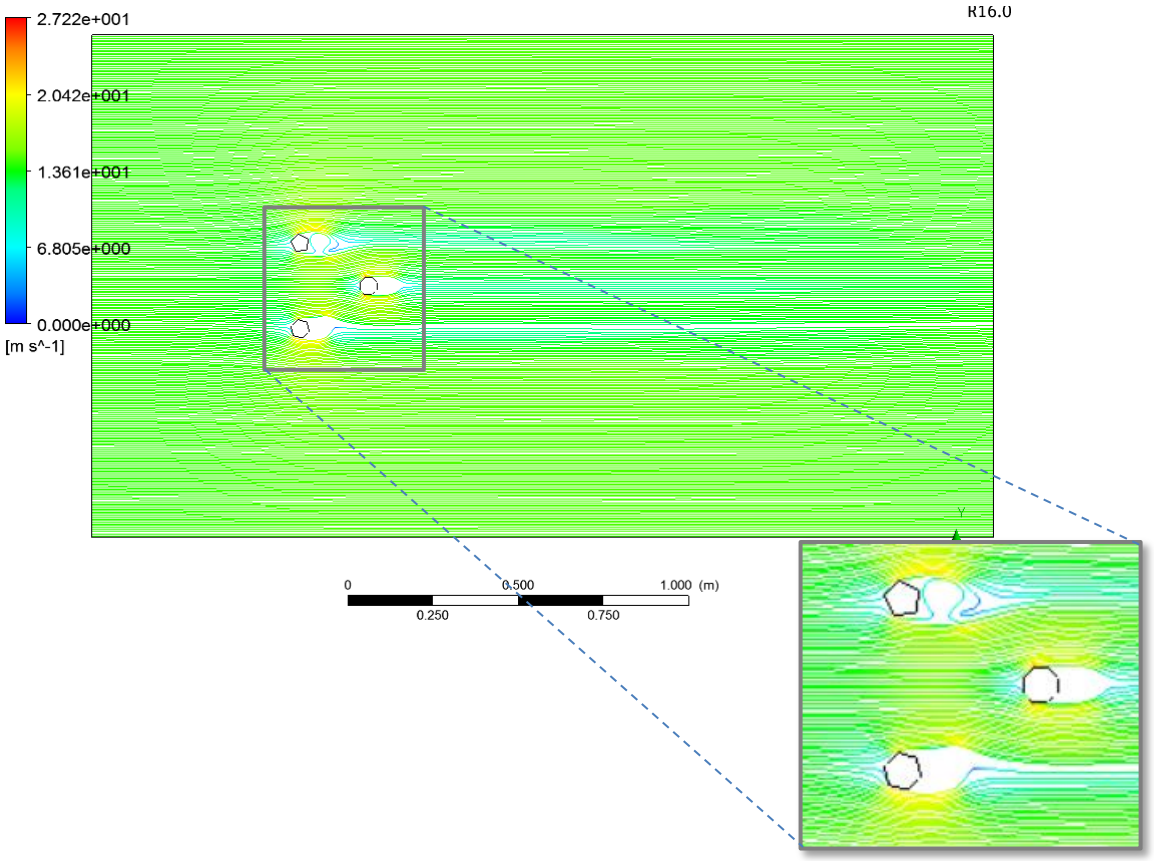

Figure 5.23: Velocity Streamline at 45^0 Angle of Attack

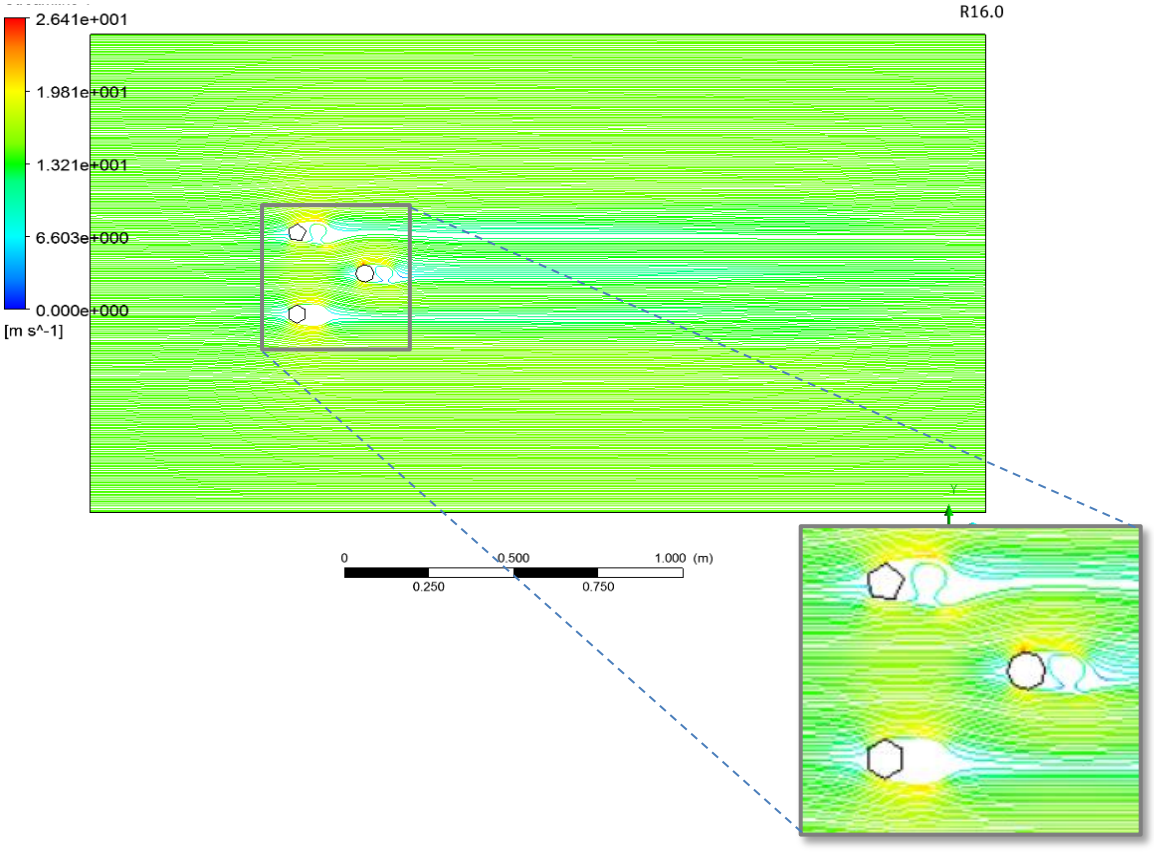

Figure 5.24: Velocity Streamline at 60^0 Angle of Attack

In the velocity contour (Fig 5.25 to 5.28), the red colors indicate the venturi effect between the cylinders and dark blue areas show the eddies behind the cylinders. The light green color (contours) in the downstream areas show how the group of cylinders influence the airflow around and behind them. The lowest velocity i.e. stagnation points are found on the front faces of cylinders at all Angle of Attack. Again at 30˚ Angle of Attack, the highest interference of airflow and flow separation is also observed.

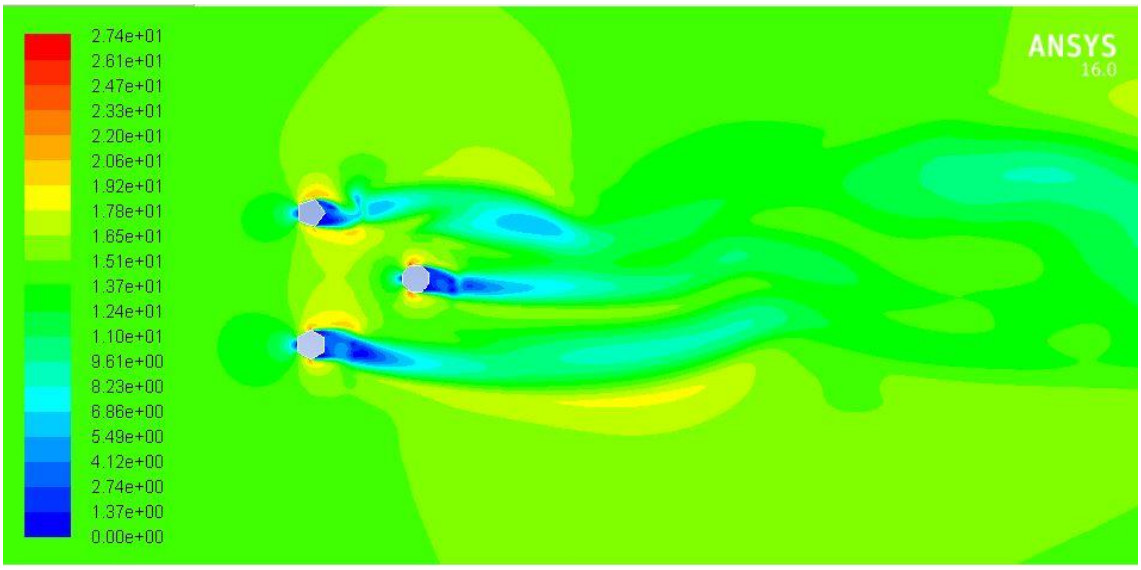

Figure 5. 25: Contours of Velocity Magnitude at 0^0 Angle of Attack

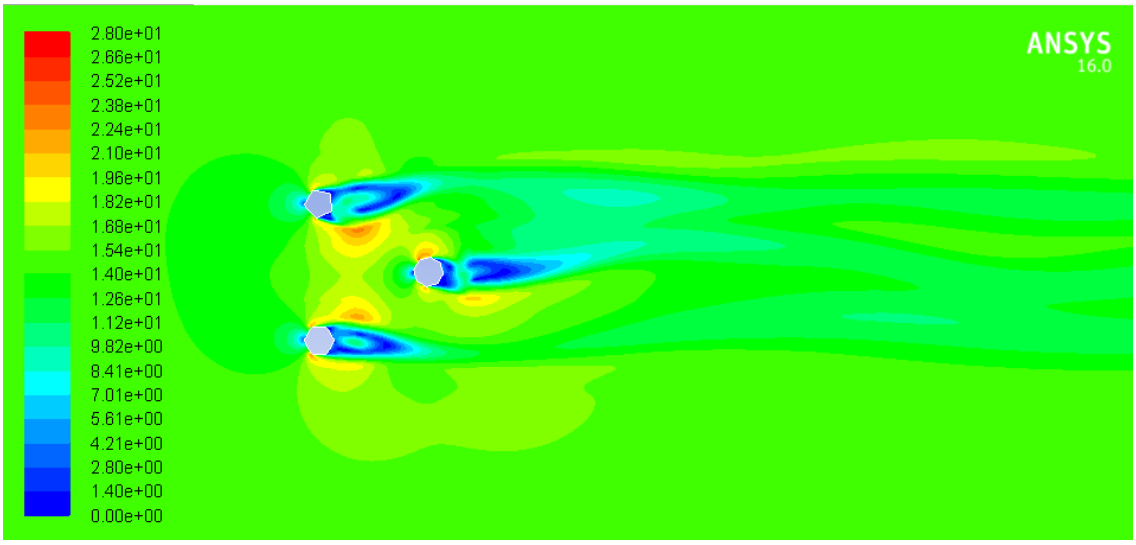

Figure 5. 26: Contours of Velocity Magnitude at 30^0 Angle of Attack

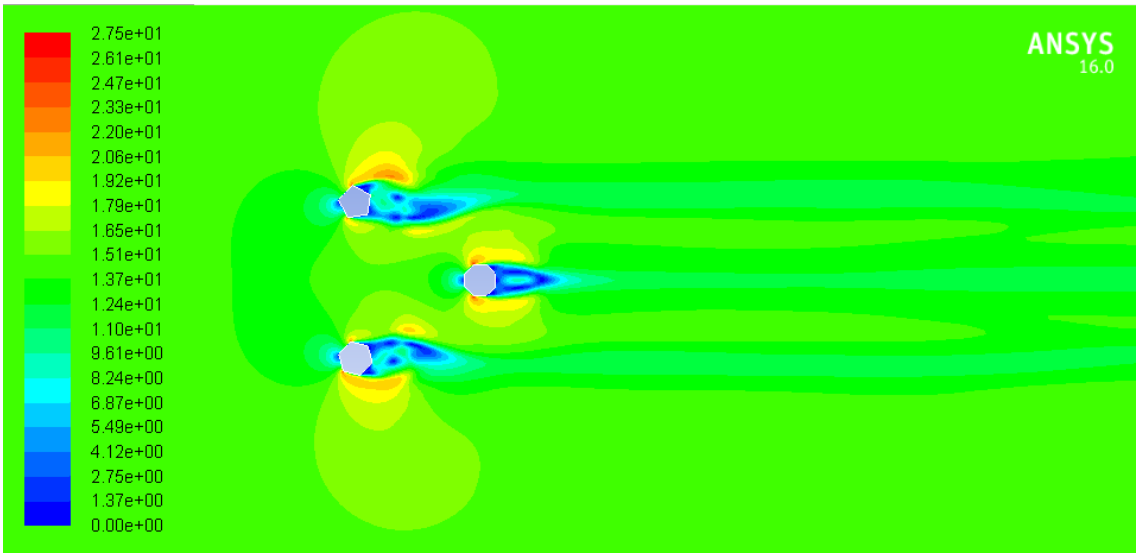

Figure 5. 27: Contours of Velocity Magnitude at 45^0 Angle of Attack

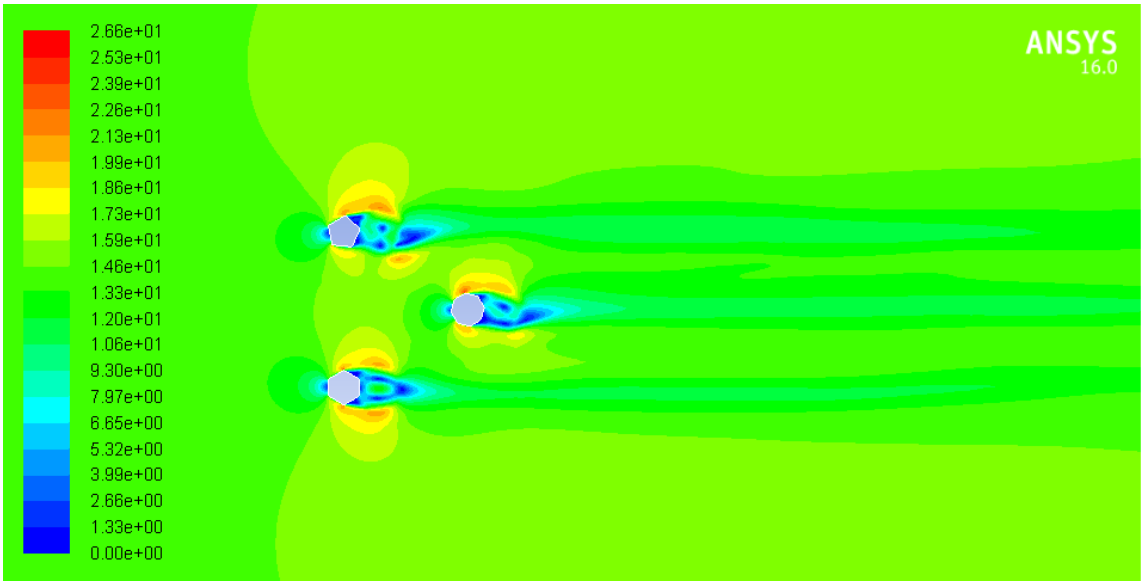

Figure 5. 28: Contours of Velocity Magnitude at 60^0 Angle of Attack

5.3 Variation of Drag and Lift Coefficient on Different Shapes

The dimensionless coefficients CD and CL are used to quantify the drag and lift respectively. A lower drag coefficient and higher lift coefficient indicates the object will have less aerodynamic or hydrodynamic resistance. In figures 5.11 and 5.12, the variation of drag and lift at different angles of attack are presented for different shapes. After analyzing the experimental values (Annex B) to the simulation, the maximum drag (1.37) and minimum lift (-0.16) is found to be attained at angle of attack of 30˚ for pentagonal cylinder, where sharp rise and drop is observed respectively. Here it should be noted that this drag is a prediction of the

force acting on the structure itself. Overall, octagonal cylinder has the lowest values of drag coefficient (0.69) as its shape is similar to the circular shape that facilitate streamline airflow. Average vales of coefficient of drag for pentagonal, hexagonal and octagonal sections are 1.13, 1.02 and 0.74 respectively.

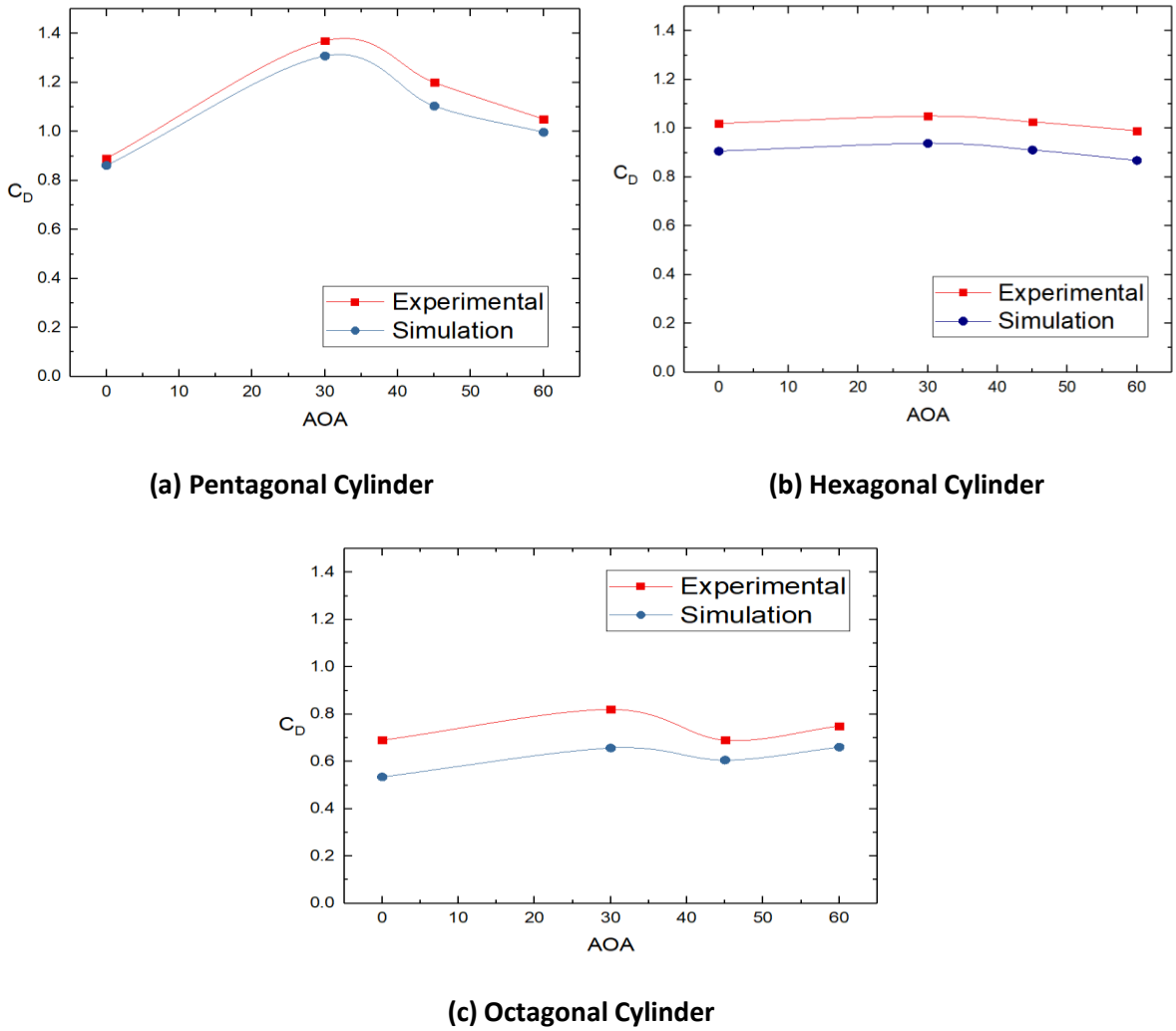

(a) Pentagonal Cylinder **(b) Hexagonal Cylinder**

(c) Octagonal Cylinder

Figure 5. 29: Variation of Coefficient of Drag at different angles of attack for Pentagonal structure, Hexagonal structure and Octagonal structure

The variation of the lift coefficient on cylinders is not significant and they are nearly zero. Within the staggered cylinders, maximum lift coefficient (0.3) is found in octagonal cylinder at 60˚ angle of attack. The minimum lift is observed at angle of attack of 45˚ for hexagonal cylinder (-0.7). Also, substantial drop to lowest value is observed due to its slightly skewed orientation at the same angle. Mentionable, at 30˚ angle of attack, although small, but the maximum eccentricity between experimental and simulation data (~0.5) is observed for hexagonal section, which may be attributed to human error in data handling. Average vales of

coefficient of lift for pentagonal, hexagonal and octagonal sections are -0.12, -0.43 and -0.15 respectively.

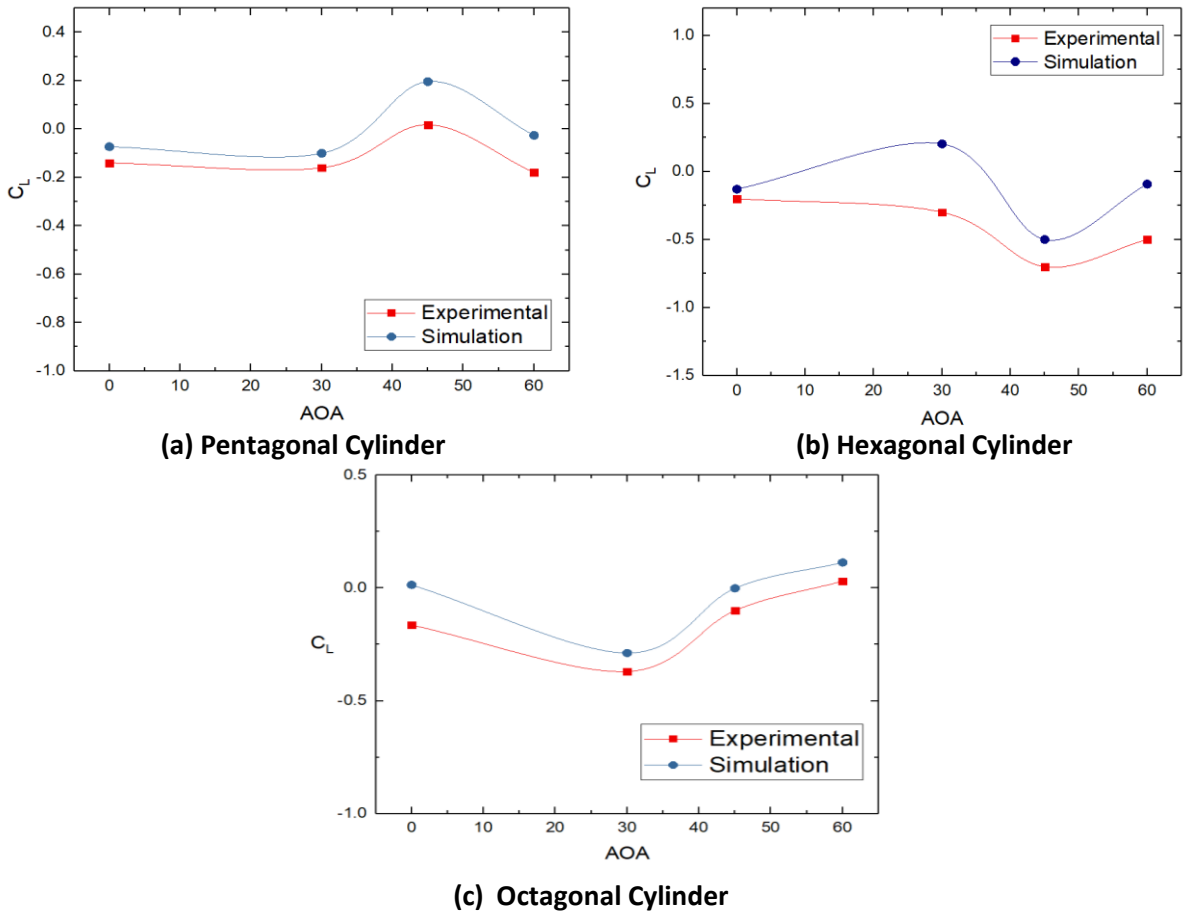

Figure 5. 30: Variation of Coefficient of Lift at Different Angles of Attack for Pentagonal Structure, Hexagonal Structure and Octagonal structure

From these representations, a suitable arrangement can be recommended for these specific shapes. Furthermore, the experimental values calculated for drag coefficient exceed the values of simulation but lags behind in case of the coefficient of lift because of the availability of smoother surface in case of simulation. In real case scenario, the roughness present and discontinuations on the surface will considerably increase the drag force acting on structure of similar arrangement. Hence, a correction factor may be used in calculation.

5.4 Error in Measurements

During measurement of the surface static pressures on the cylinders for several days, the room temperature is assumed to be constant. As such the density of the air is taken as constant in the calculation. In reality, there is minor variation of the temperature during taking all the readings,

which has been neglected in the calculation. The fluctuation of the manometer reading was observed especially on the suction side of the cylinders. But that fluctuation was not significant. While taking the reading, always the mean value of the manometer was recorded. Since fluctuation was insignificant the error in the measured values was negligible.

CHAPTER-6
CONCLUSIONS AND RECOMMENDATIONS

6.1 Conclusions

The following conclusions are drawn in regard to the wind effect on the staggered formation of the pentagonal, hexagonal and octagonal cylinders:

1. The stagnation point is found on the front faces of cylinders at all Angles of Attack.

2. Overall, the pentagonal cylinder has the highest and octagonal cylinder has the lowest values of drag coefficient as the later has a shape closest to the circular shape that facilitate streamlined airflow. Average vales of coefficient of drag for pentagonal, hexagonal and octagonal sections are 1.13, 1.02 and 0.74 respectively.

3. The variation of the lift coefficient on cylinders is not significant and they are nearly zero, but in case of 45˚ angle of attack in hexagonal cylinder, substantial drop to lowest value is observed due to its slightly skewed orientation at that angle. Average vales of coefficient of lift for pentagonal, hexagonal and octagonal sections are -0.12, -0.43 and -0.15 respectively.

4. The drag and lift coefficients complement each other well.

5. Maximum drag, interference of air flow including flow separation and backflow are observed at 30˚ angle of attack when all three cylinders have one corner and two adjacent surfaces at a steep angle facing upstream with the flow direction.

6. Minimum interference and nearly streamline flow pattern around the group of cylinders is observed at 45˚ angle of attack.

7. Overall, theoretical results agree well with the experimental results. Slight deviations observed are due to the surface roughness of the experimental models and human error.

8. The outcome of the present results may be applied while wind load is to be considered for the design of a group of buildings having similar cross-section and orientation.

6.2 Recommendations

For further study in relation to the present work the following recommendations are provided below.

1. Models with different arrangements e.g. different shapes and sizes with variation of inter-spacing between them may be taken into consideration to investigate wind loading and flow patterns.

2. Similar study with design modification in structures e.g. rounded corners, tapping on surface edges, surfaces with more roughness or extended portion etc can be carried out replacing the sharp corners to observe the effect on wind loading.

3. The effect of Reynolds number may be investigated on a single and group of cylinders.

4. The wind shear may be considered in performing the study to see its effect on the wind load.

REFERENCES

[1] Pidwirny M., "Fundamentals of Physical Geography", Michael Pidwirny & Scott Jones, 2nd Edition Online, 2006.

[2] Lawson, T.V., "Wind Loading of Buildings, Possibilities from a Wind Tunnel Investigation," University of Bristol, U.K., Bristol, Report on TVL /731A, 1975.

[3] Castro, J.P. and Fackwell, J.E., "A Note on Two- Dimensional Fence Flows with Emphasis on Wall Constant", *Journal of Wind Engineering and Industrial Aerodynamics,* Vol 3(1), March 1978.

[4] Davenport, A.G., "A Rationale for Determination of Design Wind Velocities," *Journal of American Society of Civil Engineers*, Vol. 86, pp. 39-66, 1960.

[5] Lanoville, A., Gateshore, I.S. and Parkinsoon, G.V., "An Experimental of some Effects of Turbulence on Bluff bodies," *Proceeding of the 4th International Conference on Wind Effects on Buildings and Structure,* London, UK, pp. 333-341, 1975.

[6] Baines, W. D., "Effects of Velocity Distribution on Wind Loads and Flow Patterns on Buildings," *Proceedings of a Symposium on Wind Effects on Buildings and Structures,* Teddington, UK, pp. 197-225, 1963.

[7] Barriga, A.R., Crowe, C.T and Roberson, J.A., "Pressure Distribution on a Square Cylinder at a Small Angle of attack in a Turbulent Cross Flow", *Proceedings of the 4th International Conference on Wind Effects on Buildings,* London, U.K., pp. 89-93, 1975.

[8] Bearman, P.W. and Truman, D.M., "An Investigation of the Flow Around Circular Cylinders", The Aeronautical Quarterly, Vol. 23, pp. 229-237, 1971.

[9] Biswas, N., "An Experimental Investigation of Wind load on Tall Buildings with Square Cross-section having Rounded Facet," *M. Sc. Engg Thesis*, Mechanical Engineering Department, BUET, Bangladesh, 2008.

[10] Bostock, B.R and Mair, W.A., "Pressure Distributions and Forces on Rectangular and D-Shaped Cylinders," The Aero- Dynamical Quarterly, Vol. 23, pp. 499-511, 1972.

[11] Islam, A.T.M. and Mandal, A.C., "Experimental Analysis of Aerodynamic Forces for Cross- flow on Single Rectangular Cylinder", Mechanical Engineering Research Bulletin, BUET, Dhaka, Bangladesh, Vol. 13, pp. 36-51, 1990.

[12] Farok, G.M.G., "*An Experimental Investigation of Wind Effect on Rectangular Cylinders with Rounded Corners*", *M. Sc. Engg Thesis,* Mechanical Engineering Department, BUET, Bangladesh, 2004.

[13] Davis, R.W and Moore, E.F., "A Numerical Study of Vortex Shedding from Rectangular Cylinders", *Journal of Fluid Mechanics,* Vol. 116, pp. 475-506, 1982.

[14] Lee, B.E., "The Effect of Turbulence on the Surface Pressure Field of a Square Prism", *Journal of Fluid Mechanics,* Vol. 6, pp. 263-282, 1975.

[15] Mandal, A.C. and Farok, G.M.G., "An Experimental Investigation of Static Pressure Distributions on Square and Rectangular Cylinders with Rounded Corners", *Proceedings of the 4th International Conference on Heat Transfer, Fluids Mechanics and Thermodynamics (HEFAT),* Cairo, Egypt, 2005.

[16] Hussain, H.S. and Islam, O., "Study of Wind Load on Buildings and Structures", *Journal of the Institution of Engineers, Bangladesh,* Vol. 1. No. 2-3, July - October, 1973.

[17] Hossain, M.K.M., Islam, M.Q, Mandal, A.C and Saha, S., "Wind Effect on Staggered Square Cylinders of Square and Rectangular Sections with Variable Longitudinal Spacing", Transaction of the Mechanical Engineering Division, The Institution of Engineers, Bangladesh, Vol. ME 38, pp. 52-57, 2007.

[18] Islam, A. M. T. and Mandal, A. C., "Static Pressure Distribution for Cross- flow on Single Rectangular Cylinders", Mechanical Engineering Research Bulletin, BUET, Dhaka, Bangladesh, Vol. 14, No. 1, pp. 8-23, 1991.

[19] Islam, A.M.T. and Mandal, A.C., "Effect of Longitudinal Spacing on Static Pressure Distribution of Rectangular Cylinders", Mechanical Engineering Research Bulletin, BUET, Dhaka, Bangladesh, Vol. 15, No. 1, pp. 22-47, 1992.

[20] Koening, K. and Roshiko, A., "An Experimental Study of Geometrical Effects on the Drag and Flow Field of Two Bluff Bodies Separated by a Gap", *Journal of fluid Mechanics,* Vol. 156, pp. 167-204, 1985.

[21] Leutheusser, J., "Static Wind Loadings of Grouped Buildings", *Proceedings of the 3rd International Conference on Wind Effects on Buildings,* Tokyo, Japan, pp. 211-220, 1971.

[22] Mandal, A.C. and Islam, O., "A Study of Wind Effect on a Group of Square Cylinders with Variable Transverse and Longitudinal Spacing", *The Institution of Engineers, Bangladesh,* Vol. 9. No.1, pp. 33-39, January, 1981.

[23] Matsumoto, M., "The Dynamical Forces Acting on the Vibrating Square Prism in a Steady Flow", *Proceedings of the 3rd International Conference on Wind Effects on Buildings and Structures,* Tokyo, Japan, pp. 921-930, 1971.

[24] Nakamura, Y. and Matsukawa, T., "Vortex Excitation of Rectangular Cylinders with a long side normal to the Flow", *Journal of the Fluid Mechanics,* Vol. 137, pp. 171-191, 1987.

[25] Nakamura, Y. and Ohya, Y., "The Effects of Turbulence on the Main Flow past Square Rods", *Journal of Fluid Mechanics,* Vol. 137, pp. 331-345, 1983.

[26] Nakamura, Y. and Yujioha, "Vortex Shedding from Square Prisms in Smooth and Turbulent Flows", *Journal of Fluid Mechanics,* Vol. 164, pp. 77-89, 1986.

[27] Roberson, J. A, Chi Y.L., Rutherford, G. S. and Stine, M. D., "Turbulence Effects on Drag of Sharp- edged Bodies", *Journal of Hydraulics Division,* Vol. 98, pp. 1187-1201, 1972.

[28] Roberson, J.A, Crowe, C.T and Tseng, R., "Pressure Distribution on Two and Three Dimensional Models at Small Angles of Attack in Turbulent flow", *Proceeding of the 2nd U.S. National Conference on Wind Engineering Research,* Colorado, June 22-25, 1975.

[29] Sakamoto, H. and Arie, M., "Vortex Shedding from a Rectangular Prism and a Circular Cylinder Placed Vertically in turbulent Boundary Layer", *Journal of Fluid Mechanics,* Vol. 126, pp. 147-165, 1983.

[30] Vickery, B. J., "Fluctuating Lift and Drag on a Long Cylinder of Square Cross section in a Smooth and in a Turbulent Stream", *Journal of Fluid Mechanics,* Vol. 25, pp. 481-491, 1966.

[31] Whitbread, R. E. "Model Simulation of Wind Effects on Structures", *Proceedings of a Symposium on Wind Effects on Buildings and Structures,* Teddington, U.K., pp. 283-301, 1963.

[32] Hayashi, M. Akirasakurai and Yujiohya., "Wake interference of a Row of Normal Flat Plates Arranged Side by Side in a Uniform Flow", *Journal of Fluid Mechanics,* Vol. 164, pp. 1-25, 1986.

[33] Okajima, A., "Strouhal Numbers of Rectangular Cylinders", *Journal of Fluid Mechanics,* Vol. 123, pp. 379-398, 1982.

[34] Cochran, L. S., and Cermak, J. E., "Full and Model Scale Cladding Pressures on the Texas Tech University Experimental Building", *Journal of Wind Engineering and Aerodynamics,* Vol. 43, pp. 1589-1600, 1992.

[35] Islam, T., "An Experimental Investigation of Wind Effect on Rectangular Cylinders", *M. Sc. Engg. Thesis,* Department of Mechanical Engineering, BUET, Bangladesh, 1988.

[36] Sultana, K. R., "An Experimental Investigation of Wind Load on Tall Buildings with Hexagonal Cross-Section", *M. Sc. Engg. Thesis,* Department of Mechanical Engineering, BUET, Bangladesh, 2009.

[37] Hossain, M. J., Islam, M. Q., and Ali, M., "An Experimental Investigation of Wind Load on Tall Buildings with Octagonal Cross-Section," *International Journal of Renewable Energy Research,* Vol. 3, No. 1, 2013.

[38] Nakamura, Y. and Yujioha., "Vortex Shedding from Square Prisms in Smooth and Turbulent Flows," *Journal of Fluid Mechanics,* Vol. 164, pp. 77-89, 1986.

[39] McClean, J.F. and Sumner D.D., "An Experimental Investigation of Aspect Ratio and Incidence Angle Effects for the Flow Around Surface-Mounted Finite-Height Square Prisms," *ASME Journal of Fluid Engineering,* Vol. 136(8), pp. 081206-081206-10, 2014.

[40] Anwar, P., "An Experimental Investigation of Wind Effect on Square, Pentagonal and Hexagonal Staggered Cylinders", *M. Sc. Engg. Thesis,* Department of Mechanical Engineering, BUET, Bangladesh, 2016.

[41] Bearman, P. W. and Wadcock, A. J., "The Interaction between a pair of Circular Cylinders Normal to a Stream", *Journal of the Fluid mechanics,* Vol. 61, pp. 499-511, 1973.

[42] Lawson, T. V., "Wind Loading of Buildings, Possibilities from a Wind Tunnel Investigation", University of Bristol, U.K. Report no TVL /731A, August, 1975.

[43] Cochran, L. S. and Cermak, J. E., "Full and Model Scale Cladding Pressures on the Texas Tech University Experimental Building," *Journal of Wind Engineering and Aerodynamics,* Vol. No .43, pp. 1589-1600, 1992.

[44] Franc, N., "Model Law and Experimental Technique for Determination of Wind Loads on Buildings", *Proceedings of the 1st International Conferences on Wind Effects on Building and Structure,* Teddington, London, 1963.

[45] Mandal, A.C., "A Study of Wind Effects on Square Cylinders", *M. Sc. Engg. Thesis,* Department of Mechanical Engineering, BUET, Bangladesh, 1979.

[46] Lamb, H, "Hydrodynamics", Cambridge University Press, 1932.

[47] Lanoville, A., Gateshore, I. S. and Parkinsoon, G. V., "An Experimental of Some Effects of Turbulence on Bluff Bodies", *Proceeding of the 4th International Conference on Wind Effects on Buildings and Structure,* London, U.K., pp. 333-341, 1975.

[48] Maskell, E. C., "A Theory of Blockage Effects on Bluff Bodies and Stalled Wings in a Closed Wind Tunnel", ARC R&M No. 3400, 1965.

[49] Mchuri, F. G. *et al*, "Effects of the Free Stream Turbulences on Drag Coefficients of Bluff Sharp- Edged Cylinders", *Nature,* Vol. 224, No. 5222, pp. 908-909, November 29, 1969.

[50] Pope, A. and Haper, J.J., "Low Speed Wind Tunnel Testing", John Willy and Sons, New York, 1996.

[51] Parkinson, G.V. and Modi, V.J., "Recent Research on Wind effects on Bluff Two Dimensional Bodies", *Proceedings of International Research Seminar on Wind Effects in Buildings and Structures,* Ottawa, Canada, pp. 485-514, 1967.

[52] Robertson, J. M., "Pressure field at Reattachment of Separated flows", *Proceeding of the 2nd U.S. National Conference on Wind Engineering Research,* Colorado, June 22-25, 1975.

[53] Steggel, N., "A Numerical Investigation of the Flow Around Rectangular Cylinders," *Doctor of Philosophy Thesis,* School of Mechanical and Materials Engineering., The University of Surrey, Guildford, U.K., 1998.

[54] Surry, D., "Pressure Measurements on the Texas Tech Buildings, Wind Tunnel Measurements and Comparison with Full Scale", *Journal of Wind Engineering and Aerodynamics,* Vol. 38, pp. 235-247, 1991.

APPENDIX A

Uncertainty Analysis

Sample data: 2, 2.3, 2.2, 2.1, 2.2, 2.3, 2.1, 2.2, 2.05, 2.15 inch of H_2O

If our measurement result is denoted by X, then,

$$X = \bar{X} \pm \Delta X \quad \text{.....(1)}$$

Or, $X = \bar{X} \pm \sigma$

Where, $\bar{X}$ = Average value

ΔX = Uncertainty

σ = Standard deviation

$\Delta X = \sigma$

Again, from equation (1), $X = \bar{X}\left(1 \pm \frac{\Delta X}{\bar{X}}\right)$

Here, $\frac{\Delta X}{\bar{X}}$ = Fractional Uncertainty

Percent Uncertainty = Fractional Uncertainty × 100

Now, $\bar{X} = \frac{\sum_{i=1}^{N} X_i}{N}$

or, $\bar{X} = \frac{X1 + X2 + X3 + \ldots\ldots\ldots\ldots\ldots\ldots + XN}{N}$

or, $\bar{X} = \frac{2 + 2.3 + 2.2 + 2.1 + 2.2 + 2.3 + 2.1 + 2.2 + 2.05 + 2.15}{10}$

$= 2.16$

$$\sigma = \sqrt{\frac{\sum_{i=1}^{N}(X_i - \bar{X})^2}{N-1}}$$

$$= \sqrt{\frac{(X1 - \bar{X})^2 + (X2 - \bar{X})^2 + \ldots\ldots\ldots\ldots\ldots\ldots + (XN - \bar{X})^2}{N-1}}$$

$\Rightarrow \sigma$ or $\Delta X = 0.099449$

So, $\frac{\Delta X}{\bar{X}} = \frac{0.099449}{2.16} = 0.04603838$

Percent Uncertainty = 0.04603838× 100 = 4.6%

$X = \bar{X} \pm \Delta X = 2.16 \pm 0.046038$

APPENDIX B

Experimental Data

1. Distribution of Pressure Coefficient on Pentagonal cylinder at Angle of Attack of $\alpha = 0^0$

Tapping Point	Final Reading (inch of H_2O)	Final Reading (mm of H_2O)	Initial Reading (mm of H_2O)	Differences, Δh_w (mm of H_2O)	Pressure Coefficient, Cp	Tapping Point	Final Reading (inch of H_2O)	Final Reading (mm of H_2O)	Initial Reading (mm of H_2O)	Differences, Δh_w (mm of H_2O)	Pressure Coefficient, Cp
1	1.65	41.91	48.26	6.35	0.50	14	2.2	55.88	48.26	-7.62	-0.60
2	0.69	17.59	48.26	30.67	0.80	15	2.4	60.96	48.26	-12.7	-1.00
3	0.54	13.72	48.26	34.54	0.89	16	2.1	53.34	48.26	-5.08	-0.40
4	0.75	19.05	48.26	29.21	0.76	17	2.2	55.88	48.26	-7.62	-0.60
5	1.75	44.39	48.26	3.87	0.32	18	2.3	58.42	48.26	-10.16	-0.80
6	2.05	52.07	48.26	-3.81	-0.30	19	2.1	53.34	48.26	-5.08	-0.40
7	2.7	68.58	48.26	-20.32	-1.60	20	2.2	55.88	48.26	-7.62	-0.60
8	2.8	71.12	48.26	-22.86	-1.80	21	2.05	52.07	48.26	-3.81	-0.30
9	2.45	62.23	48.26	-13.97	-1.10	22	2	50.8	48.26	-2.54	-0.20
10	2.4	60.96	48.26	-12.70	-1.00	23	2.05	52.07	48.26	-3.81	-0.30
11	2	50.8	48.26	-2.54	-0.20	24	2.15	54.61	48.26	-6.35	-0.50
12	2.3	58.42	48.26	-10.16	-0.80	25	2.35	59.69	48.26	-11.43	-0.90
13	2.4	60.96	48.26	-12.70	-1.00						

2. Distribution of Pressure Coefficient on Pentagonal cylinder at Angle of Attack of $\alpha = 30^0$

Tapping Point	Final Reading (inch of H_2O)	Final Reading (mm of H_2O)	Initial Reading (mm of H_2O)	Differences, Δh_w (mm of H_2O)	Pressure Coefficient, Cp	Tapping Point	Final Reading (inch of H_2O)	Final Reading (mm of H_2O)	Initial Reading (mm of H_2O)	Differences, Δh_w (mm of H_2O)	Pressure Coefficient, Cp
1	1.65	41.91	48.26	6.35	0.50	14	2	50.8	48.26	-2.54	-0.20
2	1.71	43.39	48.26	4.87	0.40	15	2.15	54.61	48.26	-6.35	-0.50
3	1.75	44.55	48.26	3.71	0.30	16	2.1	53.34	48.26	-5.08	-0.40
4	1.82	46.24	48.26	2.02	0.08	17	2.2	55.88	48.26	-7.62	-0.60
5	2.22	56.27	48.26	-8.01	-0.68	18	2.25	57.15	48.26	-8.89	-0.70
6	2	50.8	48.26	-2.54	-0.20	19	1.95	49.53	48.26	-1.27	-0.10
7	2.1	53.34	48.26	-5.08	-0.40	20	2.15	54.61	48.26	-6.35	-0.50
8	2.25	57.15	48.26	-8.89	-0.70	21	2.05	52.07	48.26	-3.81	-0.30
9	1.95	49.53	48.26	-1.27	-0.10	22	1.65	41.91	48.26	6.35	0.50
10	2.15	54.61	48.26	-6.35	-0.50	23	1.6	40.64	48.26	7.62	0.60
11	1.95	49.53	48.26	-1.27	-0.10	24	0.51	12.92	48.26	35.34	0.96
12	2.2	55.88	48.26	-7.62	-0.60	25	0.47	11.95	48.26	36.31	0.99
13	2.3	58.42	48.26	-10.16	-0.80						

3. Distribution of Pressure Coefficient on Pentagonal cylinder at Angle of Attack of $\alpha = 45^0$

Tapping Point	Final Reading (inch of H_2O)	Final Reading (mm of H_2O)	Initial Reading (mm of H_2O)	Differences, Δh_w (mm of H_2O)	Pressure Coefficient, Cp	Tapping Point	Final Reading (inch of H_2O)	Final Reading (mm of H_2O)	Initial Reading (mm of H_2O)	Differences, Δh_w (mm of H_2O)	Pressure Coefficient, Cp
1	1.62	41.16	48.26	7.10	0.54	14	2	50.80	48.26	-2.54	-0.20
2	0.54	13.72	48.26	34.54	0.89	15	2.3	58.42	48.26	-10.16	-0.80
3	0.67	17.05	48.26	27.21	0.69	16	2.1	53.34	48.26	-5.08	-0.40
4	1.64	41.75	48.26	6.51	0.46	17	2.2	55.88	48.26	-7.62	-0.60
5	1.8	45.72	48.26	2.54	0.20	18	2.3	58.42	48.26	-10.16	-0.80
6	2.1	53.34	48.26	-5.08	-0.40	19	2	50.81	48.26	-2.54	-0.20
7	2.2	55.88	48.26	-7.62	-0.60	20	2.3	58.42	48.26	-10.16	-0.80
8	2.35	59.69	48.26	-11.43	-0.90	21	2.1	53.34	48.26	-5.08	-0.40
9	2.1	53.34	48.26	-5.08	-0.40	22	1.79	45.35	48.26	2.91	0.24
10	2.4	60.96	48.26	-12.70	-1.00	23	1.58	40.25	48.26	8.01	0.58
11	2	50.80	48.26	-2.54	-0.20	24	0.69	17.59	48.26	30.67	0.76
12	2.18	55.37	48.26	-7.11	-0.56	25	0.53	13.55	48.26	34.71	0.92
13	2.3	58.42	48.26	-10.16	-0.80						

4. Distribution of Pressure Coefficient on Pentagonal cylinder at Angle of Attack of $\alpha = 60^0$

Tapping Point	Final Reading (inch of H_2O)	Final Reading (mm of H_2O)	Initial Reading (mm of H_2O)	Differences, Δh_w (mm of H_2O)	Pressure Coefficient, Cp	Tapping Point	Final Reading (inch of H_2O)	Final Reading (mm of H_2O)	Initial Reading (mm of H_2O)	Differences, Δh_w (mm of H_2O)	Pressure Coefficient, Cp
1	2.10	53.34	48.26	-5.08	-0.40	14	1.98	50.29	48.26	-2.032	-0.16
2	1.75	44.45	48.26	3.81	0.30	15	2.20	55.88	48.26	-7.62	-0.60
3	2.15	54.61	48.26	-6.35	-0.50	16	2.05	52.07	48.26	-3.81	-0.30
4	1.90	48.26	48.26	0.00	0.00	17	2.25	57.15	48.26	-8.89	-0.70
5	2.20	55.88	48.26	-7.62	-0.60	18	2.35	59.69	48.26	-11.43	-0.90
6	2.00	50.8	48.26	-2.54	-0.20	19	2.00	50.8	48.26	-2.54	-0.20
7	2.02	51.31	48.26	-3.048	-0.24	20	2.25	57.15	48.26	-8.89	-0.70
8	2.15	54.61	48.26	-6.35	-0.50	21	2.05	52.07	48.26	-3.81	-0.30
9	1.90	48.26	48.26	0.00	0.00	22	1.64	41.75	48.26	6.51	0.46
10	2.20	55.88	48.26	-7.62	-0.60	23	0.67	17.05	48.26	27.21	0.69
11	2.00	50.8	48.26	-2.54	-0.20	24	0.53	13.55	48.26	34.71	0.92
12	1.68	42.67	48.26	5.588	0.44	25	0.69	17.59	48.26	30.67	0.80
13	2.20	55.88	48.26	-7.62	-0.60						

5. Distribution of Pressure Coefficient on Hexagonal cylinder at Angle of Attack of $\alpha = 0^0$

Tapping Point	Final Reading (inch of H_2O)	Final Reading (mm of H_2O)	Initial Reading (mm of H_2O)	Differences, Δh_w (mm of H_2O)	Pressure Coefficient, Cp	Tapping Point	Final Reading (inch of H_2O)	Final Reading (mm of H_2O)	Initial Reading (mm of H_2O)	Differences, Δh_w (mm of H_2O)	Pressure Coefficient, Cp
1	1.65	41.91	48.26	6.35	0.50	16	2.2	55.88	48.26	-7.62	-0.60
2	1.55	39.37	48.26	8.89	0.70	17	2.1	53.34	48.26	-5.08	-0.40
3	1.45	36.83	48.26	11.43	0.90	18	2.15	54.61	48.26	-6.35	-0.50
4	1.54	39.04	48.26	9.22	0.74	19	2.15	54.61	48.26	-6.35	-0.50
5	1.57	39.94	48.26	8.32	0.65	20	2.1	53.34	48.26	-5.08	-0.40
6	1.75	44.45	48.26	3.81	0.30	21	2.2	55.88	48.26	-7.62	-0.60
7	1.6	40.64	48.26	7.62	0.60	22	2.1	53.34	48.26	-5.08	-0.40
8	1.45	36.83	48.26	11.43	0.90	23	2.15	54.61	48.26	-6.35	-0.50
9	1.75	44.45	48.26	3.81	0.30	24	2.15	54.61	48.26	-6.35	-0.50
10	1.8	45.72	48.26	2.54	0.20	25	2.1	53.34	48.26	-5.08	-0.40
11	2.2	55.88	48.26	-7.62	-0.60	26	2.15	54.61	48.26	-6.35	-0.50
12	2.15	54.61	48.26	-6.35	-0.50	27	2.05	52.07	48.26	-3.81	-0.30
13	2.18	55.37	48.26	-7.112	-0.56	28	2.35	59.69	48.26	-11.43	-0.90
14	2.2	55.88	48.26	-7.62	-0.60	29	2.55	64.77	48.26	-16.51	-1.30
15	2.1	53.34	48.26	-5.08	-0.40	30	2.44	61.976	48.26	-13.72	-1.08

6. Distribution of Pressure Coefficient on hexagonal cylinder at Angle of Attack of $\alpha = 30^0$

Tapping Point	Final Reading (inch of H_2O)	Final Reading (mm of H_2O)	Initial Reading (mm of H_2O)	Differences, Δh_w (mm of H_2O)	Pressure Coefficient, Cp	Tapping Point	Final Reading (inch of H_2O)	Final Reading (mm of H_2O)	Initial Reading (mm of H_2O)	Differences, Δh_w (mm of H_2O)	Pressure Coefficient, Cp
1	1.45	36.83	48.26	11.43	0.90	16	2.15	54.61	48.26	-6.35	-0.50
2	1.48	37.60	48.26	10.66	0.82	17	2.05	52.07	48.26	-3.81	-0.30
3	1.50	38.12	48.26	10.14	0.80	18	2.10	53.34	48.26	-5.08	-0.40
4	1.57	39.94	48.26	8.32	0.65	19	2.10	53.34	48.26	-5.08	-0.40
5	1.67	42.40	48.26	5.86	0.46	20	2.00	50.8	48.26	-2.54	-0.20
6	2.35	59.69	48.26	-11.43	-0.90	21	2.18	55.372	48.26	-7.11	-0.56
7	2.30	58.42	48.26	-10.16	-0.80	22	2.05	52.07	48.26	-3.81	-0.30
8	2.20	55.88	48.26	-7.62	-0.60	23	2.09	53.086	48.26	-4.826	-0.38
9	1.95	49.53	48.26	-1.27	-0.10	24	2.1	53.34	48.26	-5.08	-0.40
10	1.85	46.99	48.26	1.27	0.10	25	1.95	49.53	48.26	-1.27	-0.10
11	2.25	57.15	48.26	-8.89	-0.70	26	1.9	48.26	48.26	0.00	0.00
12	2.1	53.34	48.26	-5.08	-0.40	27	1.55	39.37	48.26	8.89	0.70
13	2.15	54.61	48.26	-6.35	-0.50	28	1.42	36.02	48.26	12.24	0.96
14	2.2	55.88	48.26	-7.62	-0.60	29	1.45	36.83	48.26	11.43	0.90
15	2.05	52.07	48.26	-3.81	-0.30	30	1.45	36.83	48.26	11.43	0.90

7. Distribution of Pressure Coefficient on hexagonal cylinder at Angle of Attack of $\alpha = 45^0$

Tapping Point	Final Reading (inch of H_2O)	Final Reading (mm of H_2O)	Initial Reading (mm of H_2O)	Differences, Δh_w (mm of H_2O)	Pressure Coefficient, Cp	Tapping Point	Final Reading (inch of H_2O)	Final Reading (mm of H_2O)	Initial Reading (mm of H_2O)	Differences, Δh_w (mm of H_2O)	Pressure Coefficient, Cp
1	1.42	36.02	48.26	12.24	0.96	16	2.1	53.34	48.26	-5.08	-0.40
2	1.35	34.32	48.26	13.94	0.94	17	2	50.8	48.26	-2.54	-0.20
3	1.50	38.12	48.26	10.14	0.80	18	2.1	53.34	48.26	-5.08	-0.40
4	1.55	39.37	48.26	8.89	0.70	19	2.08	52.832	48.26	-4.57	-0.36
5	1.6	40.64	48.26	7.62	0.60	20	1.98	50.292	48.26	-2.03	-0.16
6	2.1	53.34	48.26	-5.08	-0.40	21	2.2	55.88	48.26	-7.62	-0.60
7	2.01	51.05	48.26	-2.79	-0.22	22	2.08	52.832	48.26	-4.57	-0.36
8	2.04	51.82	48.26	-3.56	-0.28	23	2.12	53.848	48.26	-5.59	-0.44
9	2.05	52.07	48.26	-3.81	-0.30	24	2.1	53.34	48.26	-5.08	-0.40
10	1.95	49.53	48.26	-1.27	-0.10	25	1.96	49.784	48.26	-1.52	-0.12
11	2.18	55.37	48.26	-7.11	-0.56	26	1.7	43.18	48.26	5.08	0.40
12	2	50.8	48.26	-2.54	-0.20	27	1.55	39.37	48.26	8.89	0.70
13	2.05	52.07	48.26	-3.81	-0.30	28	1.38	34.98	48.26	13.28	0.99
14	2.08	52.83	48.26	-4.57	-0.36	29	1.42	36.02	48.26	12.24	0.96
15	1.98	50.29	48.26	-2.03	-0.16	30	1.45	36.83	48.26	11.43	0.90

8. Distribution of Pressure Coefficient on hexagonal cylinder at Angle of Attack of $\alpha = 60^0$

Tapping Point	Final Reading (inch of H_2O)	Final Reading (mm of H_2O)	Initial Reading (mm of H_2O)	Differences, Δh_w (mm of H_2O)	Pressure Coefficient, Cp	Tapping Point	Final Reading (inch of H_2O)	Final Reading (mm of H_2O)	Initial Reading (mm of H_2O)	Differences, Δh_w (mm of H_2O)	Pressure Coefficient, Cp
1	1.75	44.45	48.26	3.81	0.30	16	2.25	57.15	48.26	-8.89	-0.70
2	1.65	41.91	48.26	6.35	0.50	17	2.15	54.61	48.26	-6.35	-0.50
3	1.67	42.40	48.26	5.86	0.46	18	2.18	55.37	48.26	-7.11	-0.56
4	1.98	50.29	48.26	-2.03	-0.16	19	2.18	55.37	48.26	-7.11	-0.56
5	2.08	52.83	48.26	-4.57	-0.36	20	1.90	48.26	48.26	0.00	0.00
6	2.20	55.88	48.26	-7.62	-0.60	21	2.12	53.85	48.26	-5.59	-0.44
7	2.10	53.34	48.26	-5.08	-0.40	22	2.00	50.80	48.26	-2.54	-0.20
8	2.20	55.88	48.26	-7.62	-0.60	23	2.20	55.88	48.26	-7.62	-0.60
9	2.18	55.37	48.26	-7.11	-0.56	24	2.50	63.50	48.26	-15.24	-1.20
10	2.00	50.80	48.26	-2.54	-0.20	25	2.05	52.07	48.26	-3.81	-0.30
11	2.20	55.88	48.26	-7.62	-0.60	26	1.65	41.91	48.26	6.35	0.50
12	2.10	53.34	48.26	-5.08	-0.40	27	1.45	36.83	48.26	11.43	0.90
13	2.15	54.61	48.26	-6.35	-0.50	28	1.34	34.02	48.26	14.24	1.17
14	2.10	53.34	48.26	-5.08	-0.40	29	1.35	34.34	48.26	13.92	1.14
15	1.95	49.53	48.26	-1.27	-0.10	30	1.60	40.64	48.26	7.62	0.60

9. Distribution of Pressure Coefficient on Octagonal cylinder at Angle of Attack of $\alpha = 0^0$

Tapping Point	Final Reading (inch of H_2O)	Final Reading (mm of H_2O)	Initial Reading (mm of H_2O)	Differences, Δh_w (mm of H_2O)	Pressure Coefficient, Cp	Tapping Point	Final Reading (inch of H_2O)	Final Reading (mm of H_2O)	Initial Reading (mm of H_2O)	Differences, Δh_w (mm of H_2O)	Pressure Coefficient, Cp
1	1.5	38.1	48.26	10.16	0.80	21	2.5	63.5	48.26	-15.24	-1.20
2	1.35	34.29	48.26	13.97	1.06	22	2.1	53.34	48.26	-5.08	-0.40
3	1.33	33.78	48.26	14.48	1.1	23	2.45	62.23	48.26	-13.97	-1.10
4	1.43	36.38	48.26	11.88	0.96	24	2.35	59.69	48.26	-11.43	-0.90
5	1.60	40.64	48.26	7.62	0.60	25	2.05	52.07	48.26	-3.81	-0.30
6	1.9	48.26	48.26	0.00	0.00	26	2.50	63.5	48.26	-15.24	-1.20
7	1.85	46.99	48.26	1.27	0.10	27	2.10	53.34	48.26	-5.08	-0.40
8	1.75	44.45	48.26	3.81	0.30	28	2.45	62.23	48.26	-13.97	-1.10
9	1.7	43.18	48.26	5.08	0.40	29	2.30	58.42	48.26	-10.16	-0.80
10	1.8	45.72	48.26	2.54	0.20	30	2.05	52.07	48.26	-3.81	-0.30
11	2.4	60.96	48.26	-12.7	-1.00	31	2.60	66.04	48.26	-17.78	-1.40
12	2.1	53.34	48.26	-5.08	-0.40	32	2.20	55.88	48.26	-7.62	-0.60
13	2.4	60.96	48.26	-12.7	-1.00	33	2.60	66.04	48.26	-17.78	-1.40
14	2.2	55.88	48.26	-7.62	-0.60	34	2.50	63.5	48.26	-15.24	-1.20
15	2	50.8	48.26	-2.54	-0.20	35	2.15	54.61	48.26	-6.35	-0.50
16	2.45	62.23	48.26	-13.97	-1.10	36	2.30	58.42	48.26	-10.16	-0.80
17	2.1	53.34	48.26	-5.08	-0.40	37	2.05	52.07	48.26	-3.81	-0.30
18	2.45	62.23	48.26	-13.97	-1.10	38	1.7	43.18	48.26	5.08	0.40
19	2.3	58.42	48.26	-10.16	-0.80	39	1.62	41.24	48.26	7.02	0.56
20	2.15	54.61	48.26	-6.35	-0.50	40	1.60	40.64	48.26	7.62	0.60

10. Distribution of Pressure Coefficient on Octagonal cylinder at Angle of Attack of $\alpha = 30^0$

Tapping Point	Final Reading (inch of H_2O)	Final Reading (mm of H_2O)	Initial Reading (mm of H_2O)	Differences, Δh_w (mm of H_2O)	Pressure Coefficient, Cp	Tapping Point	Final Reading (inch of H_2O)	Final Reading (mm of H_2O)	Initial Reading (mm of H_2O)	Differences, Δh_w (mm of H_2O)	Pressure Coefficient, Cp
1	1.46	37.04	48.26	11.22	0.90	21	2.00	50.8	48.26	-2.54	-0.20
2	1.50	38.1	48.26	10.16	0.80	22	2.40	60.96	48.26	-12.7	-1.00
3	1.60	40.64	48.26	7.62	0.60	23	2.50	63.5	48.26	-15.24	-1.20
4	1.64	41.58	48.26	6.68	0.50	24	2.15	54.61	48.26	-6.35	-0.50
5	2.15	54.61	48.26	-6.35	-0.50	25	2.60	66.04	48.26	-17.78	-1.40
6	2.60	66.04	48.26	-17.78	-1.40	26	2.45	62.23	48.26	-13.97	-1.10
7	2.15	54.61	48.26	-6.35	-0.50	27	2.10	53.34	48.26	-5.08	-0.40
8	2.55	64.77	48.26	-16.51	-1.30	28	2.32	58.93	48.26	-10.67	-0.84
9	2.45	62.23	48.26	-13.97	-1.10	29	2.30	58.42	48.26	-10.16	-0.80
10	2.00	50.8	48.26	-2.54	-0.20	30	2.00	50.8	48.26	-2.54	-0.20
11	2.40	60.96	48.26	-12.7	-1.00	31	2.25	57.15	48.26	-8.89	-0.70
12	2.05	52.07	48.26	-3.81	-0.30	32	1.98	50.29	48.26	-2.032	-0.16
13	2.32	58.93	48.26	-10.67	-0.84	33	2.32	58.93	48.26	-10.67	-0.84
14	2.30	58.42	48.26	-10.16	-0.80	34	2.42	61.47	48.26	-13.21	-1.04
15	2.00	50.8	48.26	-2.54	-0.20	35	2.08	52.83	48.26	-4.57	-0.36
16	2.45	62.23	48.26	-13.97	-1.10	36	1.60	40.64	48.26	7.62	0.60
17	2.05	52.07	48.26	-3.81	-0.30	37	1.50	38.10	48.26	10.16	0.80
18	2.30	58.42	48.26	-10.16	-0.80	38	1.53	38.98	48.26	9.28	0.82
19	2.30	58.42	48.26	-10.16	-0.80	39	1.47	37.16	48.26	11.10	0.88
20	1.98	50.29	48.26	-2.03	-0.16	40	1.46	37.04	48.26	11.22	0.90

11. Distribution of Pressure Coefficient on Octagonal cylinder at Angle of Attack of $\alpha = 45^0$

Tapping Point	Final Reading (inch of H_2O)	Final Reading (mm of H_2O)	Initial Reading (mm of H_2O)	Differences, Δh_w (mm of H_2O)	Pressure Coefficient, Cp	Tapping Point	Final Reading (inch of H_2O)	Final Reading (mm of H_2O)	Initial Reading (mm of H_2O)	Differences, Δh_w (mm of H_2O)	Pressure Coefficient, Cp
1	1.68	42.67	48.26	5.588	0.44	21	2.6	66.04	48.26	-17.78	-1.40
2	1.7	43.18	48.26	5.08	0.40	22	2.15	54.61	48.26	-6.35	-0.50
3	1.5	38.1	48.26	10.16	0.80	23	2.4	60.96	48.26	-12.7	-1.00
4	1.6	40.64	48.26	7.62	0.60	24	2.38	60.45	48.26	-12.19	-0.96
5	1.79	45.47	48.26	2.794	0.22	25	2.05	52.07	48.26	-3.81	-0.30
6	2.45	62.23	48.26	-13.97	-1.10	26	2.58	65.53	48.26	-17.27	-1.36
7	2.08	52.83	48.26	-4.572	-0.36	27	2.15	54.61	48.26	-6.35	-0.50
8	2.36	59.94	48.26	-11.68	-0.92	28	2.4	60.96	48.26	-12.7	-1.00
9	2.35	59.69	48.26	-11.43	-0.90	29	2.38	60.45	48.26	-12.19	-0.96
10	2.05	52.07	48.26	-3.81	-0.30	30	2.05	52.07	48.26	-3.81	-0.30
11	2.05	52.07	48.26	-3.81	-0.30	31	2.2	55.88	48.26	-7.62	-0.60
12	2.42	61.47	48.26	-13.21	-1.04	32	1.9	48.26	48.26	0.00	0.00
13	2.4	60.96	48.26	-12.7	-1.00	33	1.68	42.67	48.26	5.588	0.44
14	2.1	53.34	48.26	-5.08	-0.40	34	1.7	43.18	48.26	5.08	0.40
15	2.52	64.01	48.26	-15.75	-1.24	35	1.68	42.67	48.26	5.588	0.44
16	2.58	65.53	48.26	-17.27	-1.36	36	1.1	27.94	48.26	20.32	1.60
17	2.1	53.34	48.26	-5.08	-0.40	37	1.35	34.29	48.26	13.97	1.10
18	2.39	60.71	48.26	-12.45	-0.98	38	1.35	34.29	48.26	13.97	1.06
19	2.38	60.45	48.26	-12.19	-0.96	39	1.37	34.92	48.26	13.34	1.00
20	2.05	52.07	48.26	-3.81	-0.30	40	1.46	37.04	48.26	11.22	0.90

12. Distribution of Pressure Coefficient on Octagonal cylinder at Angle of Attack of $\alpha = 60^0$

Tapping Point	Final Reading (inch of H_2O)	Final Reading (mm of H_2O)	Initial Reading (mm of H_2O)	Differences, Δh_w (mm of H_2O)	Pressure Coefficient, Cp	Tapping Point	Final Reading (inch of H_2O)	Final Reading (mm of H_2O)	Initial Reading (mm of H_2O)	Differences, Δh_w (mm of H_2O)	Pressure Coefficient, Cp
1	2.28	57.91	48.26	-9.652	-0.76	21	2.50	63.5	48.26	-15.24	-1.20
2	2	50.8	48.26	-2.54	-0.20	22	2.10	53.34	48.26	-5.08	-0.40
3	1.82	46.23	48.26	2.032	0.16	23	2.30	58.42	48.26	-10.16	-0.80
4	1.95	49.53	48.26	-1.27	-0.10	24	2.30	58.42	48.26	-10.16	-0.80
5	1.85	46.99	48.26	1.27	0.10	25	2.00	50.8	48.26	-2.54	-0.20
6	2.45	62.23	48.26	-13.97	-1.10	26	2.65	67.31	48.26	-19.05	-1.50
7	2.08	52.83	48.26	-4.572	-0.36	27	2.20	55.88	48.26	-7.62	-0.60
8	2.35	59.69	48.26	-11.43	-0.90	28	2.85	72.39	48.26	-24.13	-1.90
9	2.3	58.42	48.26	-10.16	-0.80	29	3.00	76.2	48.26	-27.94	-2.20
10	2	50.8	48.26	-2.54	-0.20	30	2.40	60.96	48.26	-12.7	-1.00
11	2.55	64.77	48.26	-16.51	-1.30	31	1.98	50.29	48.26	-2.03	-0.16
12	2.15	54.61	48.26	-6.35	-0.50	32	1.78	45.21	48.26	3.04	0.24
13	2.4	60.96	48.26	-12.7	-1.00	33	1.68	42.67	48.26	5.59	0.44
14	2.38	60.45	48.26	-12.19	-0.96	34	1.57	39.82	48.26	8.44	0.68
15	2.15	54.61	48.26	-6.35	-0.50	35	1.5	38.1	48.26	10.16	0.80
16	2.6	66.04	48.26	-17.78	-1.40	36	1.46	37.04	48.26	11.22	0.90
17	2.15	54.61	48.26	-6.35	-0.50	37	1.43	36.38	48.26	11.88	0.96
18	2.45	62.23	48.26	-13.97	-1.10	38	1.53	38.84	48.26	9.42	0.77
19	2.4	60.96	48.26	-12.7	-1.00	39	1.6	40.64	48.26	7.62	0.60
20	2.05	52.07	48.26	-3.81	-0.30	40	1.7	43.18	48.26	5.08	0.40

13. Variation of Drag and Lift Coefficients at Various Angles of Attack on Pentagonal Cylinder

Angle of Attack, degree (α)	**0^0**	**30^0**	**45^0**	**60^0**
Coefficient of Drag	0.89	1.37	1.2	1.05
Coefficient of Lift	-0.14	-0.16	0.0179	-0.18

14. Variation of Drag and Lift Coefficients at Various Angles of Attack on Hexagonal Cylinder

Angle of Attack, degree (α)	**0^0**	**30^0**	**45^0**	**60^0**
Coefficient of Drag	1.02	1.05	1.02599	0.99
Coefficient of Lift	-0.2	-0.3	-0.7	-0.5

15. Variation of Drag and Lift Coefficients at Various Angles of Attack on Octagonal Cylinder

Angle of Attack, degree (α)	**0^0**	**30^0**	**45^0**	**60^0**
Coefficient of Drag	0.69	0.82	0.69	0.75
Coefficient of Lift	-0.17	-0.37	-0.1	0.03